On Multiantenna Spectrum Sensing and Energy-Aware Resource Allocation in Cognitive Radio Networks

by

Guangjie Huang

A dissertation submitted to the Graduate Faculty of
Auburn University
in partial fulfillment of the
requirements for the Degree of
Doctor of Philosophy

Auburn, Alabama
August 3rd, 2013

Keywords: Cognitive radio, Cyclostationarity, Spectrum sensing, Energy efficiency,
Resource allocation, Multiple input multiple output(MIMO)

Approved by

Jitendra K. Tugnait, James B. Davis Professor of Electrical and Computer Engineering
Prathima Agrawal, Ginn Distinguished Professor of Electrical and Computer Engineering
Shiwen Mao, McWane Associate Professor of Electrical and Computer Engineering
Olav Kallenberg, Professor of Mathematics

Abstract

This dissertation covers two main parts: 1) low complexity cyclostationarity based spectrum sensing in cognitive radio, and 2) energy efficient resource allocation in cognitive radio networks. Cognitive radio allows unlicensed users (secondary users) to access the frequency spectrum allocated to licensed users (primary users). Secondary users are allowed to access the spectrum licensed to primary users in two ways: underlay and overlay. Under the overlay mode, secondary users need to sense the channel first and then decide whether to transmit based on the presence or absence of a primary signal. The underlay mode allows primary and secondary users access to the same channel simultaneously while constraining the transmitted power of secondary users so that it can be treated as background noise at primary users without exceeding the primary users noise floor. The most common sensing method is based on the energy distribution of the primary signal, however its performance is degraded when noise variance is not accurately known. For cyclostationary primary signals such as Orthogonal Frequency Division Multiplexing (OFDM) and Gaussian filtered Minimum Shift Keying (GMSK) signals, we exploit their statistical characteristics under both certain and uncertain Gaussian noise and propose a low complexity cyclostationarity-based spectrum sensing method for cognitive radio networks. Multiple receiving antennas are utilized to improve sensing performance. In addition to sensing complexity, energy efficiency has become a "hot" research topic due to the trend of sustainable energy and green wireless communication and networks. For mobile terminals with battery for power supply, the energy consumption issues are more serious because development of battery technology lags behind the development of wireless communication technologies. This dissertation also

ii

addresses energy efficient sensing and power allocation for multichannel overlay cognitive radio networks (CRN), energy efficient precoding for MIMO (multiple input multiple output) assisted spectrum sharing CRN and MIMO cognitive multiple access (C-MAC) channel.

The dissertation is organized into eight chapters. Chapter 1 provides an introduction to cognitive radio networks and related research issues. Existing spectrum sensing algorithms are addressed too. It also briefly outlines the whole dissertation. Chapter 2 through Chapter 4 are mainly concerned with low complexity cyclostationarity-based spectrum sensing for cognitive radio networks. This sensing scheme is explicitly designed for cyclostationary primary signals under white and colored Gaussian additive noise. Chapter 2 introduces the cyclostationarity background and related spectrum sensing algorithm. The cyclostationary characteristics of the OFDM and GMSK signals are illustrated as examples. The hypothesis testing framework is briefly described and existing spectrum sensing tests based on cyclostationarity are presented. In Chapter 3, a novel low complexity cyclostationarity-based spectrum sensing approach under white Gaussian noise is proposed. The theoretical performance and computational complexity advantages compared with other counterparts are given in this chapter. The simulation examples support the theoretical analysis. Chapter 4 focuses on cyclostationarity-based spectrum sensing under colored Gaussian noise. Besides sensing performance, energy efficiency related with sensing and transmission for either overlay or underlay cognitive radio networks is also studied in Chapters 5, 6 and 7. Chapter 5 focuses on energy-aware sensing and power allocation for multi-channel transmission of a single secondary link in overlay cognitive radio networks. The optimization algorithms for sensing duration, test threshold and transmission power allocation are described. Simulation results are provided in support of the proposed algorithm. Chapters 6 and 7 address energy efficient resource allocation in underlay cognitive radio networks under both transmit power constraint and interference power constraint. Chapter 6 proposes an energy efficient transmit covariance matrix (precode) to maximize energy efficiency for a single secondary link in spectrum sharing underlay CRN. Multiple antennas are employed at the secondary

transmitter and receiver. Chapter 7 further extends the work in Chapter 6 to propose an energy efficient precoding for MIMO cognitive multiple access channels. Conclusions and future work are stated in Chapter 8.

Acknowledgments

Here, I would take the chance to thank all people who help me during last four years' study at Auburn University.

First of all, I should express my deepest gratitude to my advisor Dr. Jitendra K. Tugnait who is a well-recognized scholar on digital signal processing and communication system. The dissertation would not be finished without his guidance. He always encourages me to explore research topic independently, challenges my idea, and shapes my mathematical model formulation with his broad knowledge and deep experience on digital signal processing. He also donates precious time and effort to correct my writing with patience. His kindness, brilliant ideas hint, excellent example provided, and instructions help me grow to be an eligible scientific researcher with self-discipline.

I would like to thank committed members: Dr. Prathima Agrawal, Dr. Shiwen Mao and Dr. Olav Kallenberg. I really appreciate their time and effort to read my PhD proposal and dissertation. I should give special thanks to Dr. Kevin Phelps who serves as outside reader for this dissertation.

To all the professors from whom I took courses, I own my gratitude to their instruction and knowledge that help me to finish PhD courses. I would also like to acknowledge my classmates and friends in Auburn. With their accompany, I could enjoy the past four years' life at Auburn.

Last, but not least, I will always be grateful for my parents, my brothers and sisters for their spiritual support. My mere thanks would not be sufficient to express my thanks for them.

Thanks you all again.

Table of Contents

vi

ix

List of Figures

Chapter 1

Introduction

1.1 Cognitive Radio

1.1.1 The History of Cognitive radio

The development of microelectronics has spurred the emergence of cheaper, higher speed and quality of service (QoS) devices and applications, resulting in high demand for radio spectrum. On the other hand, the frequency spectrum is a limited natural resource managed by the government agencies in a static allocation mode. The rights of frequency band are sold to licensed users with guaranteed minimum frequency interference between adjacent users. While most of the spectrum resources has been allocated to licensed users, the current radio spectrum allocation can not accommodate the dramatic emergence of new wireless communication application. However, according to [1] the utilization of current licensed spectrum is inefficient from 15% to 85%, especially the televison broadcasting band. Thus the true problem is the fixed frequency spectrum allocation rather than true shortage of frequency. To alleviate the confliction between increasing needs for frequency and inefficient spectrum usage, the concept of cognitive radio (CR) was first proposed by Mitola in 1999 [2]. It is an alternative method to allow the unlicensed users to opportunistically use frequency spectrum that is not temporally or spatially occupied by the licensed users. The potential of improving spectrum resource utilization of CR triggered Federal Communications Commission's (FCC's) work on new spectrum policy [3, 4]. FCC allows an unlicensed fixed, personal/portable device to share the TV bands, leading the begining of CR network deployment.

In academia, a large amount of work and effort has been put into CR research [2, 5, 56, 6]. The research "hot" points include: spectrum opportunity discovery such as spectrum sensing, dynamic spectrum access strategies and protocols, CR network routing and transport protocols, security issue, standardization and future application [7, 8, 9, 10].

The government officials also began to publish related new spectrum policy to pave the way for CR network applications. In the United States, based on the spectrum utilization research [1, 3], an official rule to guide unlicensed transmission of CR devices in TV bands was specified in [4]. In the United Kingdom Office of Communications (Ofcom) has proposed regulation that CR devices can access digital TV channels without interfering with PU users, jointly based on white space databases and spectrum sensing to exploit spectrum opportunity [11]. The Conference of European Post & Telecommunications Administrations (CEPT) has also specified the frequency band plan and technical requirement for CR devices to access 790-862 MHz licensed band [12].

The first industrial research on CR network was launched in the United States motivated by FCC. In 2008, the first testing CR network applied in TV bands was field tested with prototype CR devices from Adaptrum, I2R, Motorola and Philips [13]. The results showed that the performance of spectrum sensing for TV signals and wireless microphone is limited and even unreliable. Thus, FCC then recommended combination of spectrum sensing and geolocation databases for white band discovery. Then in 2009 the first public CR network was deployed and tested in Virginia [14] and finally led to a "Smart City" CR network built in North Carolina in 2010, which used CR devices from Spectrum Bridge, Microsoft and Dell [15]. The development of CR techniques and its potential application in TV white band has attracted increasing attention from the public and industry.

1.1.2 Spectrum Opportunity Discovery

The first and the most important step of CR is to detect spectrum opportunity that is also named spectrum hole or white frequency space [8, 9]. Recently emerging bunch of

proposals for discovery of spectrum opportunity can be classified into three basic types: PU signal detection, auxiliary beacons detection and geolocation databases of white spaces or spectrum holes.

The aim of PU signal detection, also named spectrum sensing, is to detect PU signals in the frequency band of interest. Spectrum sensing can be further categorized into PU transmitter signal detection and receiver detection. The former includes matched-filtering sensing, waveform-based sensing, cyclostationarity sensing and energy detector sensing [57] [60] [16] [65], which would be explained in detail in Sec. 1.2. Since the PU receiver's local oscillator leaks power, a leakage detector is used to passively identify spectrum opportunity [17].

Besides spectrum sensing, beacon transmitter is another method to detect spectrum holes. The beacon system occupies a narrow part of TV band, which periodically transmit message to secondary users to utilize idle PU channels. At the same time, strong "Stop" beacon message is designed to protect the primary users such as wireless microphone operations from interference due to secondary transmission [18]. When the PU's location and activities are known a priori such as TV bands usage, a geolocation database [19] can be built. Secondary user with GPS-aids would visit the database, and then decide when and which channel to access. CR users can also predict the spectrum opportunity by reasoning and learning from previous channel usage [20].

Spectrum sensing performance such as false alarm probability is determined directly by sensing duration. Long sensing time would result in better detection. On the other hand, too much sensing time will reduce potential network throughput since spectrum opportunity is limited. Thus, MAC layer assisted sensing scheduling is needed to balance sensing performance and transmission throughput [21, 22]. The dynamics of wireless channel such as fading can make a single sensor unable to identify PU signal, thus wasting opportunity or interfering with PU signal. To overcome the disadvantage of local sensors, collaborative sensing can exploit spatial diversity to enhance detection performance [22].

Besides MAC layer cooperative sensing utilizing spatial diversity of sensors, Ref. [23] works on relay-based cooperation that can improve cooperative spectrum sensing performance with relay diversity to overcome heavy shadowing and frequency-selective Rayleigh fading.

1.1.3 Dynamic Spectrum Access Strategies

The spectrum opportunity discovery provides the state of PU channels. Given this state, the secondary users has to decide when and how to access the channel. On the other hand, the white channel may become busy due to PU's activity and other SU's occupancy. Thus how to avoid interfering with PU signal and share spectrum with other secondary users, how to utilize spectrum for transmission and how to switch channel when current channel is not available any more, are some of the issues that a secondary user needs to face. According to [24], dynamic spectrum access can be classified into three groups: dynamic exclusive use model, open sharing model and hierarchical access model. The first model maintains the basic idea of current static spectrum allocation policy: spectrum allocated can only be used exclusively. For CR network, the secondary users try to share the spectrum with primary user who holds the spectrum rights. As a result, the only way is to do spectrum trading between PU and SU to achieve exclusive usage [25]. The primary use can sell or trade the spectrum to secondary user for profit. In [26] the stable throughput of secondary link in a cognitive radio network composed of single SU and single PU is studied. The SU queues and forwards packets for the PU to enhance transmission rate. SU also benefits from relaying PU's transmission becasue more idle channel time is created for SU itself.

Another popular access model is the hierarchical one, where there is no trading between SUs and PUs. It can be further classified into: spectrum underlay and spectrum overlay. In the spectrum underlay, the secondary user can transmit simultaneously with PU [27], with limited interference to PU signal. In the underlay model, the SU can not necessarily detect

the PU signal. Spectrum overlay is also called opportunistic spectrum access, that is secondary users can only transmit when PU signal is absent. Based on the network structure, the opportunistic spectrum access is categorized into: centralized and distributed. For centralized access, there is a central entity that controls spectrum allocation. Thus scheduling is a typical centralized access method [28]. For distributed spectrum access, special MAC layer protocols are needed. In [29] access strategies are studied to maximize single SU's throughput with PU protection. In multi-SU scenario, [30] proposes MAC designed for CR networks to guarantee co-existence of different SUs and PUs.

1.1.4 Resource Allocation and Precoding

In CR networks, the dynamics of spectrum resource induce competition among secondary users. At the same time different PU channels have different interference temperature requirement and activity models. To guarantee maximum SU's throughput, fairness among SUs and PU signal protection, resource allocation should be based on cross-layer consideration. To manage interference among secondary users and to primary users, power control is needed for spectrum access and related channel allocation is also needed [31].

In underlay spectrum sharing cognitive radio networks, MIMO (multiple input multiple output) technique is employed to enhance spectral efficiency [106, 107, 101, 100, 99], to mitigate interference to PU receiver and to maximize energy efficiency using spatial diversity. When multiple antennas are equipped at secondary users and channel state information from SU transmitter to both SU receiver and PU receiver is available, optimization on transmit covariance matrix (precoding) can be performed to maximize capacity or energy efficiency. The spatial efficient or energy efficient precoding can be applied in single secondary link, cognitive multiple access channel and/or cognitive broadcasting channel with multiple transmit antennas.

1.1.5 Cognitive Radio Network QoS Issue, Security Issue and Protocols

CR networks need awareness of the surrounding wireless environment, cooperation or interaction among secondary users, and adapt to network variations by learning and reasoning from current and previous observations. However, the erroneous spectrum sensing, dynamically changing channel state, temporally and spatially discrete spectrum resources would bring intolerant latency or traffic jitter for high layer applications with QoS requirement. As a result, new routing protocols and transport layer protocols are needed to adapt spectrum dynamics and to ensure required latency, network throughput and capacity [32]. Ref. [33] studies a distributed routing protocol based on traditional on-demand routing for ad hoc networks with multi-flow multi-frequency scheduling. An unified adaptive transport protocol for heterogeneous fourth-generation cognitive radio networks was studied in [34].

Since there is generally lack of cooperation between primary users and secondary users in CR networks, CR networks are more vulnerable than traditional wireless networks to security attacks. There are two types of attack on spectrum sensing: primary user emulation attack (PUEA) and spectrum sensing data falsification (SSDF). The work in [35] directly compared the true PU transmitter's location with estimated location of signal source to identify fake PU. Ref. [36] studied SSDF attack and proposed a statistics-based filtering method to mitigate false sensing report's affect. To alleviate CR users violating spectrum etiquettes, a monitoring and punishing mechanisms may be embedded into hardware in CR devices [2].

1.1.6 Cognitive Radio Network Standard and applications

Aiming to resolve the spectrum scarcity problem and to improve spectrum utilization, cognitive radio has triggered standardization from all levels such as International Telecommunication Union (ITU), Institute of Electrical and Electronics Engineers (IEEE), European Association for Standardizing Information and Communication Systems (ECMA) and European Telecommunications Standards Institute (ETSI) [9, 8]. ITU-R 1B has developed

definitions, usage scenarios of cognitive radio systems (CRS) and its relation with software defined radio (SDR) [37]. IEEE 802 group and SCC41 group are developing standardization of cognitive radio and have proposed CR standards 802.22 [38], 802.11af [39], SCC41 [40] and 802.19. IEEE 802.22 wireless regional area network (WRAN) is the first international CR standard. WRAN is a cellular network designed for rural area, including base station (BS) and customer premises equipment (CPE). IEEE 802.11af is evolved from current Wi-Fi [41], based on the FCC policy to allow personal and/or portable devices [4]. IEEE 801.19 aims to provide coexistence among independent unlicensed wireless network, such as 802.22, 802.16 on TV band. IEEE SCC41, formally named IEEE 1900, is a CR standard to regulate higher-layer protocols than MAC and PHY for dynamic access network (DSA). ECMA proposes the first standard ECMA 392 that personal/portable cognitive devices utilize white space in TV bands [42]. The TC RSS working group of ETSI has proposed a technical report on how cognitive radio network operate on UHF white space frequency bands, primary user protection and system requirements [43].

In [10] a survey on emerging cognitive radio network application is studied. The first future potential cognitive radio network is on TV bands in the United States. The secondary CR network is MBANS. There is another trend that leads traditional power grid into smart grid with cognitive ability. For the public's benefits, CR can also be applied into public safety networks, cellular networks and wireless medical networks.

1.2 Existing Spectrum Sensing Algorithms in Cognitive Radio

The goal of cognitive radio is to achieve maximum spectrum utilization while interference to licensed users is kept to a minimum. To avoid interference to license users (also named primary users), the unlicensed users (also named secondary users) should detect the presence of primary users' signal before accessing the specified spectrum band. On the other hand, the secondary users should cancel transmission immediately once they detect the signal of primary users. As a result, advanced spectrum sensing techniques are need for application of

cognitive radios. For local or non-cooperative spectrum sensing, researchers have proposed many solutions, including matched-filter sensing, waveform-based sensing, cyclostationarity sensing and energy detector sensing [65, 60, 16].

1.2.1 Energy Detector

Energy detector is the most popular one due to its simplicity and no needs for primary users' signal [44, 45, 46]. The energy detector compares the power metric of signal with a threshold to decide the presence or absence of the primary signal. However, the test threshold is related to power or variance of noise, which is not available in many scenarios. In [45], the authors propose a power spectrum density (PSD) estimation method for noise through a assessment window, which is assumed to be free of primary signal. Thus, it does not require exact knowledge of noise. Ref. [47] improves the PSD estimation bias and variance in [45] by replacing Welch windowed periodogram with multitaper estimator. The multi-taper method is proved to decrease the bias and variance for PSD estimation in [46].

1.2.2 Coherent Detector

When the primary user signal is deterministic and known to the secondary users, matched filter can be used for coherently spectrum sensing. Even only part of the signal structure is known, such as pilot aided channel estimation, we can still achieve coherent detection[48].

1.2.3 Cyclostationary Detector

Some of man-made signals are cyclostationary due to signal structure, modulation, coding or pilot added for channel estimation. For these cyclostationary signals, their statistics such as autocorrelation function exhibit periodicity, which can be used for detection of primary user signal under noise and interference background [59, 73, 49, 64, 68, 67, 71].

1.2.4 Other Spectrum Sensing Algorithms

Other spectrum sensing algorithms include covariance-based detection and wavelet-based detection. When the received PU signal exhibits spatial correlation due to multi-antenna receiver, oversampling or dispersive channel, we can utilize such correlation to distinguish PU signal from background noise[50]. Wavelet-based detection [51] has been used to estimate the power spectrum density (PSD) of the PU signal with discrete changes between adjacent sub frequency bands and smooth changes within each sub frequency band.

1.3 Overview of the Dissertation

In this dissertation, we investigate low complexity cyclostationarity based sensing and energy efficient design for sensing and power allocation in cognitive radio networks. Based on the cyclostationarity of the primary signal, we propose low complexity sensing for both single antenna and multiple antennas assisted secondary users. For battery-supported mobile secondary users, we study the effect of energy on sensing and transmission, and then an energy efficient sensing and power allocation scheme is proposed for multichannel secondary transmission in cognitive radio network. We further propose energy efficient resource allocation for either single secondary link or cognitive multiple access channel in spectrum sharing underlay cognitive radio networks. The main contents of the dissertation are presented in Chapter 2 through Chapter 7.

Chapter 2 through Chapter 4 focus on low complexity cyclostationarity based spectrum sensing under both white and colored uncertain Gaussian noise, in which multiple receive antennas are utilized to enhance sensing performance. This sensing scheme is explicitly designed for the cognitive radio networks where primary users' signals exhibit cyclostationarity. To opportunistically access the spectrum allocated to the primary users, the secondary users need to first sense the presence of cyclostationary signals from primary users to avoid transmission conflict.

In Chapter 2, the cyclostationarity background and corresponding existing spectrum sensing schemes are introduced. First, the cyclostationary characteristics of OFDM and GMSK signals are derived theoretically and illustrated with simulations. Second, the concept of statistical hypothesis testing is reviewed before introducing existing cyclostationary sensing algorithms.

Chapter 3 presents the details of spectrum sensing of cyclostationary primary user (PU) signals in white Gaussian noise with both single and multiple receiving antennas. A novel algorithm based on looking for a cycle frequency at a particular time lag in the cyclic autocorrelation function (CAF) of the noisy PU signal is proposed. We explicitly exploit the knowledge that under the null hypothesis of PU signal absent, the measurements originate from white Gaussian noise with possibly unknown variance. Our formulation allows us to computationally simplify the spectrum sensing detector, obviating the need for estimating an unwieldy covariance matrix needed in prior works. We consider both single and multiple antenna receivers. Supporting simulation examples are provided and they verify our performance analysis and also show that our approaches either outperform or are at least as good as existing approaches while being computationally much cheaper.

The cyclostationarity-based spectrum sensing under uncertain (colored) Gaussian noise is addressed in Chapter 4. Detection of cyclostationary primary user (PU) signals in colored Gaussian noise for cognitive radio systems is considered based on looking for a cycle frequency at a particular time lag in the cyclic autocorrelation function (CAF) of the noisy PU signal. We explicitly exploit the knowledge under the null hypothesis of PU signal absent, the measurements originate from colored Gaussian noise with possibly unknown correlation function. We consider both single and multiple antenna receivers. A performance analysis of the proposed detector is carried out. Supporting simulation examples are provided using a OFDM PU signal and they show that our proposed approaches are computationally much cheaper than the Dandawate-Giannakis and related approaches while having quite similar detection performance for a given false alarm rate.

In Chapter 5, energy-aware design of sensing and power allocation strategies for multi-channel cognitive radio networks is presented and analyzed. Frequency spectrum and energy are two key resources of green cognitive radio networks with battery-powered wireless terminals. The issues of how to utilize sparse frequency spectrum and limited energy resource pose challenges to the design of sensing and power allocation strategies that affect both throughput and energy consumption. In this dissertation, we first construct an utility function that incorporates throughput as reward and energy consumption as cost for a time slotted multi-channel cognitive radio network. An optimization problem to maximize the utility function is formulated involving optimization of both sensing parameters (sensing duration, local test threshold) and power allocation strategy. The problem is non-convex, however, we decouple it into two separate convex problems and propose an iterative algorithm to obtain a sub-optimal solution. The simulation results show that our iterative algorithm converges fast and performs better than an "only power allocation optimization" approach and an existing approach that ignores energy efficiency.

In Chapter 6, energy efficient spectrum sharing in cognitive radio network is designed and analyzed. We formulate the design of energy efficiency maximization for a single secondary link in an underlay spectrum sharing cognitive radio network under an SU (secondary user) transmit-power constraint and an upperbound on the interference power at the PU (primary user). We propose energy efficient precoding (beamforming) for the SU transmitter to maximize energy efficiency defined as the transmission rate to power ratio, when the terminals in the system are equipped with multiple antennas. The underlying channels are assumed to be known at the SU transmitter. The nonlinear optimization (fractional programming) problem is transformed into a parametrized convex optimization problem and the corresponding solution is discussed. Computer simulation examples are provided to illustrate the proposed approach and to explore the trade-off between energy efficiency and spectrum efficiency.

Based on energy efficient precoding for MIMO assisted single secondary link in Chapter 6, we further study weighted energy efficiency maximization for multiple-input multiple-output cognitive multiple access channels under both secondary user transmit power constraint and primary user interference power constraint in Chapter 7. Energy efficiency is defined as the ratio of weighted sum rate and energy consumption including both transmission and circuit energy consumption. The nonlinear (fractional programming) energy efficiency optimization problem is transformed into a series of parametrized convex optimization problems. A combination of bisection search method and cyclic coordinate ascent-based iterative water-filling algorithm is proposed to solve the parametrized problem. Computer simulation examples are provided to illustrate the proposed approach and to explore the trade-off between energy efficiency and spectrum efficiency.

Conclusions and related future work are presented in Chapter 8.

Chapter 2

Cyclostationarity Background and Corresponding Spectrum Sensing Tests

2.1 Introduction

Due to the signal structure, modulation, pilot or carriers, man-made signal exhibits periodicity in its mean, correlation function or spectral descriptors. Such signal sequences can be called (wide-sense) cyclostationary processes. A discrete time zero-mean complex cyclostationary process $x(t)$ is characterized by its time-varying correlation function as [59, 67]

$$R_{xx}(t, t + \tau) = E\{x(t)x^*(t + \tau)\}. \tag{2.1}$$

The correlation function $R_{xx}(t, t + \tau)$ can be further expressed in Fourier series (FS) form [59, 68] as follows

$$R_{xx}(t, t + \tau) = \sum_{\alpha \in \mathcal{A}} R(\alpha; \tau)e^{j2\pi\alpha t} \tag{2.2}$$

where $R(\alpha; \tau)$ is called the cyclic autocorrelation function (CAF) at cycle frequency $\alpha \in \mathcal{A}$ given by (M is the observation length)

$$R(\alpha; \tau) = \lim_{M \to \infty} \frac{1}{M} \sum_{t=1}^{M} R_{xx}(t, t + \tau)e^{-j2\pi\alpha t} \tag{2.3}$$

and $\mathcal{A}$ is the set of cycle frequencies [59]

$$\mathcal{A} \triangleq \{\alpha, 0 \leq \alpha < 1 \text{ and } R(\alpha; \tau) \not\equiv 0\}. \tag{2.4}$$

For some cyclostationary processes, CAF varnishes to zero but conjugate CAF $R_{(*)}(\alpha; \tau)$ is large enough to be detected

$$R_{(*)}(\alpha; \tau) = \lim_{M \to \infty} \frac{1}{M} \sum_{t=1}^{M} R_{xx^*}(t, t + \tau)e^{-j2\pi\alpha t} \tag{2.5}$$

where $R_{xx^*}(t, t + \tau) = E\{x(t)x(t + \tau)\}$.

Later we will consider vector random processes arising due to a multiantenna receiver with $p \geq 1$ antennas. Therefore, we will consider a $p \times 1$ discrete time zero-mean complex-valued cyclostationary signal $x(t)$ with time-varying autocorrelation function $R_{xx}(t, t+\tau) := E\{x(t)x^H(t+\tau)\}$. The corresponding Fourier series decomposition and nonconjugate CAFs of $R_{xx}(t, t + \tau)$ can be obtained according to (2.2) and (2.3). Similar comments apply to conjugate CAFs. In the following section, we illustrate the cyclostationarity exhibited in Orthogonal Frequency Division Multiplexing (OFDM) and Gaussian Minimum Shift Keying (GMSK) signals.

Notation: B_{ij} denotes the ijth element of the matrix $\mathbf{B}$, x_i denotes the ith element of vector $\mathbf{x}$, and $\mathbf{I}$ is the identity matrix. The superscripts $*$ and H denote the complex conjugate and the Hermitian (conjugate transpose) operations, respectively. $\delta_{i,j}$ denotes the Kronecker delta: $= 1$ if $i = j$, 0 otherwise. Given a column vector $\mathbf{x}$, diag$\{\mathbf{x}\}$ denotes a square matrix with elements of $\mathbf{x}$ along its main diagonal and zeros everywhere else. For a real Gaussian variable x with mean μ and variance σ^2, its distribution is described as $x \sim \mathcal{N}(\mu, \sigma^2)$. For circularly symmetric complex Gaussian vector $\mathbf{x}$ with mean vector μ and the covariance matrix $\mathbf{\Sigma}$, the probability distribution is denoted as $\mathbf{x} \sim \mathcal{CN}(\mu, \mathbf{\Sigma})$.

2.2 Cyclostationary Characteristics of OFDM and GMSK Signals

2.2.1 OFDM Signal

An OFDM signal exhibits nonconjugate cyclostationarity [68], which is suitable for cyclostationarity-based spectrum sensing. In an OFDM system, the Phase Shift Keying

(PSK) or Quadrature Amplitude Modulation (QAM) modulated information symbols are transmitted over multiple orthogonal carriers in parallel. A typical baseband OFDM signal can be expressed as

$$s(t) = \sqrt{\frac{1}{N_c}} \sum_{n=-\infty}^{\infty} \sum_{i=0}^{N_c-1} d_{n,i} e^{j2\pi i(t-nT_s-\epsilon)/T_u} g_R(t - nT_s - \epsilon) e^{-j2\pi \frac{N_c-1}{2} t/T_u} \tag{2.6}$$

where $d_{n,i}$ is the nth information symbol modulated on the ith sub-carrier, N_c is the number of sub-carriers, and ϵ is the unknown symbol timing. T_s is the OFDM symbol length and $T_s = T_u + T_g$, where T_u is the useful OFDM symbol length and T_g is the cyclic prefix length. $g_R(t)$ is the rectangular impulse function of length T_s.

The time varying nonconjugate autocorrelation of the OFDM signal can be expressed as [68, 67]

$$R_{ss}(t, t+\tau) = \frac{\sigma_d^2}{N_c} \frac{sin(\pi N_c \tau/T_u)}{sin(\pi \tau/T_u)} \sum_{n=-\infty}^{\infty} g_R(t - nT_s - \epsilon) g_R^*(t - nT_s - \epsilon + \tau) \tag{2.7}$$

where $\sigma_d^2 = E\{d_{n,i} d_{n,i}^*\}$. It is easy to show that $R_{ss}(t, t+\tau)$ is periodic in t with a period T_s. As a result, the OFDM signal exhibits nonconjugate cyclostationarity with a cyclic frequency $\alpha = k/T_s = kf_s$, where $k = 0, \pm 1, \pm 2, \ldots$. The cyclic autocorrelation function of OFDM signal can be calculated as [68, 67]

$$R(\alpha; \tau) = \begin{cases} \frac{\sigma_d^2}{N_c} \frac{sin(\pi N_c \tau/T_u) sin[\pi k f_s(T_s-\tau)]}{\pi k sin(\pi \tau/T_u)} e^{-j2\pi k f_s \epsilon}, & \alpha = k/T_s, |\tau| < T_s, \\ 0, & otherwise. \end{cases} \tag{2.8}$$

Consequently, although the OFDM signal does not exhibit conjugate cyclostationarity, its nonconjugate cyclostationarity with a basic cycle frequency equal to the symbol rate of the OFDM system $\alpha = 1/T_s$ is large enough for detection.

Assume OFDM signal is sampled at the Nyquist rate such that the sampling interval is $\frac{T_s}{N_c+N_{cp}}$. For each OFDM symbol, there are N_{cp} samples for the cyclic prefix and N_c samples

15

for useful OFDM symbol. Assume only one cyclic frequency $\frac{1}{T_s}$ and one time lag T_u is considered. Due to Nyquist sampling, the corresponding cyclic frequency and time lag in discrete time domain is $\alpha = \frac{1}{N_c + N_{cp}}$ and $\tau = N_c$ respectively. Let $\sigma_s = \sigma_d$, of which σ_s^2 is the power of the OFDM signal. The theoretical cyclic autocorrelation function with parameters α, τ and σ_s is calculated as [67]

$$R(\alpha; \tau) = -\frac{\sigma_s^2}{\pi} sin\left(\pi \frac{N_{cp}}{N_c + N_{cp}} \right).$$ (2.9)

Based on (2.8), we set $N_c = 8$, $T_s/T_u = 5/4$ and plot a 3D theoretical CAF figure in Fig. 2.1.
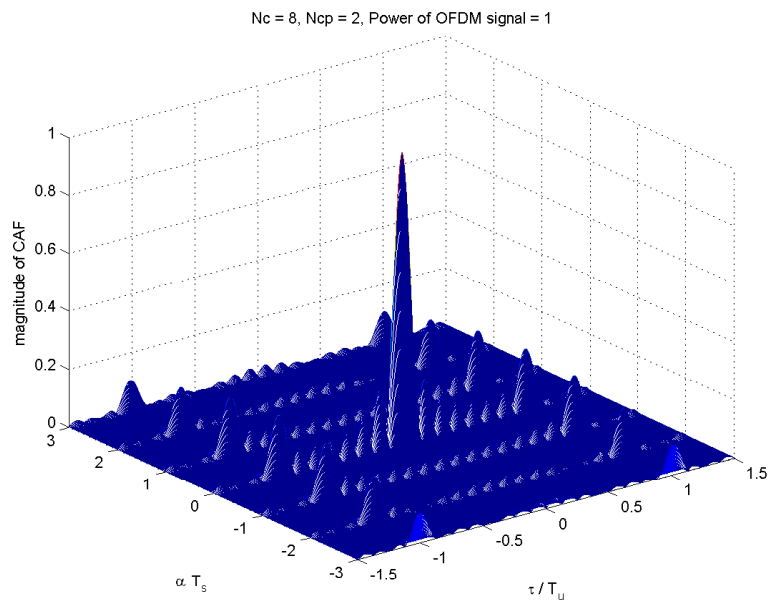
Figure 2.1: Theoretical CAF function with 8 subcarriers and normalized power

2.2.2 GMSK Signal

GMSK modulation is used in Global System for Mobile Communications (GSM) system. It exhibits conjugate cyclostationarity [68]. GMSK can also be treated as a 2-level FSK modulation with a modulation index $h = 0.5$. The complex envelope of a GMSK signal is

16

[67]

$$s(t) = exp\left[j2\pi h \sum_{n=-\infty}^{\infty} d_n \int_{-\infty}^{t} g(\tau - nT_s)d\tau\right] \tag{2.10}$$

with the symbol sequence $d_n \in \{-1, 1\}$, symbol rate $f_s = 1/T_s$ and frequency impulse $g(t)$ given as

$$g(t) = \frac{1}{T_s}\text{rect}(\frac{t}{T_s}) * p_{Gauss}(t) \tag{2.11}$$

where rect(t) is rectangular pulse and $p_{Gauss}(t)$ is a Gaussian impulse with the time bandwidth product BT_s (B is the bandwidth), which is equal to 0.3 for the GSM system. In practice, the Gaussian impulse is cut to a length LT_s with $L \leq 3$. With $L = 4$, a GMSK signal can be approximated [52] as

$$s(t) \approx \sum_{n=-\infty}^{\infty} z_n c_0(t - nT_s) \tag{2.12}$$

with elementary impulse form $c_0(t)$ and the modulating symbol sequence z_n [53] such that

$$z_n = exp\left[j\pi h \sum_{i=-\infty}^{n} d_i\right] = exp[j\frac{\pi}{2}(d_n + \sum_{i=-\infty}^{n-1} d_i)]$$

$$= jd_n z_{n-1}. \tag{2.13}$$

Using this approximation, the conjugate time varying autocorrelation function of the signal can be calculated as [68, 67]

$$R_{ss^*}(t, t + \tau) \simeq \sum_{n=-\infty}^{+\infty} z_{-\infty}^2 (-1)^n c_0(t - \epsilon - nT_s) \times c_0(t - \epsilon - nT_s + \tau) \tag{2.14}$$

where ϵ is the unknown symbol timing and $z_{-\infty}^2 \in \{-1, 1\}$ is a constant determined by the initial state of z_n. It is easy to show that $R_{ss^*}(t, t + \tau)$ is periodic with a period $2T_s$. Hence, GMSK exhibits conjugate cyclostationarity with cycle frequencies $a_k = k/(2T_s) = kf_s/2$ for

integer k. Then we obtain the conjugate cyclic autocorrelation function (CAF) as

$$
R_{ss(*)}(\alpha, \tau) = \begin{cases} \frac{z_{-\infty}^2}{T_s} \int_{-\infty}^{\infty} C_0(\theta) C_0(\frac{k}{2T_s} - \theta) e^{-j2\pi\epsilon\frac{k}{2T_s}} e^{j2\pi\tau(\frac{k}{2T_s} - \theta)} d\theta, & \alpha = kf_s/2, k \text{ } odd, \\ 0, & otherwise \end{cases}
$$

(2.15)

where $C_0(\theta)$ is the Fourier transform of $c_0(t)$. Similar deduction can be applied to nonconjugate CAF functions with a basic cycle frequency $\alpha_f = 1/T_s = f_s$. Then we have [67]

$$
R(\frac{k}{T_s}, \tau) = \frac{1}{T_s} \int_{-\infty}^{\infty} e^{-j2\pi(\theta - \frac{k}{T_s})\tau} e^{-j2\pi\epsilon\frac{k}{T_s}} C_o(\theta) C_0^*(\theta - \frac{k}{T_s}) d\theta
$$

(2.16)

where $k = 0, \pm 1, \pm 2, \ldots$

Since the function $C_0(\theta)$ of GMSK has narrow spectrum in the GSM system, the nonconjugate CAF functions are totally suppressed for all cycle frequencies. On the other hand, conjugate CAF function with cycle frequencies $\pm\frac{1}{2Ts}$ is not suppressed, which can be used for identification of GMSK signals.

2.3   Introduction to Statistical Hypothesis Testing

In this section, we briefly review binary hypothesis tests under the Neyman-Pearson criterion [54]. The goal of detection is to identify a PU signal $s(t)$ embedded in white Gaussian noise $n(t)$. For simplicity, we assume $s(t) = 0$ or 1 to represent absence or presence of PU signals. Assume $n(t) \sim \mathcal{N}(0, \sigma^2)$ and let $x(t)$ denotes the received signal. For analytical simplicity, the detection is based on only one sample of $x(t)$, represented as $x[0]$. Then we have to decide whether $s(t)$ is present with noise $n(t)$ or only $n(t)$ is present, which can be formulated as

$$
\begin{aligned}
H_0 : \quad & x[0] = n[0], \\
H_1 : \quad & x[0] = s[0] + n[0]
\end{aligned}
$$

(2.17)

where H_0 represents the null hypothesis, H_1 is the alternative hypothesis, $s[0] = 1$ and $n[0] \sim N(0, \sigma^2)$. Then, the distribution of received signal sample $x[0]$ would be

$$
\begin{aligned}
p(x|H_0) &= \frac{1}{\sqrt{2\pi\sigma^2}} exp(-\frac{1}{2\sigma^2} x[0]^2), \\
p(x|H_1) &= \frac{1}{\sqrt{2\pi\sigma^2}} exp(-\frac{1}{2\sigma^2} (x[0] - 1)^2).
\end{aligned}
\tag{2.18}
$$

Based on Neyman-Pearson (NP) detection rule, to maximize detection probability for a given false alarm probability α, we design the NP test to decide H_1 if

$$
\begin{aligned}
L(x) &= \frac{p(x|H_1)}{p(x|H_0)} \\
&= \frac{\frac{1}{\sqrt{2\pi\sigma^2}} exp(-\frac{1}{2\sigma^2}(x[0]-1)^2)}{\frac{1}{\sqrt{2\pi\sigma^2}} exp(-\frac{1}{2\sigma^2} x[0]^2)} > \eta
\end{aligned}
\tag{2.19}
$$

where the test threshold η is given by

$$
P_{fa} = \int_{x:L(x)>\eta} p(x|H_0)dx = \alpha
\tag{2.20}
$$

and $L(x)$ is termed as the likelihood ratio function. As a result, the detection probability of NP test is defined as

$$
P_d = \int_{x:L(x)>\eta} p(x|H_1)dx.
\tag{2.21}
$$

2.4 Existing Cyclostationarity-based Spectrum Sensing Algorithms

Since white Gaussian noise is wide-sense stationary (without cyclostationarity), the primary signal with cyclostationarity can be detected based on its nontrivial CAFs at some cycle frequencies and time lag. In the following subsections, existing cyclostationarity based spectrum sensing algorithms are reviewed.

Dandawate-Giannakis test [59, 67, 64]

First we introduce the test in [59]. Define

$$\hat{\mathbf{c}} := \begin{bmatrix} \operatorname{Re}\hat{R}_{11,x}(\alpha;\tau) \\ \operatorname{Im}\hat{R}_{11,x}(\alpha;\tau) \end{bmatrix}, \quad F(2\pi f) := \sum_{t=1}^{M} x(t)x^*(t+\tau)e^{-j2\pi ft}, \tag{2.22}$$

$$\hat{S} := \frac{1}{ML_w} \sum_{s=-(L_w-1)/2}^{s=(L_w-1)/2} W(s)F(\alpha - \frac{s}{M})F(\alpha - \frac{s}{M}), \tag{2.23}$$

$$\hat{S}^* := \frac{1}{ML_w} \sum_{s=-(L_w-1)/2}^{s=(L_w-1)/2} W(s)F^*(\alpha - \frac{s}{M})F(\alpha + \frac{s}{M}), \tag{2.24}$$

$$\hat{\Gamma} := \begin{bmatrix} \operatorname{Re}\left\{\frac{\hat{S}+\hat{S}^*}{2}\right\} & \operatorname{Im}\left\{\frac{\hat{S}-\hat{S}^*}{2}\right\} \\ \operatorname{Im}\left\{\frac{\hat{S}+\hat{S}^*}{2}\right\} & \operatorname{Re}\left\{\frac{\hat{S}^*-\hat{S}}{2}\right\} \end{bmatrix} \tag{2.25}$$

where $W(s)$ is a spectral smoothing window of odd length L_w. The test of [59] is given by

$$\mathcal{T}_{2c} := M\hat{\mathbf{c}}^T\hat{\Gamma}^{-1}\hat{\mathbf{c}} \underset{\mathcal{H}_0}{\overset{\mathcal{H}_1}{\gtrless}} \gamma \quad \text{where} \quad \mathcal{T}_{2c} \overset{\mathcal{H}_0}{\sim} \chi_2^2. \tag{2.26}$$

A multi-antenna version of this test for conjugate CAFs may be found in [73]. A Kaiser window function has been used for $W(s)$ in [59, 67, 68, 64, 73]. It is given by

$$W(s) = \begin{cases} I_0\left(\beta\sqrt{1-(\frac{s}{L_w/2})^2}\right), & -\frac{L_w-1}{2} \le s \le \frac{L_w+1}{2} \\ 0, & \text{elsewhere} \end{cases}$$

where I_0 is zero-order modified Bessel function of the first kind and β and L_w are parameters to be selected.

It should be pointed out that the tests of [59, 67, 68, 64, 73] are not generalized likelihood ratio tests (GLRTs), contrary to the claims made therein. Consider [59] and let $\mathbf{c}$ denote the true value of $\hat{\mathbf{c}}$ under $\mathcal{H}_1$ (it is zero under $\mathcal{H}_0$) and let Γ denote the true value of $\hat{\Gamma}$. As

discussed in [64, Sec. II.B], the likelihood ratio (LR) for this problem ($\hat{\mathbf{c}}$ is the "observation" and $f(\cdot)$ denotes probability density function) is given by

$$\Lambda = \frac{f(\hat{\mathbf{c}} \mid \mathcal{H}_1)}{f(\hat{\mathbf{c}} \mid \mathcal{H}_0)} = \frac{\exp\left(-\frac{1}{2}M(\hat{\mathbf{c}} - \mathbf{c})^T\Gamma^{-1}(\hat{\mathbf{c}} - \mathbf{c})\right)}{\exp\left(-\frac{1}{2}M\hat{\mathbf{c}}^T\Gamma^{-1}\hat{\mathbf{c}}\right)}. \tag{2.27}$$

The unknown under $\mathcal{H}_0$ is Γ and the unknowns under $\mathcal{H}_1$ are $\mathbf{c}$ and Γ. In GLRT, one replaces the unknowns with their maximum likelihood (ML) estimates. Under $\mathcal{H}_1$ the ML estimate of $\mathbf{c}$ is given by $\hat{\mathbf{c}}$ [55, Sec. 3.2], making the numerator in (2.27) a constant (one). Under $\mathcal{H}_0$ a positive-definite estimate of Γ does not exist; by [55, Sec. 3.2] the ML estimate of Γ would have been $\hat{\mathbf{c}}\hat{\mathbf{c}}^T$ if we had rank($\hat{\mathbf{c}}\hat{\mathbf{c}}^T$)=2, but it is of rank one. In [64, Sec. II.B], $\hat{\Gamma}$ is used as the ML estimate of Γ which is not the case. It is more appropriate to view $\mathcal{T}_{2c}$ in (2.26) as an *ad hoc* test statistic resulting in a CFAR test; same remark applies to [67, 68, 64, 73] (all based on [59]).

Jallon Test [63]

This test applies to OFDM signals only. We will state the relevant results of [63] in the notation of our dissertation. Given an OFDM signal as discussed in Sec. 2.2.1, the test statistic of [63, Sec. 3] is given by

$$\hat{J}_x(N_b) := \frac{1}{2N_b + 1}\sum_{k=-N_b}^{k=N_b}\left|\hat{R}_{11,x}(k\alpha_0; N_c)\right|^2 \underset{\mathcal{H}_0}{\overset{\mathcal{H}_1}{\gtrless}} \eta_{J_1}, \quad \alpha_0 = \frac{1}{N_c + N_{cp}} = \frac{1}{N}, \tag{2.28}$$

with N_b picked to be the largest integer $< \frac{N_c}{N_{cp}}$. In [63] one is testing the estimated CAF at a single lag $\tau = N_c$ but at $2N_b + 1$ cycle frequencies in the set $\{\frac{k}{N}, \; k = -N_b, -N_b+1, \cdots, N_b\}$ $= \{\frac{k}{N}, \; k = N - N_b, N - N_b + 1, \cdots, N - 1, 0, 1, \cdots, N_b\}$. Under $\mathcal{H}_0$, [63, Cor. 1] states that asymptotically $\frac{M}{\sigma_1^4}(2N_b + 1)\hat{J}_x(N_b) \sim \chi^2(2(2N_b + 1))$ where $\sigma_1^2 = E\{|x_1(t)|^2 \mid \mathcal{H}_0\}$. This is incorrect in that a factor of two is missing; correct asymptotic distribution under $\mathcal{H}_0$ is given by $\frac{2M}{\sigma_1^4}(2N_b + 1)\hat{J}_x(N_b) \sim \chi^2(2(2N_b + 1))$, the reason being that a complex zero-mean Gaussian random variable Y with variance σ^2 consists of independent real and imaginary

21

parts, each with zero-mean and variance $\sigma^2/2$ whereas [63] seems to use variance σ^2 for real and imaginary parts of Y. Notice that in order to calculate the test threshold in (2.28), one needs the knowledge of the noise variance σ_1^2. Lack of this knowledge is not addressed in [63], but is discussed in [62, Sec. 3] (in the context of spread signals) where one estimates σ_1^2 and use it to normalize the test statistic as

$$\hat{J}_{2x}(N_b) := \frac{2M}{\hat{R}_{11,x}^2(0)}(2N_b+1)\hat{J}_x(N_b) \underset{\mathcal{H}_0}{\overset{\mathcal{H}_1}{\gtrless}} \eta_{J_2}, \quad \text{where} \quad \hat{J}_{2x}(N_b) \overset{\mathcal{H}_0}{\sim} \chi^2(2(2N_b+1)). \quad (2.29)$$

Note that the factor of two error in [63] regarding the test statistic distribution under $\mathcal{H}_0$ is also present in [62]. If one considers only a single cycle frequency at α_0 in (2.29) (and set $N_b = 0$), then (2.29) reduces to our proposed detector in Chapter. 3.

Tani-Fantacci Test [71]

This test applies to OFDM signals only. We will state the relevant results of [71] in the notation of our dissertation. Given an OFDM signal as discussed in Sec. 2.2.1, the test statistic of [71, Sec. IV.A] is given by

$$T_\alpha := \left| \frac{\hat{R}_{11}^\alpha(N_c)}{\hat{R}_{11}^{\alpha+S}(N_c)} \right| \underset{\mathcal{H}_0}{\overset{\mathcal{H}_1}{\gtrless}} \eta_T, \quad \alpha = \frac{1}{N_c + N_{cp}} = \frac{1}{N}, \quad (2.30)$$

where

$$\hat{R}_{11}^\alpha(\tau) := \frac{1}{M}\sum_{n=1}^{M}\left(\frac{1}{L}\sum_{k=n}^{n+L-1}x(k)x^*(k+\tau)\right)e^{-j2\pi\alpha n} \quad (2.31)$$

and L is picked to be shorter than the OFDM symbol duration. One picks the (fundamental) cycle frequency $\alpha = \alpha_0 = \frac{1}{N}$ (for sampled OFDM signal) and S is an arbitrary integer value that does not belong to the set of cycle frequencies $\{\frac{k}{T_s}, \ k = 1, 2, \cdots\}$ for continuous-time OFDM signal. It is established in [71] that under $\mathcal{H}_0$, asymptotically T_α follows a Cauchy distribution.

2.5 Conclusions

In this chapter, the background of cyclostationarity and corresponding spectrum sensing schemes based on it are introduced. We also briefly introduce the concept of binary hypothesis test. In following Chapter 3, the details of our proposed low complexity cyclostationarity-based spectrum sensing with both single and multiple receiving antennas are presented. Those existing cyclostationary spectrum sensing cited in this chapter are treated as counterparts of our proposed algorithm in the simulation chapter under different scenarios.

Chapter 3

On Cyclic Autocorrelation Based Spectrum Sensing for Cognitive Radio Systems in
Gaussian Noise

Detection of cyclostationary primary user (PU) signals in white Gaussian noise for cognitive radio systems is considered based on looking for a cycle frequency at a particular time lag in the cyclic autocorrelation function (CAF) of the noisy PU signal. We explicitly exploit the knowledge that under the null hypothesis of PU signal absent, the measurements originate from white Gaussian noise with possibly unknown variance. Our formulation allows us to computationally simplify the spectrum sensing detector, obviating the need for estimating an unwieldy covariance matrix needed in prior works. We consider both single and multiple antenna receivers. A performance analysis of the proposed detector is carried out. Supporting simulation examples are provided using both OFDM and GMSK PU signals and they verify our performance analysis and also show that our approaches either outperform or are at least as good as existing approaches while being computationally much cheaper.

3.1 Introduction

Cognitive radio allows for usage of licensed frequency bands (rights held by primary users (PUs)) by unlicensed users (secondary or cognitive users) when the licensed spectrum bands are unoccupied (a function of time and location). Therefore, one of the first steps to be accomplished by a cognitive user is *spectrum sensing*: analysis of the received electromagnetic transmissions to search for unoccupied spectrum bands (*spectrum holes*). One of the ways to accomplish this is energy detection/spectral analysis and consequent (statistical) hypothesis testing [56, 57, 60, 65]. Based on the received signal $x(t)$, the cognitive user has to decide if the primary user (PU) is present or not. This may be formulated as a binary hypothesis

testing problem

$$x(t) = \begin{cases} n(t) & : \mathcal{H}_0 \\ s(t) + n(t) & : \mathcal{H}_1 \end{cases} \tag{3.1}$$

where $\mathcal{H}_0$ is the null hypothesis that cognitive user is receiving just noise $n(t)$, and $\mathcal{H}_1$ is the alternative that PU signal $s(t)$ is also present. A popular approach is that of energy detection; see [56, 57, 60, 65] and references therein. One designs a CFAR (constant false alarm rate) test requiring prior knowledge of some of the signal statistics under $\mathcal{H}_0$. For instance, $n(t)$ is taken to be thermal noise with known variance.

Energy detection based approaches can not distinguish among different types of primary user or secondary user signals. Cyclostationarity detection allows classifying signals exhibiting cyclostationarity at different cycle frequencies [64] and/or different time lags. As noted in [67], one can use cyclostationarity detection for recognizing the individual air interfaces, a task at which energy detector would fail. Existing cyclostationarity detectors for cognitive radio systems reported in [67, 64, 73] are all based on [59] where one looks for a cycle frequency at a particular time lag in the cyclic autocorrelation function (CAF) of the (noisy) PU signal; extensions to multiple cycle frequencies and/or multiple lags may also be found in some of these papers. Under the alternative hypothesis, CAF is nonzero whereas under the null hypothesis it is zero. Signal characteristics under the null hypothesis are not exploited except for noting that its CAF would be zero. Implementation of the approaches of [59, 67, 64, 73] requires computation of the covariance matrix of estimated CAF's real and imaginary parts. [In general, this covariance matrix does not have an analytical expression even when the PU signal is precisely known.] In practice, it is estimated from the data, is computationally expensive and it needs a frequency smoothing window [59] to smooth certain cyclic periodograms in the frequency domain. In this chapter we explicitly exploit the knowledge that under the null hypothesis of PU signal absent, the measurements originate from white Gaussian noise with possibly unknown variance. Such a framework is explicitly

stated in [73, Eqns. (1),(2)], and although not explicitly stated in [67, 64], is extensively employed in simulation examples presented therein.

Other existing approaches based on single antenna receivers include [62], [63], [66] and [71]. In [62] detection of spread signals using the signal nonconjugate CAF at multiple lags and multiple cycle frequencies is considered under white Gaussian noise with possibly unknown variance. In [63] detection of orthogonal frequency division multiplex (OFDM) signals using the signal nonconjugate CAF at a single time lag and multiple cycle frequencies is considered under white Gaussian noise with known variance. In [66] several single antenna cyclostationarity detectors under white Gaussian noise have been considered including a peak detector [66, (12)] which utilizes the noisy signal CAF at multiple cycle frequencies and a single time-lag. This detector of [66, (12)] is the same as that of [63]; both assume known noise variance and both can be modified to handle unknown noise variance following [62]. (It should be noted that sensitivity of the detector in [66, (12)] to uncertainty in noise variance was recognized in [66] but was not fixed as in [62], rather a different detector was proposed.) Our proposed detector when specialized to single antenna is similar to that in [62], [63] and [66, (12)], except that we use a single time lag and a single cycle frequency. As noted in [64] (and others), cyclostationarity detection allows discrimination among signals exhibiting cyclostationarity at different cycle frequencies and/or time lags. Use of multiple cycle frequencies or time lags can reduce this discrimination capability where an interfering cyclostationary signal may be detected as a PU cyclostationary signal. In our simulation examples we will discuss such cases where the detector of [63] detects a certain interfering signal as a PU signal whereas our proposed detector does not. Further discussion of [63] is postponed to Sec. 2.4. In [71] a single cycle frequency and single time lag cyclostationarity detector has been presented for OFDM signals under noise variance uncertainty. It is different from that in [62], [63], [66] and from our proposed detector; further details regarding [71] are in Sec. 2.4.

The proposed detectors are useful in several practical scenarios such as detection of OFDM signals in digital video broadcasting (DVB) standard DVB-T (under IEEE 802.22 Working Group proposals), as discussed in [63]. As noted in [64] OFDM is employed by many of the current as well as future wireless communications systems including 3GPP Long Term Evolution (LTE), IEEE 802.11a/g WLANs, DVB standards DVB-T and DVB-H, as well as IEEE 802.16 and WiMax wireless metropolitan area networks. Finally, a GSM network as the primary system and coexisting with an OFDM based secondary WLAN system has been considered in [68]. Our conjugate CAF based detectors for detecting GMSK signals in the presence of interfering OFDM signals apply to the application considered in [68].

Our formulation allows us to simplify the spectrum sensing detector, both conceptually and computationally, and obviates the need for estimating the unwieldy covariance matrix needed in [59, 67, 64, 73]. We consider both single and multiple antenna receivers. Under single antenna receivers, our detector is similar to that in [62], [63] and [66, (12)], except that we use a single time lag and a single cycle frequency which allows discrimination among signals exhibiting cyclostationarity at different cycle frequencies and/or time lags, unlike receivers of [62], [63] and [66, (12)] that utilize multiple cycle frequencies and/or multiple time lags. Also unlike[62], [63], [66, (12)] and [71], we investigate multiple antenna receivers where we exploit cyclic cross-correlations among different antennas. Exploitation of cyclic cross-correlations among different antennas has also been considered in [73] for GMSK signals where [73] extends the single-antenna approach of [59] inheriting its computational complexity. A performance analysis of the proposed detectors is presented in Sec. V. Computational complexity issues are discussed in Sec. VI. Supporting simulation examples are provided using OFDM or GMSK PU signals are presented in Sec. VII where we compare our detectors with those of [59], [73], [63] and [71].

Notation: B_{ij} denotes the ijth element of the matrix $\mathbf{B}$, x_i denotes the ith element of vector $\mathbf{x}$, and $\mathbf{I}$ is the identity matrix. The superscripts $*$ and H denote the complex conjugate and the Hermitian (conjugate transpose) operations, respectively. $\delta_{i,j}$ denotes

the Kronecker delta: $= 1$ if $i = j$, 0 otherwise. Given a column vector $\mathbf{x}$, $\text{diag}\{\mathbf{x}\}$ denotes a square matrix with elements of $\mathbf{x}$ along its main diagonal and zeros everywhere else. We use $\text{cov}(\mathbf{x}, \mathbf{y}^*) := E\{\mathbf{x}\mathbf{y}^H\} - E\{\mathbf{x}\}E\{\mathbf{y}^H\}$ and let $\text{cum}_4(x_1, x_2, x_3, x_4)$ denote the joint 4th cumulant of random variables x_i ($i = 1, 2, 3, 4$). Note that $\text{cum}_4(x_1, x_2, x_3, x_4) = E\{x_1 x_2 x_3 x_4\} - E\{x_1 x_2\}E\{x_3 x_4\} - E\{x_1 x_3\}E\{x_2 x_4\} - E\{x_1 x_4\}E\{x_2 x_3\}$ when all x_i's are zero-mean.

3.2 Cyclostationarity Background

A discrete-time zero-mean complex-valued cyclostationary signal $x(t)$ is characterized by a time-varying autocorrelation function $R_{xx}(t, t + \tau) := E\{x(t)x^*(t + \tau)\}$ which has a Fourier series representation [59, 67]

$$R_{xx}(t, t + \tau) = \sum_{\alpha \in \mathcal{A}} R_{xx}(\alpha; \tau)e^{j2\pi\alpha t} \tag{3.2}$$

where given $\mathbf{x}(t)$ for $t = 0, 1, \cdots, M - 1$, the *cyclic autocorrelation function* (CAF) $R_{xx}(\alpha; \tau)$ at cycle frequency $\alpha \in \mathcal{A}$ is given by

$$R_{xx}(\alpha; \tau) = \lim_{M \to \infty} \frac{1}{M} \sum_{t=0}^{M-1} R_{xx}(t, t + \tau)e^{-j2\pi\alpha t} \tag{3.3}$$

and $\mathcal{A}$ is the set of cycle frequencies [59]

$$\mathcal{A} := \{\alpha \,|\, 0 \leq \alpha < 1, \ R_{xx}(\alpha; \tau) \not\equiv 0\}. \tag{3.4}$$

A conjugate CAF is defined as

$$R_{xx(*)}(\alpha; \tau) = \lim_{M \to \infty} \frac{1}{M} \sum_{t=0}^{M-1} R_{xx^*}(t, t + \tau)e^{-j2\pi\alpha t} \tag{3.5}$$

where $R_{xx^*}(t, t+\tau) := E\{x(t)x(t+\tau)\}$. Ref. [59] considers conjugate CAFs whereas [67, 64] consider both types of CAFs. For (wide-sense) stationary (WSS) signals, $R_{xx}(\alpha; \tau) = 0$ as well as $R_{xx(*)}(\alpha; \tau) = 0$ for any $\alpha \neq 0$.

3.2.1 Multivariate Processes

Later we will consider vector random processes arising due to a multiantenna receiver with $p \geq 1$ antennas. Therefore, we will consider a $p \times 1$ discrete-time zero-mean complex-valued cyclostationary signal $\mathbf{x}(t)$ with time-varying autocorrelation function $\mathbf{R}_{xx}(t, t+\tau) := E\{\mathbf{x}(t)\mathbf{x}^H(t+\tau)\}$ which has a Fourier series representation [59, 67]

$$\mathbf{R}_{xx}(t, t+\tau) = \sum_{\alpha \in \mathcal{A}} \mathbf{R}_{xx}(\alpha; \tau)e^{j2\pi\alpha t} \tag{3.6}$$

where the nonconjugate *cyclic autocorrelation function* (CAF) $\mathbf{R}_{xx}(\alpha; \tau)$ at cycle frequency $\alpha \in \mathcal{A}$ is given by

$$\mathbf{R}_{xx}(\alpha; \tau) = \lim_{M \to \infty} \frac{1}{M} \sum_{t=1}^{M} \mathbf{R}_{xx}(t, t+\tau)e^{-j2\pi\alpha t}. \tag{3.7}$$

Similar comments apply to conjugate CAFs.

3.3 Large Sample Statistics of Sample CAF

Our focus will be on the binary hypothesis testing problem involving p-dimensional processes $(p \geq 1)$

$$\mathbf{x}(t) = \begin{cases} \mathbf{n}(t) & : \mathcal{H}_0 \\ \mathbf{s}(t) + \mathbf{n}(t) & : \mathcal{H}_1 \end{cases} \tag{3.8}$$

where $\mathbf{n}(t)$ is zero-mean white Gaussian (as in [73]) and $\mathbf{s}(t) = \sum_{l=0}^{L_c} \mathbf{h}(l)s_{pu}(t-l)$ where $s_{pu}(t)$ is a scalar cyclostationary signal (emitted by a primary user) with a known cycle frequency α and known lag τ such that $R_{s_{pu}s_{pu}}(\alpha; \tau) \neq 0$, and p-column $\mathbf{h}(l)$ is the complex channel impulse response. Our approach (similar to [59, 67, 64, 73]) is to test the estimated CAF of the observations at a pair (α, τ) to check whether it is nonzero. However, unlike [59,

67, 64, 73]), we explicitly exploit the known statistics of observations under $\mathcal{H}_0$ (namely, we have white Gaussian noise with possibly unknown variances). In this section we investigate large sample statistics of estimated CAF when we have Gaussian noise as observations. We are interested only in nonzero cycle frequencies.

3.3.1 Nonconjugate CAF

These results are appropriate for OFDM signals.

Spatially and Temporally White Gaussian Noise

Consider a $p \times 1$ WSS proper (circularly symmetric) complex-valued zero-mean white Gaussian sequence $\mathbf{x}(t) = \mathbf{n}(t)$ with covariance $\Sigma_n = E\{\mathbf{n}(t)\mathbf{n}^H(t)\} = \text{diag}\left\{\sigma_1^2,\ \sigma_2^2,\ \cdots,\sigma_p^2\right\}$. Since $\mathbf{x}(t)$ is WSS, $\mathbf{R}_{xx}(t, t+\tau) = \mathbf{R}_{xx}(\tau) = \Sigma_n\delta_{\tau,0}$. Also, since $\mathbf{x}(t)$ is proper, $E\{\mathbf{x}(t)\mathbf{x}^T(t+\tau)\} \equiv 0$. Given an observation length of M samples, we estimate the (nonconjugate) CAF $\mathbf{R}_{xx}(\alpha; \tau)$ as

$$\hat{\mathbf{R}}_{xx}(\alpha; \tau) = \frac{1}{M}\sum_{t=1}^{M}\mathbf{x}(t)\mathbf{x}^H(t+\tau)e^{-j2\pi\alpha t}. \tag{3.9}$$

It is easy to see that $\lim_{M\to\infty} E\{\hat{\mathbf{R}}_{xx}(\alpha; \tau)\} = \mathbf{R}_{xx}(\alpha; \tau)$. Let ($x_i$ is the i-th component of $\mathbf{x}$)

$$\hat{R}_{ik,x}(\alpha; \tau) := \frac{1}{M}\sum_{t=1}^{M}x_i(t)x_k^*(t+\tau)e^{-j2\pi\alpha t}. \tag{3.10}$$

Then

$$E\{\hat{R}_{ik,x}(\alpha; \tau)\} = R_{ik,x}(\tau)\left[\frac{1}{M}\sum_{t=1}^{M}e^{-j2\pi\alpha t}\right] \tag{3.11}$$

where $R_{ik,x}(\tau) := E\{x_i(t)x_k^*(t+\tau)\}$. We have

$$E\{x_i(t_1)x_j^*(t_1 + \tau_1)e^{-j2\pi\alpha t_1}x_k^*(t_2)x_l(t_2 + \tau_2)e^{j2\pi\beta t_2}\}$$

$$= \text{cum}_4\left(x_i(t_1), x_j^*(t_1 + \tau_1), x_k^*(t_2), x_l(t_2 + \tau_2)\right)e^{-j2\pi(\alpha t_1 - \beta t_2)}$$

30

$$+R_{ij,x}(\tau_1)R_{kl,x}^*(\tau_2)e^{-j2\pi(\alpha t_1-\beta t_2)} + R_{ik,x}(t_2-t_1)R_{lj,x}(t_1-t_2-\tau_2+\tau_1)e^{-j2\pi(\alpha t_1-\beta t_2)}.$$

$$(3.12)$$

For Gaussian sequences, the 4th cumulants are identically zero. Hence,

$$\text{cov}\left(\hat{R}_{ij,x}(\alpha;\tau_1),\hat{R}_{kl,x}^*(\beta;\tau_2)\right) = E\left\{\hat{R}_{ij,x}(\alpha;\tau_1)\hat{R}_{kl,x}^*(\beta;\tau_2)\right\} - E\left\{\hat{R}_{ij,x}(\alpha;\tau_1)\right\}E\{\hat{R}_{kl,x}^*(\beta;\tau_2)\}$$

$$= \frac{1}{M^2}\sum_{t_1=1}^{M}\sum_{t_2=1}^{M}\left[R_{ik,x}(t_2-t_1)R_{lj,x}(t_1-t_2-\tau_2+\tau_1)e^{-j2\pi(\alpha t_1-\beta t_2)}\right] =: A. \qquad (3.13)$$

Using the fact that $\mathbf{x}(t)$ is white Gaussian, it follows that

$$A = \frac{1}{M^2}\sum_{t=1}^{M}R_{ik,x}(0)R_{lj,x}(\tau_1-\tau_2)e^{-j2\pi(\alpha-\beta)t} = \frac{1}{M^2}R_{ik,x}(0)R_{lj}(\tau_1-\tau_2)\left[\sum_{t=1}^{M}e^{-j2\pi(\alpha-\beta)t}\right].$$

$$(3.14)$$

We have

$$\frac{1}{M}\sum_{t=1}^{M}e^{-j2\pi(\alpha-\beta)t} = \begin{cases} 1 & \text{for } \alpha = \beta \in \mathcal{A} \\ \frac{e^{-j\pi(\alpha-\beta)(M+1)}}{M}\frac{\sin(\pi(\alpha-\beta)M)}{\sin(\pi(\alpha-\beta))} & \text{for } \alpha \neq \beta, \quad \alpha,\beta \in \mathcal{A}. \end{cases} \qquad (3.15)$$

It then follows that

$$\lim_{M\to\infty} MA = R_{ik,x}(0)R_{lj,x}(\tau_1-\tau_2)\delta_{\alpha,\beta}. \qquad (3.16)$$

But under $\mathcal{H}_0$, $\mathbf{x}(t)$ is spatially and temporally white, leading to

$$\lim_{M\to\infty} M\text{cov}\left(\hat{R}_{ij,x}(\alpha;\tau_1),\hat{R}_{kl,x}^*(\beta;\tau_2)\right) = R_{ii,n}(0)R_{jj,n}(0)\delta_{i,k}\delta_{j,l}\delta_{\tau_1,\tau_2}\delta_{\alpha,\beta} \qquad (3.17)$$

where $R_{ii,n}(0) = \sigma_i^2$, $i = 1,2,\cdots,p$.

Using (3.10) it follows that

$$\hat{R}_{ik,x}^*(\alpha;\tau) = \hat{R}_{ki,x}(-\alpha;-\tau) = \hat{R}_{ki,x}(1-\alpha;-\tau). \qquad (3.18)$$

Therefore, from (3.17) and (3.18), we have

$$\lim_{M \to \infty} M\text{cov}\left(\hat{R}_{ij,x}(\alpha;\tau_1), \hat{R}_{kl,x}(\beta;\tau_2)\right) = \lim_{M \to \infty} M\text{cov}\left(\hat{R}_{ij,x}(\alpha;\tau_1), \hat{R}_{lk,x}^*(-\beta;-\tau_2)\right)$$

$$= R_{ii,n}(0)R_{jj,n}(0)\delta_{i,l}\delta_{j,k}\delta_{\tau_1,-\tau_2}\delta_{\alpha,-\beta}. \tag{3.19}$$

Also, by [59, 67, 64], asymptotically (as $M \to \infty$), $\hat{R}_{ik,x}(\alpha;\tau)$ is a Gaussian random variable (complex-valued but not necessarily circularly symmetric) and "vectorized" matrix $\hat{\mathbf{R}}_{xx}(\alpha;\tau)$ is a Gaussian random vector for any α and τ.

White Gaussian Noise– Single Cycle Frequency and Single Lag

We will test the observations for the presence of cyclostationarity at a single cyclic frequency α and a single lag τ; extensions to multi-cycles and multi-lags are straightforward but tedious, hence are not considered in this chapter. Note that for white Gaussian noise, $\mathbf{R}_{xx}(\alpha;\tau) = 0$ for any $\alpha \neq 0$ and any τ. Setting $\beta = \alpha \neq 0$ and $\tau_1 = \tau_2 = \tau \geq 0$ in (3.17) and (3.19), we have

$$\lim_{M \to \infty} M\text{cov}\left(\hat{R}_{ij,x}(\alpha;\tau), \hat{R}_{kl,x}^*(\alpha;\tau)\right) = R_{ii,n}(0)R_{jj,n}(0)\delta_{i,k}\delta_{j,l}, \tag{3.20}$$

$$\lim_{M \to \infty} M\text{cov}\left(\hat{R}_{ij,x}(\alpha;\tau), \hat{R}_{kl,x}(\alpha;\tau)\right) = 0. \tag{3.21}$$

Invoking asymptotic Gaussianity, it then follows that

$$\lim_{M \to \infty} \sqrt{M}\hat{R}_{ij,x}(\alpha;\tau) \sim \mathcal{N}_c\left(0, R_{ii,n}(0)R_{jj,n}(0)\right) \quad \forall i,j \tag{3.22}$$

where $\mathcal{N}_c(\mathbf{m}, \Sigma)$ denotes a circularly symmetric (proper) complex Gaussian (vector) distribution with mean $\mathbf{m}$ and covariance matrix Σ. Furthermore, $\hat{R}_{ij,x}(\alpha;\tau)$ is asymptotically independent of $\hat{R}_{kl,x}(\alpha;\tau)$ if $i \neq k$ or $j \neq l$.

3.3.2 Conjugate CAF

These results are appropriate for GMSK signals. Given an observation length of M samples, we estimate the conjugate CAF $\mathbf{R}_{xx(*)}(\alpha;\tau) := \lim_{M\to\infty} \frac{1}{M} \sum_{t=1}^{M} E\{\mathbf{x}(t)\mathbf{x}^T(t+\tau)\}e^{-j2\pi\alpha t}$ as

$$\hat{\mathbf{R}}_{xx(*)}(\alpha;\tau) = \frac{1}{M} \sum_{t=1}^{M} \mathbf{x}(t)\mathbf{x}^T(t+\tau)e^{-j2\pi\alpha t}. \tag{3.23}$$

Spatially and Temporally White Gaussian Noise– Single Cycle Frequency, Single Lag

When $\mathbf{n}(t)$ is proper and $\mathbf{x}(t) = \mathbf{n}(t)$, it follows easily that $E\{\hat{\mathbf{R}}_{xx(*)}(\alpha;\tau)\} = 0$ and

$$\mathrm{cov}\left(\hat{R}_{(*)ij,x}(\alpha;\tau), \hat{R}_{(*)kl,x}(\alpha;\tau)\right) = E\{\hat{R}_{(*)ij,x}(\alpha;\tau)\hat{R}_{(*)kl,x}(\alpha;\tau)\} = 0 \tag{3.24}$$

where $R_{(*)ik,x}(\tau) := E\{x_i(t)x_k(t+\tau)\}$. Mimicking Sec. 3.3.1 we have

$$\mathrm{cov}\left(\hat{R}_{(*)ij,x}(\alpha;\tau), \hat{R}^*_{(*)kl,x}(\alpha;\tau)\right) = E\{\hat{R}_{(*)ij,x}(\alpha;\tau)\hat{R}^*_{(*)kl,x}(\alpha;\tau)\}$$

$$= \frac{1}{M^2} \sum_{t_1=1}^{M} \sum_{t_2=1}^{M} \left[R_{ik,n}(t_2-t_1)R_{jl,n}(t_2-t_1) + R_{il,n}(t_2-t_1+\tau)R_{jk,n}(t_2-t_1-\tau)\right]e^{-j2\pi\alpha(t_1-t_2)}$$

$$= \frac{1}{M^2} \sum_{t=1}^{M} \left[R_{ik,n}(0)R_{jl,n}(0) + R_{il,n}(0)R_{jk,n}(0)\delta_{\tau,0}\right]. \tag{3.25}$$

Hence we have

$$\lim_{M\to\infty} M\mathrm{cov}\left(\hat{R}_{(*)ij,x}(\alpha;\tau), \hat{R}^*_{(*)kl,x}(\alpha;\tau)\right)$$

$$= \begin{cases} 2R_{ii,n}(0)R_{jj,n}(0) & \text{if } i=k=l=j \text{ and } \tau=0 \\ R_{ii,n}(0)R_{jj,n}(0) & \text{if } (i,j)=(k,l) \text{ but } i \neq j, \text{ or } (i,j)=(l,k) \text{ and } \tau=0 \\ 0 & \text{otherwise .} \end{cases}$$

$$\tag{3.26}$$

Invoking asymptotic Gaussianity, it then follows that under $\mathcal{H}_0$

$$\lim_{M\to\infty} \sqrt{M}\hat{R}_{(*)ij,x}(\alpha;\tau) \sim \mathcal{N}_c\left(0, (1+\delta_{\tau,0}\delta_{i,j})R_{ii,n}(0)R_{jj,n}(0)\right) \quad \forall i,j. \qquad (3.27)$$

Noting that since $\lim_{M\to\infty} \hat{R}_{(*)ij,x}(\alpha;\tau) = \lim_{M\to\infty} \hat{R}_{(*)ji,x}(\alpha;\tau)$ and $\hat{R}_{(*)ij,x}(\alpha;0) = \hat{R}_{(*)ji,x}(\alpha;0)$, unlike nonconjugate CAFs, in case of conjugate CAFs, $\hat{R}_{(*)ij,x}(\alpha;\tau)$ is asymptotically independent of $\hat{R}_{(*)kl,x}(\alpha;\tau)$ for $i \neq k$ or $j \neq l$ if $i \geq j$ and $k \geq l$ (or if $i \leq j$ and $k \leq l$).

3.4 Test Statistics

Based on the large sample statistics of CAFs of white Gaussian noise discussed in Sec. 3.3, we now propose *ad hoc* CFAR (constant false alarm rate) detectors for detection of nonzero nonconjugate as well as conjugate CAFs. They are *ad hoc* as they do not follow any optimality criterion.

3.4.1 Nonconjugate CAF: OFDM Signals

Consider the binary hypothesis testing problem (3.8). The PU channel impulse response and the noise variances are unknown. We do know that noise is zero-mean complex (proper) Gaussian, spatially uncorrelated and temporally white. Also, $s_{pu}(t)$ in (3.8) is a scalar cyclostationary signal (emitted by PUs) with a known cycle frequency α and known lag τ such that $R_{s_{pu}s_{pu}}(\alpha;\tau) \neq 0$. The binary hypothesis testing problem in this case can be formulated as

$$\begin{aligned} \mathcal{H}_0 &: \quad R_{ij,x}(\alpha;\tau) = 0 \ \ \forall i,j = 1,2,\cdots,p \\ \mathcal{H}_1 &: \quad R_{ij,x}(\alpha;\tau) \not\equiv 0 \ \text{ for some } i,j, \ \text{ where } i,j = 1,2,\cdots,p. \end{aligned} \qquad (3.28)$$

Under both hypotheses, we have $\lim_{M\to\infty} E\{\hat{\mathbf{R}}(\alpha;\tau)\} = \mathbf{R}(\alpha;\tau)$. Under $\mathcal{H}_0$, by the results of Sec. 3.3.1, $\hat{R}_{ij}(\alpha;\tau)$ has zero-mean $\forall i,j$, and under $\mathcal{H}_1$, it has non-zero mean for some i,j; therefore, $|R_{ij}(\alpha;\tau)| > 0$ for some i,j. Let $\tilde{\mathbf{r}}$ denote the $p^2 \times 1$ vector composed of elements

$\hat{R}_{ij,x}(\alpha;\tau)/\sqrt{R_{ii,n}(0)R_{jj,n}(0)}$ for all distinct (i,j). Then by (3.22), we have $\lim_{M\to\infty}\sqrt{M}\tilde{\mathbf{r}} \overset{\mathcal{H}_0}{\sim}$ $\mathcal{N}_c(0,\mathbf{I})$ leading to $2M\tilde{\mathbf{r}}^H\tilde{\mathbf{r}} \overset{\mathcal{H}_0}{\sim} \chi^2_{2p^2}$ where χ^2_n denotes the central chi-square distribution with n degrees of freedom (dof). Since $|R_{ij}(\alpha;\tau)| > 0$ for some i,j, we have $E\{\tilde{\mathbf{r}}^H\tilde{\mathbf{r}} \,|\, \mathcal{H}_1\} > E\{\tilde{\mathbf{r}}^H\tilde{\mathbf{r}} \,|\, \mathcal{H}_0\}$. Furthermore, since the true values $R_{ii,n}(0)$, $(i = 1, 2, \cdots, p)$, are not available, we replace them by $\hat{R}_{ii,x}(0)$ and consider the following *ad hoc* test motivated by $2M\tilde{\mathbf{r}}^H\tilde{\mathbf{r}}$ and $E\{\tilde{\mathbf{r}}^H\tilde{\mathbf{r}} \,|\, \mathcal{H}_1\} > E\{\tilde{\mathbf{r}}^H\tilde{\mathbf{r}} \,|\, \mathcal{H}_0\}$:

$$\mathcal{T} := 2M\sum_{i=1}^{p}\sum_{j=1}^{p} \frac{|\hat{R}_{ij,x}(\alpha;\tau)|^2}{\hat{R}_{ii,x}(0)\hat{R}_{jj,x}(0)} \overset{\mathcal{H}_1}{\underset{\mathcal{H}_0}{\gtrless}} \eta \tag{3.29}$$

where

$$\hat{R}_{ii,x}(0) := \frac{1}{M}\sum_{t=1}^{M} |x_i(t)|^2 \tag{3.30}$$

and the threshold η is picked to achieve a pre-specified probability of false alarm $P_{fa} = P\{\mathcal{T} \geq \eta \,|\, \mathcal{H}_0\}$. By the results of Sec. 3.3.1, we can find (shown next) asymptotic distribution of $\mathcal{T}$ under $\mathcal{H}_0$ and design a CFAR test. Such CFAR tests are not optimal in any sense but do yield a constant false-alarm rate, a desirable property, under model parameter uncertainties. CFAR tests have been used in radar and other problems under parameter uncertainty [61, Sec. 8.1].

We now turn to calculation of η. It follows from (3.22) that asymptotically (as $M \to \infty$),

$$2M\frac{|\hat{R}_{ij,x}(\alpha;\tau)|^2}{R_{ii,x}(0)R_{jj,x}(0)} \overset{\mathcal{H}_0}{\sim} \chi^2_2. \tag{3.31}$$

Eqn. (3.20) applied to white Gaussian noise also implies that as $M \to \infty$, $\hat{R}_{ii,x}(0)$ converges in the mean-square sense, hence in probability (i.p.), to $R_{ii}(0)$ [70, Appendix B]. Together with (3.31) this results implies that asymptotically [70, Lemma B.4]

$$2M\frac{|\hat{R}_{ij,x}(\alpha;\tau)|^2}{\hat{R}_{ii,x}(0)\hat{R}_{jj,x}(0)} \overset{\mathcal{H}_0}{\sim} \chi^2_2. \tag{3.32}$$

As noted in Sec. 3.3.1, any element of $\hat{\mathbf{R}}_{xx}(\alpha; \tau)$ is asymptotically independent of all other elements, therefore, in (3.29) we have mutually independent random variables for distinct ij pairs. Since there are p^2 such terms in $\mathcal{T}$, asymptotically

$$\mathcal{T} \stackrel{\mathcal{H}_0}{\sim} \chi^2_{2p^2}. \tag{3.33}$$

3.4.2   Conjugate CAF: GMSK Signals

We will take $\tau = 0$ since that is where the GMSK CAF is the strongest [68]. Following Secs. 3.3.2 and 3.4.1, we propose the test statistic

$$\mathcal{T}_{conj} := 2M \sum_{i=1}^{p} \sum_{j=i}^{p} \frac{|\hat{R}_{(*)ij,x}(\alpha; 0)|^2}{(1 + \delta_{i,j})\hat{R}_{ii,x}(0)\hat{R}_{jj,x}(0)} \underset{\mathcal{H}_0}{\overset{\mathcal{H}_1}{\gtrless}} \eta_{conj}. \tag{3.34}$$

Using the results of Sec. 3.3.2 and noting that there are $(p^2 + p)/2$ terms in the double summation in (3.34), it follows that

$$\mathcal{T}_{conj} \stackrel{\mathcal{H}_0}{\sim} \chi^2_{p^2+p} \tag{3.35}$$

which allows us to calculate the test threshold η_{conj} corresponding to a specified P_{fa}.

3.4.3   Single Antenna Case: Nonconjugate CAF

Proposed Test

For $p = 1$ (single antenna), the proposed nonconjugate CAF test reduces to

$$2M \frac{|\hat{R}_{11,x}(\alpha; \tau)|^2}{\hat{R}^2_{11,x}(0)} \underset{\mathcal{H}_0}{\overset{\mathcal{H}_1}{\gtrless}} \eta. \tag{3.36}$$

3.5 Detection Probability

In this section we derive the asymptotic distribution of the proposed test statistics of Sec. 3.4 under $\mathcal{H}_1$ for a specified PU signal. We will assume a non-random channel; for random channels, our results offer conditional detection probability conditioned on the channel.

3.5.1 Nonconjugate CAF

Under $\mathcal{H}_1$, we have $R_{ij,x}(\alpha; \tau) \neq 0$ for at least one pair (i, j). Let $\hat{\mathbf{r}}$ denote the $p^2 \times 1$ vector composed of elements $\tilde{R}_{ij,x}(\alpha; \tau) := \hat{R}_{ij,x}(\alpha; \tau)/\sqrt{\hat{R}_{ii,x}(0)\hat{R}_{jj,x}(0)}$ for all distinct (i, j), with $\mathbf{m}_1 := E\{\hat{\mathbf{r}}\}$ composed of elements $R_{ij,x}(\alpha; \tau)/\sqrt{R_{ii,x}^{(1)}(0)R_{jj,x}^{(1)}(0)}$ (for large M) where $R_{ii,x}^{(1)}(0) := E\{x_i(t)\, x_i^*(t)\,|\,\mathcal{H}_1\}$. Let $\Sigma_1 := \lim_{M\to\infty}(1/M)\mathrm{cov}(\hat{\mathbf{r}}, \hat{\mathbf{r}}^*)$. Then invoking the asymptotic Gaussianity [59, 67, 64], under $\mathcal{H}_1$ and for low SNRs,

$$\lim_{M\to\infty} \sqrt{M}\,(\hat{\mathbf{r}} - \mathbf{m}_1) \sim \mathcal{N}_c\left(0, \Sigma_1\right). \tag{3.37}$$

[Note that $\lim_{M\to\infty} M\mathrm{cov}\left(\hat{R}_{ij,x}(\alpha; \tau), \hat{R}_{ij,x}(\alpha; \tau)\right) \neq 0$ when the PU signal is present, hence $\hat{R}_{ij,x}(\alpha; \tau)$ is not proper, but is approximately proper for "low" SNRs.] Then for large M,

$$2M\hat{\mathbf{r}}^H\Sigma_1^{-1}\hat{\mathbf{r}} \overset{\mathcal{H}_1}{\sim} \chi_{2p^2}^2(\lambda_1), \tag{3.38}$$

where $\chi_n^2(\lambda_1)$ denotes noncentral chi-square distribution with n degrees of freedom and noncentrality parameter λ_1, and $\lambda_1 = 2M\mathbf{m}_1^H\Sigma_1^{-1}\mathbf{m}_1$. Under **low SNR**, $\Sigma_1 \approx \mathbf{I} \Rightarrow 2M\hat{\mathbf{r}}^H\Sigma_1^{-1}\hat{\mathbf{r}} \approx \mathcal{T}$ and $\lambda_1 \approx 2M\mathbf{m}_1^H\mathbf{m}_1$. Thus,

$$\mathcal{T} \overset{\mathcal{H}_1}{\sim} \chi_{2p^2}^2(\lambda_1) \tag{3.39}$$

where (assuming $\mathbf{s}(t) = \sum_{l=0}^{L_c}\mathbf{h}(l)s_{pu}(t-l)$)

$$\lambda_1 = 2M\sum_{i=1}^{p}\sum_{j=1}^{p}\frac{|R_{ij,x}(\alpha; \tau)|^2}{R_{ii,x}^{(1)}(0)R_{jj,x}^{(1)}(0)}, \quad R_{ii,x}^{(1)}(0) = \sigma_i^2 + E\{|s_i(t)|^2\,|\,h_i(l),\ 0 \leq l \leq L_c\}. \tag{3.40}$$

Therefore, given a specified false alarm probability P_{fa}, the threshold η satisfies $P_{fa} = \int_\eta^\infty f_{\mathcal{T}}(x)\, dx$ where $\mathcal{T} \sim \chi^2_{2p^2}$. The resultant probability of PU detection P_d is then $P_d = P\{\mathcal{T} \geq \eta \,|\, \mathcal{H}_1,\, \mathbf{h}(l),\, 0 \leq l \leq L_c\} = \int_\eta^\infty f_{\mathcal{T}}(y)\, dy$ where $\mathcal{T} \sim \chi^2_{2p^2}(\lambda_1)$.

3.5.2 Conjugate CAF

We will follow the same line of arguments as in Sec. 3.5.1. Under $\mathcal{H}_1$, we have $R_{(*)ij,x}(\alpha; 0) \neq 0$ for at least one pair (i, j). Let $\hat{\mathbf{r}}_{(*)}$ denote the $\frac{p^2+p}{2} \times 1$ vector composed of elements $\tilde{R}_{(*)ij,x}(\alpha; 0) := \hat{R}_{(*)ij,x}(\alpha; 0)/\sqrt{(1 + \delta_{i,j})\hat{R}_{ii,x}(0)\hat{R}_{jj,x}(0)}$ for $1 \leq i \leq j \leq p$, with $\mathbf{m}_2 := E\{\hat{\mathbf{r}}_{(*)}\}$ composed of elements $R_{(*)ij}(\alpha; 0)/\sqrt{(1 + \delta_{i,j})R_{ii}^{(1)}(0)R_{jj}^{(1)}(0)}$ (for large M). Let $\lim_{M \to \infty} (1/M)\mathrm{cov}(\hat{\mathbf{r}}_{(*)}, \hat{\mathbf{r}}^*_{(*)}) =: \Sigma_2$. Then invoking the asymptotic Gaussianity [59, 67, 64], under $\mathcal{H}_1$ and for low SNRs,

$$\lim_{M \to \infty} \sqrt{M}\left(\hat{\mathbf{r}}_{(*)} - \mathbf{m}_2\right) \sim \mathcal{N}_c\left(0, \Sigma_2\right). \tag{3.41}$$

[Note that, as in Sec. 3.5.1, $\lim_{M \to \infty} M\mathrm{cov}\left(\hat{R}_{(*)ij,x}(\alpha; 0), \hat{R}_{(*)ij,x}(\alpha; 0)\right) \neq 0$ when the PU signal is present, hence $\hat{R}_{(*)ij,x}(\alpha; 0)$ is not proper, but is approximately proper for "low" SNRs.] Then for large M,

$$2M\hat{\mathbf{r}}_{(*)}^H \Sigma_1^{-1} \hat{\mathbf{r}}_{(*)} \overset{\mathcal{H}_1}{\sim} \chi^2_{p^2+p}(\lambda_2), \tag{3.42}$$

where $\lambda_2 = 2M\mathbf{m}_2^H \Sigma_2^{-1} \mathbf{m}_2$. Under **low SNR**, $\Sigma_2 \approx \mathbf{I} \Rightarrow 2M\hat{\mathbf{r}}_{(*)}^H \Sigma_2^{-1} \hat{\mathbf{r}}_{(*)} \approx \mathcal{T}_{conj}$ and $\lambda_2 \approx 2M\mathbf{m}_2^H \mathbf{m}_2$. Thus,

$$\mathcal{T}_{conj} \overset{\mathcal{H}_1}{\sim} \chi^2_{p^2+p}(\lambda_2) \tag{3.43}$$

where

$$\lambda_2 = 2M \sum_{i=1}^p \sum_{j=i}^p \frac{\left|R_{(*)ij,x}(\alpha; 0)\right|^2}{(1 + \delta_{i,j})R_{ii,x}^{(1)}(0)R_{jj,x}^{(1)}(0)}. \tag{3.44}$$

3.6 Computational Complexity

Here we will compare computational complexity of our proposed tests with that of [59] (used in the single antenna case ($p = 1$) for testing a single cycle frequency at a single

lag in [67] and extended to multiple cycle frequencies in [64]), [73] (extension of [59] to the multiple antennas case $(p > 1)$), [63] and [71]. We will express computational complexity in terms of number of complex multiplications needed to implement the various approaches; the respective counts for various approaches are listed in Table 3.1. Given an observation sample size of M samples, for computing the CAF at given τ and α, we need $2M$ multiplications. To compute the (stationary) autocorrelation at zero lag we need M multiplications. This yields a count of $3M$ multiplications for the proposed test (3.36) for single antenna. For the proposed multi-antenna detectors (3.29) or (3.34) with p antennas, we have to calculate p^2 CAFs (cyclic auto- and cross-correlations) and p stationary autocorrelation functions, yielding a count of $Mp(1 + 2p)$ complex multiplications for (3.29) and a count of $Mp(p + 2)$ multiplications for (3.34). For the test of [59] described in Sec. 2.4, one needs $2M$ multiplications to calculate the CAF at given τ and α, $(M/2)\log_2(2M)$ multiplications for the FFT involved (to compute the cyclic periodogram), and $M + 4L_w$ multiplications for smoothing the two cyclic periodograms. This yields the number of complex multiplications needed as $3M + \frac{M}{2}\log_2 M + 4L_w$. The extension to $p > 1$ given in [73] requires $p^2\left(3M + \frac{M}{2}\log_2 M + 4L_w\right)$ complex multiplications for nonconjugate CAF-based test and $\frac{p^2 + p}{2}\left(3M + \frac{M}{2}\log_2 M + 4L_w\right)$ multiplications for conjugate CAF-based test. As seen by comparing (3.36) and (2.28), the test (2.28) of [63] requires $(2N_b + 1)2M + M$ multiplications for $p = 1$. Using the results of [71, Sec. IV-C], the test (2.30) requires $3M$ complex multiplications.

3.7 Simulation Examples

We now present some computer simulation examples using OFDM and GMSK signals to illustrate our detectors and to compare their performance and computational complexity with some existing detectors. In all presented examples noise variance is assumed to be unknown.

3.7.1 Example 1: Single Antenna Receiver

The primary signal is an OFDM signal with number of subcarriers $N_c = 32$ and cyclic prefix of length $N_{cp} = 8$. The number of OFDM symbols were taken to be $N_{ofdm} = 100$, 10 or 1, with the corresponding observation size of $M = N_{ofdm}(N_c + N_{cp}) = 4000$, 400 or 40, respectively. The subcarrier modulation was QPSK. The false alarm probability is 0.01 and all results are averaged over 2000 Monte Carlo runs. For PU signal detection we picked the (normalized) cycle frequency $\alpha = 1/(N_c + N_{cp}) = 1/N$ and time lag $\tau = N_c$. We used zero-mean circularly symmetric complex-Gaussian additive white noise. The OFDM signal was passed through either a constant channel with unit gain or a flat Rayleigh fading channel.

In Fig. 3.1 we compare the theoretical performance based on (3.33) and (3.39) with the simulations-based performance for the proposed detector when number of antennas $p = 1$ and the channel is unit gain. The theoretical CAF for the OFDM signal was obtained from [67] (for rectangular pulse shape) for use in computing the non-centrality parameter λ_1. It is seen that the agreement between theory and simulations is quite good for larger observation samples. In Fig. 3.2 we compare P_d performance (as a function of SNR for $P_{fa} = 0.01$) of our proposed approach with that of [59] (also used in [67, 64]) via simulations when number of antennas $p = 1$ and the channel is flat Rayleigh fading channel. For the approach of [59] we used Kaiser windows with parameters $(\beta, L_w) = (1,65)$, $(1,513)$ and $(1,513)$ for $M = 40$, 400 and 4000, respectively. It is seen that the proposed approach is superior to [59] for smaller observation sizes. On the other hand, using the results of Table 3.1, we find that the [59] needs 4.05, 4.15 and 3.17 times more complex multiplications than the proposed approach for $M = 40$, 400 and 4000, respectively. Notice that both the proposed test (3.36) and test (2.26) of [59] use the same CAF but normalize it differently. While (3.36) explicitly uses white Gaussian nature of noise to normalize using $\hat{R}_{11,x}^2(0)$, (2.26) uses a "generic" covariance estimator $\hat{\Gamma}$ which needs far more parameters (spectral smoothing window, FFT in (2.22), etc.) which likely makes the estimate $\hat{\Gamma}$ of higher variance than $\hat{R}_{11,x}^2(0)$. This fact (likely higher variance of $\hat{\Gamma}$ under both $\mathcal{H}_0$ and $\mathcal{H}_1$, as compared to the variance of $\hat{R}_{11,x}^2(0)$) would

seem to account for poorer performance of Dandawate-Giannakis test (2.26) as compared to the proposed test (3.36) for "smaller" observation samples M; for larger M the variances of normalization factors become small enough to have negligible difference in performance. However, the computational complexity advantage of test (3.36) over test (2.26) remains. In Fig. 3.3 for a constant-gain channel and OFDM PU signal in white Gaussian noise, we show the number of observation samples needed to achieve $P_d = 0.9$ versus SNR, with $P_{fa} = 0.01$. It is seen that the proposed test is superior to [59] for SNR$\geq$0 dB and has same performance for SNR$<$ 0dB, while being computationally cheaper (as discussed earlier). In Fig. 3.4 we compare P_d performance (as a function of SNR for $P_{fa} = 0.01$) of the proposed test (3.36) with the Tani-Fantacci test (2.30) [71] for an AWGN channel when $M = 2000$ (we took $L = 38 < N = 40$ in (2.31)). It is seen that the proposed test vastly outperforms the Tani-Fantacci test while by Table 3.1, the computational complexity of the two approaches is the same. Comparisons with the Jallon test (2.28) are deferred to Sec. 3.7.2.

3.7.2 Example 2: Cyclostationary Interference

First we consider a constant-gain channel and an OFDM PU signal ($p = 1$) as in Example 1 ($N_c = 32$, $N_{cp} = 8$) but under three different scenarios: (i) white noise alone, (ii) white noise and an OFDM interfering signal with $N_c = 64$, $N_{cp} = 16$, QPSK modulation (called "Type I" interference hereinafter), with interfering signal power equal to noise power (0dB SNR for interfering signal), and (iii) white noise and an OFDM interfering signal with $N_c = 32$, $N_{cp} = 16$, QPSK modulation (called "Type II" interference hereinafter), with interfering signal power 10dB below the noise power (-10dB SNR for interfering signal). Fig. 3.5 shows the performance (based on 2000 runs) of the nonconjugate CAF detector (3.36) and the test (2.28) of [63] under the three scenarios when $M = 2000$ and $P_{fa} = 0.01$. With fixed noise power and interference power fixed relative to noise power, we varied the PU signal power to achieve the desired PU SNR (it does not include interference signal power). For test (2.28) we consider two cases: $N_b = 0$ (smallest value) and $N_b = 3$ (largest

$N_b < \frac{N_c}{N_{cp}} = \frac{32}{8} = 4$ based on the PU signal parameters, the largest N_b recommended by [63]). Under white noise alone, [63] with $N_b = 3$ significantly outperforms the proposed test (about 3dB SNR advantage for achieving $P_d = 0.9$) since test (2.28) of [63] uses more PU cycle frequencies. This advantage is preserved under Type I interference. However, under Type II interference, test (2.28) of [63] fails in that it views interference as a PU signal (even at SNR=-20dB P_d is significantly higher than the design P_{fa} of 0.01, unlike scenarios (i) and (ii)): CAFs of both PU signal and Type II interference peak at $\tau = N_c = 32$. While the proposed test (3.36) tuned to $\alpha = 1/40$ and $\tau = 32$ is able to reject Type II interference (it only worsens the effective SNR), Jallon's test (2.28) tuned to $\tau = 32$ and cycle frequencies $k/40$, $k = -3, -2, \cdots, 3$ also responds to significant CAF of interference at $\tau = 32$ and zero cycle frequency. Note that we picked Type II interference SNR to be -10dB; for 0dB SNR P_d for test (2.28) is almost 1 even at low SNRs. As noted earlier, cyclostationarity detection allows discrimination among signals exhibiting cyclostationarity at different cycle frequencies and/or time lags. As in the case of Type II interference in this example, use of multiple cycle frequencies or time lags can reduce this discrimination capability where an interfering cyclostationary signal may be detected as a PU cyclostationary signal. Finally, using the results of Table 3.1 for $p = 1$, note that Jallon's detector needs $1 + (4/3)N_b$ times more complex multiplications than the proposed approach for any observation sample size. Thus [63] has five times higher computational complexity for $N_b = 3$ while it obtains a 3dB SNR advantage for achieving $P_d = 0.9$ over our proposed detector under white noise. When $N_b = 0$, Jallon's and the proposed detectors have same computational complexity, but the SNR advantage now is less than 0.3 dB.

Fig. 3.6 shows the performance of the nonconjugate CAF detector and the approach of [59] in the presence of an interfering signal in addition to noise, for a constant gain channel. The PU signal is an OFDM signal with N_c=64, $N_{cp} = 16$ and QPSK modulation, whereas the interfering signal is also OFDM but with N_c=32, $N_{cp} = 8$ and QPSK modulation. The nonconjugate detector looks for (normalized) $\alpha = 1/80$ at $\tau = 64$. The SNR for the

interfering signal was fixed at 0dB (i.e., noise power equals interfering signal power). With fixed noise power, we varied the PU signal power to achieve the desired PU SNR. Fig. 3.6 shows the P_d for $P_{fa} = 0.01$, $M = 2000$, $p = 1$ antenna, 2000 runs, and varying PU SNR. We also show the results when the interfering signal is absent. The nonconjugate CAF detector is able to distinguish between the PU signal and the interfering signal (which, as noted in [64] and others, an energy detector fails to do). There is about a 3dB loss in performance compared to the case when the interference is absent, for both the proposed approach and that of [59]; this is not surprising since interference plus noise power is 3dB higher than noise power. Furthermore, the proposed approach is superior to [59] (about 2dB SNR advantage for achieving $P_d = 0.9$).

3.7.3   Example 3: Multi-Antenna Receiver, OFDM PU signal

Now we consider $p = 4$ antennas and an OFDM signal as in Example 3.7.1. In Fig. 3.7 we compare P_d performance (as a function of SNR for $P_{fa} = 0.01$) of our proposed approach with that of [73] (modified to handle nonconjugate CAFs, an extension of [59] to multiple antenna receiver) via simulations when observation samples $M = 4000$ (100 OFDM symbols) and the channel is flat Rayleigh-fading vector channel with independent components (each Rayleigh fading), and spatially uncorrelated zero-mean circularly symmetric complex-Gaussian additive white noise. For the approach of [73], we used Kaiser window with parameters $(\beta, L_w) = (1,513)$. We tested for $\alpha = 1/40$ and $\tau = 32$. It is seen that the performance of the proposed approach is about the same as that of [73]. Using the results of Table 3.1 for nonconjugate CAFs, we find that the [73] needs 4.22 times more complex multiplications than the proposed approach for $M = 4000$; thus the proposed approach is to be preferred when both performance and computational complexity are considered. In Fig. 3.8 we compare the theoretical performance based on (3.33) and (3.39) with the simulations-based performance for the proposed detector when number of antennas $p = 4$, $M = 4000$, $P_{fa} = 0.01$ and the channel is non-random with unit gain. It is seen that the agreement

between theory and simulations is good. Note that the asymptotic distribution (3.39) under $\mathcal{H}_1$ is a low-SNR approximation which accounts for some difference in theory and simulations at SNRs around -10 to -9 dB ("higher" end).

3.7.4 Example 4: Multi-Antenna Receiver, GMSK PU signal

Now we consider a GMSK PU signal with N=16 samples per symbol. We seek to detect the PU signal using conjugate CAF at the normalized cycle frequency $\alpha = \frac{1}{32}$ and lag $\tau = 0$. The channel was either constant gain or flat Rayleigh fading, with circularly symmetric complex Gaussian additive noise. Figs. 3.9 and 3.10 show the P_d performance (as a function of SNR for $P_{fa} = 0.01$) of our proposed approach and that of [73] for constant-gain and Rayleigh fading channels, respectively, based on 10000 runs when number of antennas $p = 4$ and M=320. For the approach of [73], we used Kaiser window with parameters (β, L_w) = (1,65). In both figures there is little difference between the two approaches. Using the results of Table 3.1 for conjugate CAFs, we find that the [73] needs 3.32 times more complex multiplications than the proposed approach for M =320; thus the proposed approach is to be preferred when both performance and computational complexity are considered.

3.8 Conclusions

Detection of cyclostationary primary user (PU) signals in white Gaussian noise for cognitive radio systems was considered based on looking for a cycle frequency at a particular time lag in the cyclic autocorrelation function (CAF) of the noisy PU signal. We explicitly exploit the knowledge that under the null hypothesis of PU signal absent, the measurements originate from white Gaussian noise with possibly unknown variance. Our formulation allows us to simplify the spectrum sensing detector, and obviates the need for estimating an unwieldy covariance matrix needed in the Dandawate-Giannakis [59] and related approaches. We considered both single and multiple antenna receivers and both nonconjugate and conjugate CAFs. A performance analysis of the proposed detectors was carried out. Supporting

simulation examples were presented to compare our detectors with those of [59], [73], [63] and [71], and to demonstrate the capability to discriminate among signals exhibiting cyclostationarity at different cycle frequencies and/or time lags. Our proposed approaches are computationally cheaper than the Dandawate-Giannakis and related approaches [59], [73] while having quite similar detection performance. Our proposed approach significantly outperforms [71] while having same computational complexity. In white noise channels, the single-antenna detector of [63] has a 3dB SNR advantage for achieving a detection probability of 0.9 over our proposed detector but requires five times more complex multiplications. Also, Jallon's test [63] fails to reject a class of cyclostationary interfering signals whereas our proposed detector is successful.

Table 3.1: Number of complex multiplications for M observation samples with white Gaussian noise

	Proposed	[59, 73]	Jallon [63]	Tani-Fantacci [71]
$p=1$	$3M$	$3M + \frac{M}{2}\log_2 M + 4L_w$	$(2N_b + 1)2M + M$	$3M$
$p > 1$: nonconjugate CAF	$Mp(1 + 2p)$	$p^2\left(3M + \frac{M}{2}\log_2 M + 4L_w\right)$		
$p > 1$: conjugate CAF	$Mp(p + 2)$	$\frac{p^2+p}{2}\left(3M + \frac{M}{2}\log_2 M + 4L_w\right)$		
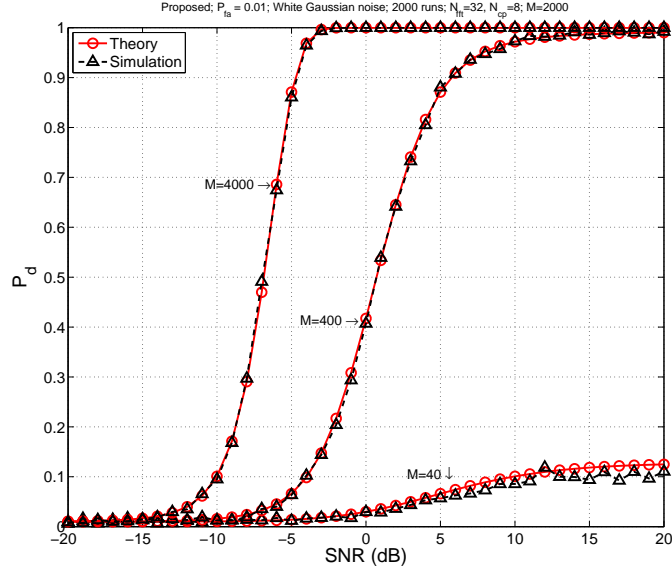
Figure 3.1: Example 1: Performance analysis: theoretical and simulation-based performance comparison of probability of detection P_d versus SNR for the proposed single-antenna spectrum sensing under different observation lengths: OFDM signal (number of subcarriers N_c=32, cyclic prefix length $N_{cp} = 8$), non-random channel with unit gain, $P_{fa} = 0.01$, $p = 1$, 2000 Monte Carlo runs.
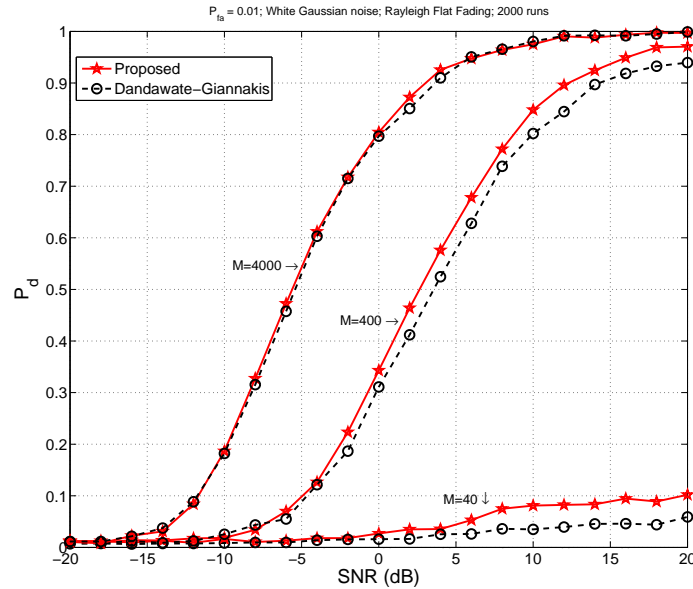
Figure 3.2: Example 1: Simulation-based comparison of P_d versus SNR with single antenna under Rayleigh flat-fading: $P_{fa} = 0.01$, $p = 1$, 2000 Monte Carlo runs, OFDM signal (number of subcarriers N_c=32, cyclic prefix length $N_{cp} = 8$). The approach labeled "Dandawate-Giannakis" is used in [59, 67, 64].
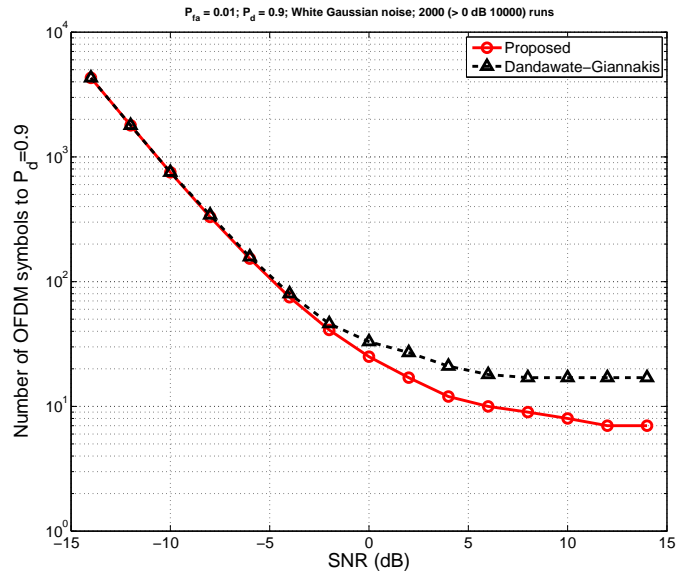
Figure 3.3: Example 1: Number of symbols needed to achieve $P_d = 0.9$ versus SNR with single antenna under non-random channel with constant gain: $p = 1$, $P_{fa} = 0.01$, 2000 runs for SNR≤0dB and 10000 runs for SNR>0dB, OFDM signal (number of subcarriers N_c=32, cyclic prefix length $N_{cp} = 8$). The approach labeled "Dandawate-Giannakis" is used in [59, 67, 64].
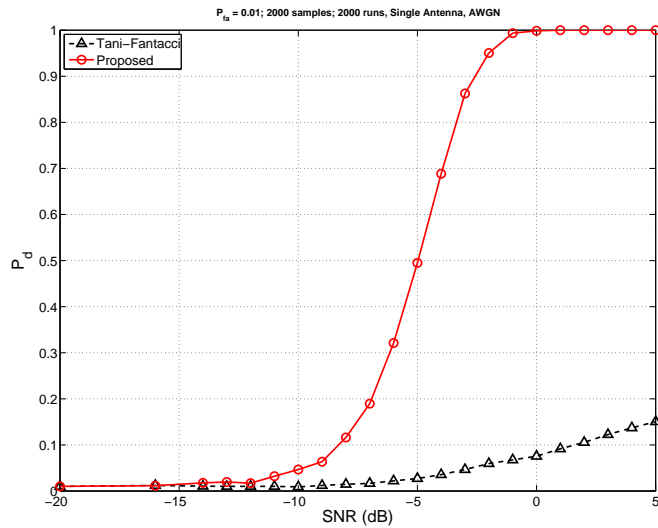
Figure 3.4: Example 1: Simulation-based comparison of P_d versus SNR with single antenna under non-random channel with constant gain: $P_{fa} = 0.01$, $p = 1$, $M = 2000$, 2000 Monte Carlo runs, OFDM signal (number of subcarriers N_c=32, cyclic prefix length $N_{cp} = 8$). The approach labeled "Tani-Fantacci" is that of [71].
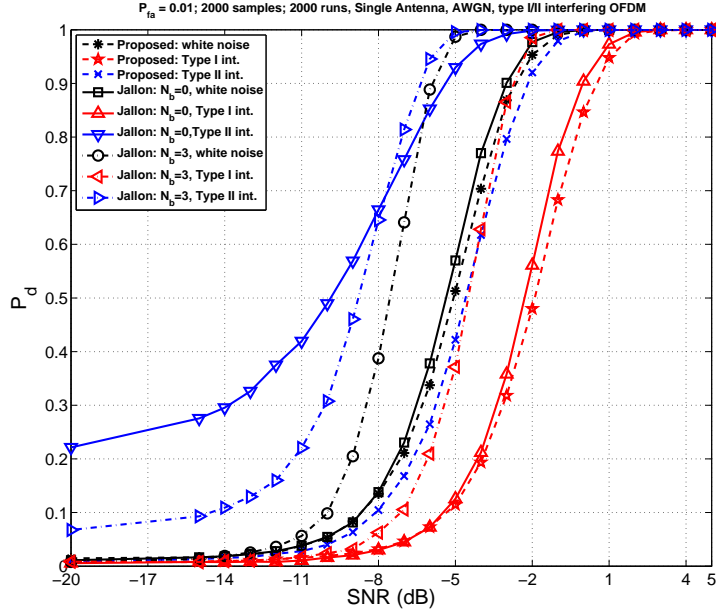
Figure 3.5: Example 2: Simulation-based comparison of P_d versus SNR with single antenna under non-random channel with constant gain and possible presence of cyclostationary interference: $P_{fa} = 0.01$, $p = 1$, $M = 2000$, 2000 Monte Carlo runs, OFDM signal (number of subcarriers N_c=32, cyclic prefix length $N_{cp} = 8$). The approach labeled "Jallon" is that of [63]. Type I interference is an OFDM signal with number of subcarriers N_c=64 and cyclic prefix length $N_{cp} = 16$ whereas Type II interference is an OFDM signal with number of subcarriers N_c=32 and cyclic prefix length $N_{cp} = 16$. The SNR for Type I interfering signal was fixed at 0dB (i.e., noise power equals interfering signal power) whereas that for Type II interfering signal was fixed at -10dB. With fixed noise power, we varied the PU signal power to achieve the desired PU SNR (horizontal axis).

48
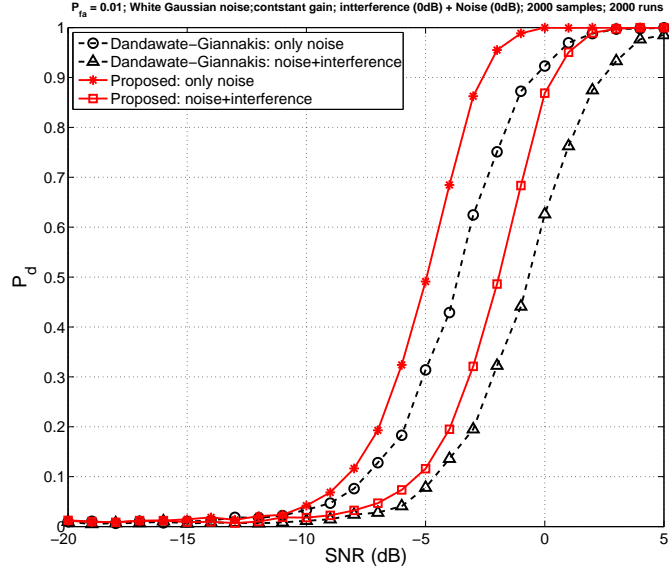
Figure 3.6: Example 2: Simulation-based comparison of P_d versus SNR with single antenna under non-random channel with constant gain and possible presence of cyclostationary interference: $P_{fa} = 0.01$, $p = 1$, $M = 2000$, 2000 Monte Carlo runs, OFDM signal (number of subcarriers N_c=64, cyclic prefix length $N_{cp} = 16$). The approach labeled "Dandawate-Giannakis" is used in [59, 67, 64]. Interference is an OFDM signal with number of subcarriers N_c=32 and cyclic prefix length $N_{cp} = 8$. The SNR for the interfering signal was fixed at 0dB (i.e., noise power equals interfering signal power). With fixed noise power, we varied the PU signal power to achieve the desired PU SNR (horizontal axis).
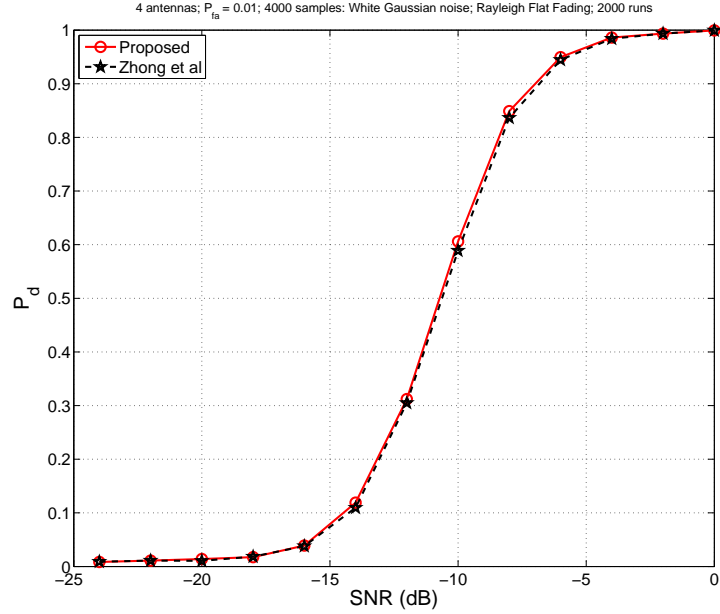
Figure 3.7: Example 3: Simulation-based comparison of probability of detection versus SNR with $p = 4$ antennas under Rayleigh flat-fading and $M = 4000$: $P_{fa} = 0.01$, 2000 Monte-Carlo runs, OFDM signal (number of subcarriers N_c=32, cyclic prefix length $N_{cp} = 8$). The approach labeled "Zhong et al" is from [73].
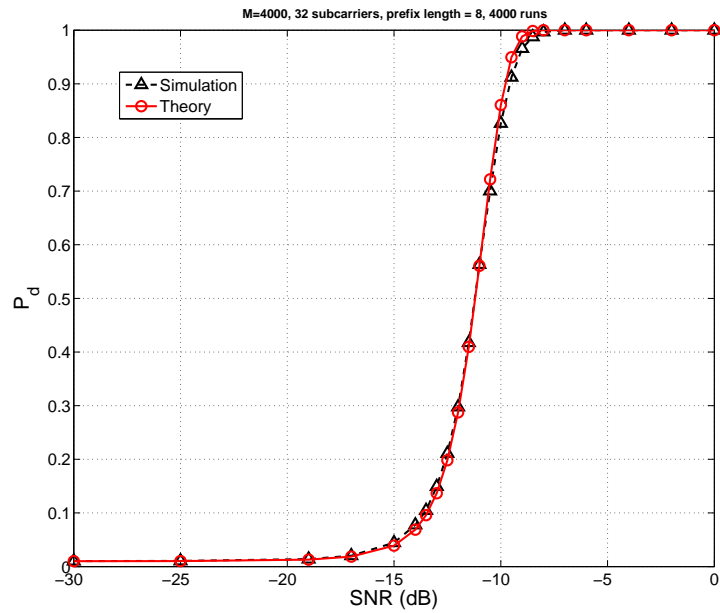
Figure 3.8: Example 3: Performance analysis: theoretical and simulation-based performance comparison of probability of detection P_d versus SNR for the proposed multi-antenna spectrum sensing: OFDM signal (number of subcarriers N_c=32, cyclic prefix length $N_{cp} = 8$), non-random channel with unit gain, $P_{fa} = 0.01$, $p = 4$, $M = 4000$, 4000 runs.
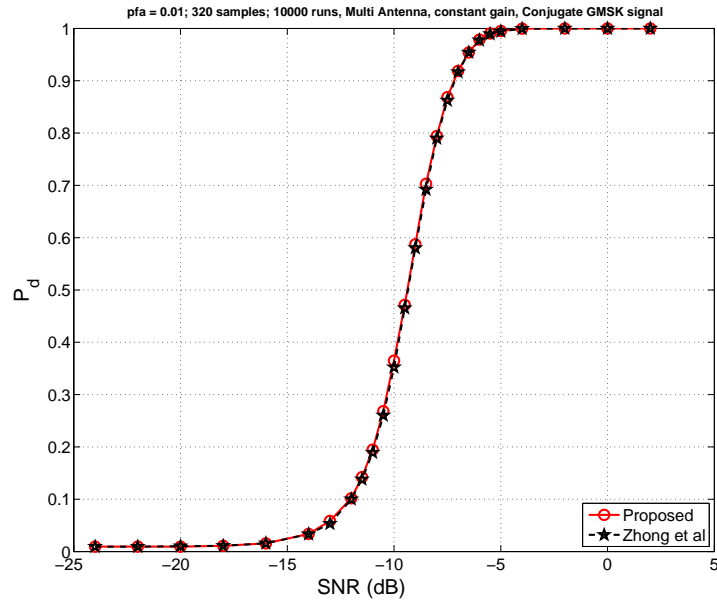
Figure 3.9: Example 4: Simulation-based comparison of probability of detection versus SNR for GMSK signal with 16 samples per symbol, with $p = 4$ antennas under non-random channel with constant gains and $M = 320$: $P_{fa} = 0.01$, 10000 runs. The approach labeled "Zhong et al" is from [73].
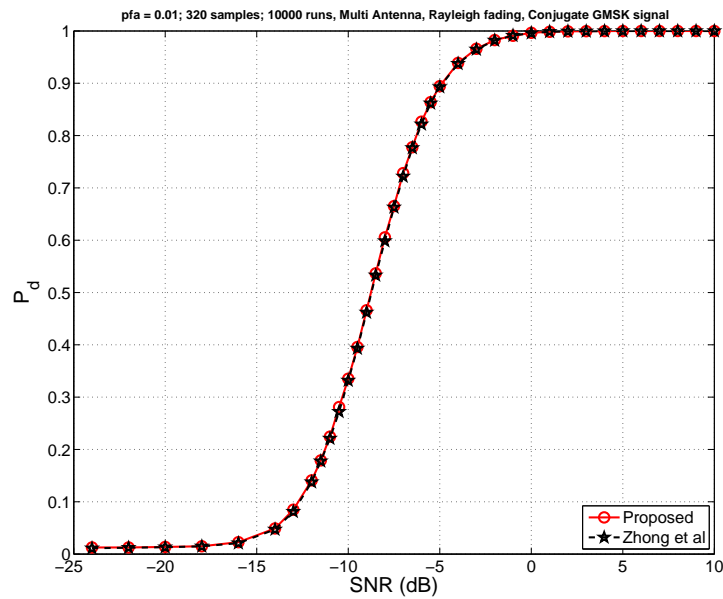
Figure 3.10: Example 4: Simulation-based comparison of probability of detection versus SNR for GMSK signal with 16 samples per symbol, with $p = 4$ antennas under Rayleigh flat-fading and $M = 320$: $P_{fa} = 0.01$, 10000 runs. The approach labeled "Zhong et al" is from [73].

51

Chapter 4

Cyclostationarity Based Spectrum Sensing Under Uncertain Gaussian Noise

Detection of cyclostationary primary user (PU) signals in colored Gaussian noise for cognitive radio systems is considered based on looking for single or multiple cycle frequencies at single or multiple time lags in the cyclic autocorrelation function (CAF) of the noisy PU signal. We explicitly exploit the knowledge that under the null hypothesis of PU signal absent, the measurements originate from possible colored Gaussian noise with unknown correlation function. Our formulation allows us to simplify the spectrum sensing detector and obviates the need for estimating an unwieldy covariance matrix needed in some prior works. We consider both single and multiple antenna receivers, and both nonconjugate and conjugate CAFs. A performance analysis of the proposed detector is carried out. Supporting simulation examples are provided to demonstrate the efficacy of the proposed approaches and to compare them with some existing approaches. Our proposed approaches are computationally cheaper than the Dandawate-Giannakis and related approaches while having quite similar detection performance for a given false alarm rate.

4.1 Introduction

Cognitive radio allows for usage of licensed frequency bands (rights held by primary users (PUs)) by unlicensed users (secondary or cognitive users) when the licensed spectrum bands are unoccupied (a function of time and location). Therefore, one of the first steps to be accomplished by a cognitive user is *spectrum sensing*: analysis of the received electromagnetic transmissions to search for unoccupied spectrum bands (*spectrum holes*). One of the ways to accomplish this is energy detection/spectral analysis and consequent (statistical) hypothesis testing [56, 57, 60, 65]. Based on the received signal $x(k)$ (k denotes discrete-time), the

52

cognitive user has to decide if the PU is present or not. This may be formulated as a binary hypothesis testing problem where under the null hypothesis $\mathcal{H}_0$, the cognitive user is receiving just noise $x(k) = n(k)$, and under the alternative $\mathcal{H}_1$, PU signal $s(k)$ is also present with $x(k) = s(k) + n(k)$. A popular approach is that of energy detection; see [56, 57, 60, 65] and references therein. One designs a CFAR (constant false alarm rate) test requiring prior knowledge of some of the signal statistics under $\mathcal{H}_0$. For instance, $n(k)$ is taken to be thermal noise with known variance.

Detectors for orthogonal frequency division multiplex (OFDM) signals over additive white Gaussian noise (AWGN) channels with possible unknown noise variance have been considered in [75] using likelihood ratio tests. The formulation of [75] does not consider colored noise or frequency-selective channels, unlike this chapter. Autocorrelation based detection of OFDM signals is investigated in [58] for both AWGN and multipath channels under the assumption of white noise. In [76] spectrum sensing of a second-order cyclostationary signal (such as OFDM) received at multiple antennas is investigated under white Gaussian noise and flat fading. It is noted in [76, Sec. VII] that "The covariance structure is changed if the noise is colored, and the performance of the proposed detector will degrade. This is a problem for future study." We consider colored noise in this chapter. In a typical system due to filtering at the front-end to exclude out-of-band signals (and other operations such as sampling), the noise at the receiver is seldom (exactly) white. Furthermore, any interfering OFDM signal (with signal parameters such as cycle frequencies, not of interest) can be modeled as a Gaussian process (by invoking the central limit theorem for large enough number of subcarriers [58]). Such signals propagating through multipath channels are then colored Gaussian processes.

Energy detection based and quite a few other approaches can not distinguish among different types of primary user or secondary user signals. Cyclostationarity detection allows classifying signals exhibiting cyclostationarity at different cycle frequencies [64] and/or different time lags. As noted in [67], one can use cyclostationarity detection for recognizing

53

the individual air interfaces, a task at which energy detector would fail. Existing cyclostationarity detectors for cognitive radio systems reported in [67, 64, 73] are all based on [59] where one looks for a cycle frequency at a particular time lag in the cyclic autocorrelation function (CAF) of the (noisy) PU signal; extensions to multiple cycle frequencies and/or multiple lags may also be found in some of these papers. Under the alternative hypothesis, CAF is nonzero whereas under the null hypothesis it is zero. Signal characteristics under the null hypothesis are not exploited except for noting that its CAF would be zero. Implementation of the approaches of [59, 67, 64, 73] requires computation of the covariance matrix of estimated CAF's real and imaginary parts. (In general, this covariance matrix does not have an analytical expression even when the PU signal is precisely known.) In practice, it is estimated from the data, is computationally expensive and it needs a frequency smoothing window [59] to smooth certain cyclic periodograms in the frequency domain. In this chapter we explicitly exploit the knowledge that under the null hypothesis of PU signal absent, the measurements originate from possibly colored Gaussian noise with possibly unknown correlation function. This framework subsumes white Gaussian noise. Such a framework (white Gaussian noise) is explicitly stated in [73, Eqns. (1),(2)], and although not explicitly stated in [67, 64], is extensively employed in simulation examples presented therein.

Other existing approaches based on single antenna receivers include [62], [63], [66] and [71]. In [62] detection of spread signals using the signal nonconjugate CAF at multiple lags and multiple cycle frequencies is considered under white Gaussian noise with possibly unknown variance. In [63] detection of OFDM signals using the signal nonconjugate CAF at a single time lag and multiple cycle frequencies is considered under white Gaussian noise with known variance. In [66] several single antenna cyclostationarity detectors under white Gaussian noise have been considered including a peak detector [66, (12)] which utilizes the noisy signal CAF at multiple cycle frequencies and a single time-lag. Our proposed detector when specialized to single antenna and white Gaussian noise is similar to that in [62], [63] and [66, (12)], except that we exclude the use of zero cycle frequency, the

contribution of the stationary part of the signal. In [71] a single cycle frequency and single time lag cyclostationarity detector has been presented for OFDM signals under noise variance uncertainty. It is different from that in [62], [63], [66] and from our proposed detector; further details regarding [71] are in Sec. 2.4.

Preliminary conference versions of this chapter have appeared in [74] and [72]. In [74] cyclostaionarity detectors in white Gaussian noise with unknown variance based on single cycle frequency and single time lag have been considered whereas in [72] cyclostaionarity detectors in colored Gaussian noise with unknown correlation function based on single cycle frequency and single time lag have been investigated. In this chapter we discuss detectors based on multiple cyclic frequencies and multiple time lags in colored Gaussian noise. Also we consider both nonconjugate and conjugate CAFs appropriate for OFDM and GMSK signals, respectively, whereas both [74] and [72] are restricted to nonconjugate CAFs.

The proposed detectors are useful in several practical scenarios such as detection of OFDM signals in digital video broadcasting (DVB) standard DVB-T (under IEEE 802.22 Working Group proposals), as discussed in [63]. As noted in [64] OFDM is employed by many of the current as well as future wireless communications systems including 3GPP Long Term Evolution (LTE) [69], IEEE 802.11a/g WLANs, DVB standards DVB-T and DVB-H, as well as IEEE 802.16 and WiMAX wireless metropolitan area networks. Finally, a GSM network as the primary system and coexisting with an OFDM based secondary WLAN system has been considered in [68]. Our conjugate CAF based detectors for detecting GMSK signals in the presence of interfering OFDM signals apply to the application considered in [68]. Note that we exploit only the temporal and spatial (in the multiantenna case) properties of the received signal, as in [59, 67, 64, 73], but not its spectral properties such as cyclic spectrum (or power spectrum) in that we can only detect presence or absence of the PU signal in the "full" PU band instead of distinguishing between occupancy or vacancy of various subbands in the full band. This is a limitation that our approach shares with that of [59, 67, 64, 73].

Our formulation allows us to simplify the spectrum sensing detector, both conceptually and computationally, and obviates the need for estimating the unwieldy covariance matrix needed in [59, 67, 64, 73]. We consider both single and multiple antenna receivers. Under single antenna receivers, our detector is similar to that in [62], [63] and [66, (12)] when specialized to single antenna and white Gaussian noise. Also unlike[62], [63], [66, (12)] and [71], we investigate multiple antenna receivers where we exploit cyclic cross-correlations among different antennas. Exploitation of cyclic cross-correlations among different antennas has also been considered in [73] for GMSK signals where [73] extends the single-antenna approach of [59] inheriting its computational complexity.

As in [59, 67, 64, 73], our approach is to test the estimated CAF of the observations at selected cycle frequencies and lags: their mean value is zero under colored Gaussian noise and is nonzero when the desired PU signal is present. Since we do not assume any knowledge about the structure of the colored noise (its variance or correlation function) or the underlying channel (flat or frequency selective), an optimal detector based on the likelihood ratio or generalized likelihood ratio test, does not appear to be possible. We devise tests based on the large sample properties of the estimated CAF without requiring knowledge of the noise or the channel structure. The rest of the chapter is organized as follows. In Sec. II we present some background material pertaining to cyclostationary signals and their CAF. In Sec. III we derive some large sample statistics of the sample CAFs of colored Gaussian sequences which are then used in Sec. IV to propose novel detectors to detect PU signals exhibiting nonconjugate or conjugate cyclostaionarity. The results of Secs. III and IV are new. A performance analysis of the proposed detectors is presented in Sec. V. Computational complexity issues are discussed in Sec. VI. Supporting simulation examples are provided using OFDM or GMSK PU signals are presented in Sec. VII where we compare our detectors with those of [59], [64], [73] and [71].

Notation: Variable B_{ij} denotes the ijth element of the matrix $\mathbf{B}$, x_i denotes the ith element of vector $\mathbf{x}$, and $\mathbf{I}$ is the identity matrix. The superscripts $*$ and H denote the

complex conjugate and the Hermitian (conjugate transpose) operations, respectively. The function $\delta_{i,j}$ denotes the Kronecker delta function, i.e. $\delta_{i,j} = 1$ if $i = j$, 0 otherwise. Given a column vector $\mathbf{x}$, diag$\{\mathbf{x}\}$ denotes a square matrix with elements of $\mathbf{x}$ along its main diagonal and zeros everywhere else. We use cov$(\mathbf{x}, \mathbf{y}^*) := E\{\mathbf{x}\mathbf{y}^H\} - E\{\mathbf{x}\}E\{\mathbf{y}^H\}$ and let cum$_4(x_1, x_2, x_3, x_4)$ denote the joint 4th cumulant of random variables x_i ($i = 1, 2, 3, 4$). Note that cum$_4(x_1, x_2, x_3, x_4) = E\{x_1 x_2 x_3 x_4\} - E\{x_1 x_2\}E\{x_3 x_4\} - E\{x_1 x_3\}E\{x_2 x_4\} - E\{x_1 x_4\}E\{x_2 x_3\}$ when all x_i's are zero-mean. The notation $\mathcal{N}_c(\mathbf{m}, \Sigma)$ denotes a circularly symmetric (proper) complex Gaussian (vector) distribution with mean $\mathbf{m}$ and covariance matrix Σ, and $\mathcal{N}_r(\mathbf{m}, \Sigma)$ denotes the same for a real-valued Gaussian vector.

4.2 Cyclostationarity Background

A discrete-time zero-mean complex-valued cyclostationary signal $x(k)$ is characterized by a time-varying autocorrelation function $R_{xx}(k, k+\tau) := E\{x(k)x^*(k+\tau)\}$ which has a Fourier series representation [59, 67]

$$R_{xx}(k, k+\tau) = \sum_{\alpha \in \mathcal{A}} R_{xx}(\alpha; \tau)e^{j2\pi\alpha k} \tag{4.1}$$

where given M samples of observations $x(k)$ for $k = 1, 2, \cdots, M$, the *cyclic autocorrelation function* (CAF) $R_{xx}(\alpha; \tau)$ at cycle frequency $\alpha \in \mathcal{A}$ is given by

$$R_{xx}(\alpha; \tau) = \lim_{M \to \infty} \frac{1}{M} \sum_{k=1}^{M} R_{xx}(k, k+\tau)e^{-j2\pi\alpha k} \tag{4.2}$$

and $\mathcal{A}$ is the set of cycle frequencies [59]

$$\mathcal{A} := \{\alpha \,|\, 0 \leq \alpha < 1, \; R_{xx}(\alpha; \tau) \not\equiv 0\}. \tag{4.3}$$

A conjugate CAF is defined as

$$R_{xx(*)}(\alpha;\tau) = \lim_{M\to\infty} \frac{1}{M} \sum_{k=1}^{M} R_{xx^*}(k, k+\tau)e^{-j2\pi\alpha k} \qquad (4.4)$$

where $R_{xx^*}(k, k+\tau) := E\{x(k)x(k+\tau)\}$. Ref. [59] considers conjugate CAFs whereas [67, 64] consider both types of CAFs. For wide-sense stationary (WSS) signals, $R_{xx}(\alpha;\tau) = 0$ as well as $R_{xx(*)}(\alpha;\tau) = 0$ for any $\alpha \neq 0$.

4.2.1 Multivariate Processes

Later we will consider vector random processes arising due to a multiantenna receiver with $p \geq 1$ antennas. Therefore, we will consider a $p \times 1$ discrete-time zero-mean complex-valued cyclostationary signal $\mathbf{x}(k)$ with time-varying autocorrelation function $\mathbf{R}_{xx}(k, k+\tau) := E\{\mathbf{x}(k)\mathbf{x}^H(k+\tau)\}$ which has a Fourier series representation [59, 67]

$$\mathbf{R}_{xx}(k, k+\tau) = \sum_{\alpha\in\mathcal{A}} \mathbf{R}_{xx}(\alpha;\tau)e^{j2\pi\alpha k} \qquad (4.5)$$

where the nonconjugate *cyclic autocorrelation function* (CAF) $\mathbf{R}_{xx}(\alpha;\tau)$ at cycle frequency $\alpha \in \mathcal{A}$ is given by

$$\mathbf{R}_{xx}(\alpha;\tau) = \lim_{M\to\infty} \frac{1}{M} \sum_{k=1}^{M} \mathbf{R}_{xx}(k, k+\tau)e^{-j2\pi\alpha k}. \qquad (4.6)$$

Similar comments apply to conjugate CAFs.

4.3 Large Sample Statistics of Sample CAF

In this section we investigate large sample statistics of estimated CAF when we have colored Gaussian noise as observations. These results are exploited later in Sec. 4.4 to propose detectors for detection of cyclostationary PU signals. Our focus will be on the

binary hypothesis testing problem involving p-dimensional processes ($p \geq 1$)

$$\mathbf{x}(k) = \begin{cases} \mathbf{n}(k) & : \mathcal{H}_0 \\ \mathbf{s}(k) + \mathbf{n}(k) & : \mathcal{H}_1 \end{cases} \tag{4.7}$$

where $\mathbf{n}(k)$ is zero-mean, spatially uncorrelated, temporally colored Gaussian and $\mathbf{s}(k) = \sum_{l=0}^{L_c} \mathbf{h}(l) s_{pu}(k - l)$ where $s_{pu}(k)$ is a scalar cyclostationary signal (emitted by a primary user) with at least one known cycle frequency α and at least one known lag τ such that $R_{s_{pu}s_{pu}}(\alpha; \tau) \neq 0$, and p-column $\mathbf{h}(l)$ is the complex channel impulse response. Our approach (similar to [59, 67, 64, 73]) is to test the estimated CAF of the observations at pairs (α_i, τ_i), $i \geq 1$, to check whether it is nonzero. However, unlike [59, 67, 64, 73], we explicitly exploit the known statistics of observations under $\mathcal{H}_0$ (namely, we have colored Gaussian noise with possibly unknown correlation function). We are interested only in nonzero cycle frequencies.

4.3.1 Nonconjugate CAF

These results are appropriate for OFDM signals.

Spatially White and Temporally Correlated Gaussian Noise

Consider a $p \times 1$ WSS proper (circularly symmetric) complex-valued zero-mean colored Gaussian sequence $\mathbf{x}(k) = \mathbf{n}(k)$ with correlation function $\mathbf{R}_{xx}(k, k + \tau) = \mathbf{R}_{nn}(k, k + \tau) = \mathbf{R}_{nn}(\tau) = \text{diag}\{R_{ii,n}(\tau), 1 \leq i \leq p\}$. Also, since $\mathbf{n}(k)$ is proper, $E\{\mathbf{n}(k)\mathbf{n}^T(k + \tau)\} \equiv 0$. Given an observation length of M samples, we estimate the (nonconjugate) CAF $\mathbf{R}_{xx}(\alpha; \tau)$ as

$$\hat{\mathbf{R}}_{xx}(\alpha; \tau) = \frac{1}{M} \sum_{k=1}^{M} \mathbf{x}(k)\mathbf{x}^H(k + \tau)e^{-j2\pi\alpha k}. \tag{4.8}$$

It is easy to see that $\lim_{M\to\infty} E\{\hat{\mathbf{R}}_{xx}(\alpha;\tau)\} = \mathbf{R}_{xx}(\alpha;\tau)$. Let ($x_i$ is the i-th component of $\mathbf{x}$)

$$\hat{R}_{ik,x}(\alpha;\tau) := \frac{1}{M}\sum_{m=1}^{M} x_i(m)x_k^*(m+\tau)e^{-j2\pi\alpha m}. \tag{4.9}$$

We prove Lemma 1 in the Appendix Sec. A.

Lemma 1 . For $\mathbf{x}(k) = \mathbf{n}(k)$, a WSS proper zero-mean Gaussian sequence, we have

$$\lim_{M\to\infty} M\mathrm{cov}\left(\hat{R}_{ij,n}(\alpha;\tau_1), \hat{R}_{kl,n}^*(\beta;\tau_2)\right) = \tilde{\gamma}_{ij,n}(\alpha;\tau_1-\tau_2)\delta_{i,k}\delta_{j,l}\delta_{\alpha,\beta} \tag{4.10}$$

and

$$\lim_{M\to\infty} M\mathrm{cov}\left(\hat{R}_{ij,n}(\alpha;\tau_1), \hat{R}_{kl,n}(\beta;\tau_2)\right) = \lim_{M\to\infty} M\mathrm{cov}\left(\hat{R}_{ij,n}(\alpha;\tau_1), \hat{R}_{lk,n}^*(-\beta;-\tau_2)\right)$$

$$= \tilde{\gamma}_{ij,n}(\alpha;\tau_1+\tau_2)\delta_{i,l}\delta_{j,k}\delta_{\alpha,-\beta}. \tag{4.11}$$

where $R_{ik,x}(\tau) := E\{x_i(t)x_k^*(t+\tau)\}$ and

$$\tilde{\gamma}_{ij,n}(\alpha;\tau_1-\tau_2) := \sum_{m=-\infty}^{\infty} R_{ii,n}(-m)R_{jj,n}(m+\tau_1-\tau_2)e^{-j2\pi\alpha m} \quad \bullet \tag{4.12}$$

Finite Memory Colored Gaussian Noise

We now make a further assumption that correlation function of noise is "effectively" zero for lags $> L_n$ where (the upperbound) L_n is known, i.e.

$$\mathbf{R}_{nn}(\tau) = 0 \text{ for } |\tau| > L_n. \tag{4.13}$$

By (4.10), (4.11) and (4.13), for $\alpha, \beta \in \mathcal{A}$, we have

$$\lim_{M\to\infty} M\mathrm{cov}\left(\hat{R}_{ij,n}(\alpha;\tau_1), \hat{R}_{kl,n}^*(\beta;\tau_2)\right) = \begin{cases} \tilde{\gamma}_{ij,n}(\alpha;0)\delta_{i,k}\delta_{j,l}\delta_{\alpha,\beta}, & \text{for } \tau_1 = \tau_2 \\ 0 & \text{for } |\tau_1-\tau_2| > 2L_n, \end{cases} \tag{4.14}$$

60

$$\lim_{M \to \infty} M \mathrm{cov} \left(\hat{R}_{ij,n}(\alpha; \tau_1), \hat{R}_{kl,n}(\beta; \tau_2) \right) = 0. \tag{4.15}$$

Also, by [59, 67, 64], asymptotically (as $M \to \infty$), $\hat{R}_{ik,x}(\alpha; \tau)$ is a Gaussian random variable (complex-valued but not necessarily circularly symmetric) and "vectorized" matrix $\hat{\mathbf{R}}_{xx}(\alpha; \tau)$ is a Gaussian random vector for any α and τ, for $\mathbf{x}(t)$ under either $\mathcal{H}_0$ or $\mathcal{H}_1$ and whether $\mathbf{x}(t)$ is finite memory or not. Invoking asymptotic Gaussianity, it then follows that

$$\lim_{M \to \infty} \sqrt{M} \hat{R}_{ij,n}(\alpha; \tau) \sim \mathcal{N}_c \left(0, \tilde{\gamma}_{ij,n}(\alpha; 0) \right) \quad \forall i, j. \tag{4.16}$$

Furthermore, $\hat{R}_{ij,x}(\alpha; \tau)$ is asymptotically independent of $\hat{R}_{kl,x}(\alpha; \tau)$ if $i \neq k$ or $j \neq l$. Moreover, $\hat{R}_{ij,x}(\alpha; \tau_1)$ is asymptotically independent of $\hat{R}_{kl,x}(\beta; \tau_2)$ if $\alpha \neq \beta$ ($\alpha, \beta \in \mathcal{A}$) or $\tau_1 \neq \tau_2$, for any i, j, k, l. As discussed in Sec. 2.2.1, for OFDM signals the nonconjugate CAF peaks at $\tau = \pm N_c$ (N_c = number of subcarriers). If we take $\tau_1 = N_c$ and $\tau_2 = -N_c$, we need to have $L_n < 2N_c$ for (4.14) to hold true.

4.3.2 Conjugate CAF

These results are appropriate for GMSK signals. Given an observation length of M samples, we estimate the conjugate CAF $\mathbf{R}_{xx(*)}(\alpha; \tau) := \lim_{M \to \infty} \frac{1}{M} \sum_{k=1}^{M} E\{\mathbf{x}(k)\mathbf{x}^T(k + \tau)\}e^{-j2\pi\alpha k}$ as

$$\hat{\mathbf{R}}_{xx(*)}(\alpha; \tau) = \frac{1}{M} \sum_{k=1}^{M} \mathbf{x}(k)\mathbf{x}^T(k + \tau)e^{-j2\pi\alpha k}. \tag{4.17}$$

Spatially White and Temporally Correlated Gaussian Noise

Mimicking Sec. 4.3.1 we obtain Lemma 2 whose proof is given in the Appendix Sec. B.

Lemma 2 . For $\mathbf{x}(k) = \mathbf{n}(k)$, a WSS proper zero-mean Gaussian sequence, we have

$$\lim_{M \to \infty} M \mathrm{cov}(\hat{R}_{(*)ij,n}(\alpha; \tau_1), \hat{R}^*_{(*)kl,n}(\beta; \tau_2)) = \sum_{m=-\infty}^{\infty} [R_{ik,n}(m)R_{jl,n}(m + \tau_2 - \tau_1)$$

$$+ R_{il,n}(m + \tau_2)R_{jk,n}(m - \tau_1)]e^{j2\pi\alpha m}\delta_{\alpha,\beta} \quad \bullet \quad (4.18)$$

Finite Memory Colored Gaussian Noise

For GMSK signals, the nonconjugate CAF peaks at $\tau = 0$. Confining our attention to $\tau_1 = \tau_2 = 0$, for finite-memory, spatially-uncorrelated, colored Gaussian noise, we obtain

$$\lim_{M \to \infty} M \text{cov} \left(\hat{R}_{(*)ij,n}(\alpha; 0), \hat{R}^*_{(*)kl,n}(\beta; 0) \right)$$

$$= \begin{cases} 2 \sum_{m=-L_n}^{L_n} R^2_{ii,n}(m) e^{j2\pi\alpha m} \delta_{\alpha,\beta} \text{ if } i = k = l = j \\ \sum_{m=-L_n}^{L_n} R_{ii,n}(m) R_{jj,n}(m) e^{j2\pi\alpha m} \delta_{\alpha,\beta} \\ \qquad \text{if } (i,j) = (k,l) \text{ but } i \neq j, \text{ or } (i,j) = (l,k) \\ 0 \text{ otherwise .} \end{cases} \qquad (4.19)$$

Invoking asymptotic Gaussianity, it then follows that for finite-memory colored Gaussian noise

$$\lim_{M \to \infty} \sqrt{M} \hat{R}_{(*)ij,n}(\alpha; 0) \sim \mathcal{N}_c \left(0, \sum_{m=-L_n}^{L_n} (1 + \delta_{i,j}) R_{ii,n}(m) R_{jj,n}(m) e^{j2\pi\alpha m} \right) \quad \forall i, j. \qquad (4.20)$$

Noting that since $\lim_{M \to \infty} \hat{R}_{(*)ij,x}(\alpha; \tau) = \lim_{M \to \infty} \hat{R}_{(*)ji,x}(\alpha; \tau)$ and $\hat{R}_{(*)ij,x}(\alpha; 0) = \hat{R}_{(*)ji,x}(\alpha; 0)$, unlike nonconjugate CAFs, in case of conjugate CAFs, $\hat{R}_{(*)ij,x}(\alpha; \tau)$ is asymptotically independent of $\hat{R}_{(*)kl,x}(\alpha; \tau)$ for $i \neq k$ or $j \neq l$ if $i \geq j$ and $k \geq l$ (or if $i \leq j$ and $k \leq l$).

4.4   Test Statistics

Based on the large sample statistics of CAFs of colored Gaussian noise discussed in Sec. 4.3, we now propose *ad hoc* CFAR (constant false alarm rate) detectors for detection of nonzero nonconjugate as well as conjugate CAFs. They are *ad hoc* as they do not follow any optimality criterion. Since we do not assume any knowledge about the structure of the colored noise (its variance or correlation function) or the underlying channel (flat or frequency selective), an optimal detector based on the likelihood ratio or generalized likelihood ratio test, does not appear to be possible. We will assume that the finite-memory assumption

(4.13) holds true in this section. The desired PU signals are assumed to have nonzero CAF at certain known non-zero cycle frequencies and lags whereas CAF of colored noise is zero at all lags and nonzero cycle frequencies. The proposed tests exploit the large sample statistics of the estimated CAF to yield CFAR detectors.

4.4.1   Nonconjugate CAF: OFDM Signals

Consider the binary hypothesis testing problem (4.7). The PU channel impulse response and the noise correlation function are unknown. We do know that noise is zero-mean complex (proper) Gaussian, spatially uncorrelated and temporally possibly colored (and of finite memory). Also, $s_{pu}(t)$ in (4.7) is a scalar cyclostationary signal (emitted by PUs) with $K \geq 1$ known cycle frequency and lag pairs (α_k, τ_k), $k = 1, 2, \cdots, K$, such that $R_{s_{pu}s_{pu}}(\alpha_k; \tau_k) \neq 0$ and $|\tau_1 - \tau_2| > L_n$ so that (4.14) holds true. The binary hypothesis testing problem in this case can be formulated as

$$
\begin{aligned}
\mathcal{H}_0 &: \quad R_{ij,x}(\alpha_k; \tau_k) = 0 \ \ \forall i, j, k \\
\mathcal{H}_1 &: \quad R_{ij,x}(\alpha_k; \tau_k) \not\equiv 0 \ \ \text{for some } i, j, k.
\end{aligned}
\tag{4.21}
$$

Under both hypotheses, we have $\lim_{M \to \infty} E\{\hat{\mathbf{R}}(\alpha; \tau)\} = \mathbf{R}(\alpha; \tau)$. Under $\mathcal{H}_0$, by the results of Sec. 4.3.1, $\hat{R}_{ij}(\alpha_k; \tau_k)$ has zero-mean $\forall i, j, k$, and under $\mathcal{H}_1$, it has non-zero mean for some i, j, k; therefore, $|R_{ij}(\alpha_k; \tau_k)| > 0$ for some i, j, k. Define (see also (4.12))

$$
\bar{\gamma}_{ij,n}(\alpha_k) := \sum_{m=-L_n}^{L_n} R_{ii,n}(-m) R_{jj,n}(m) e^{-j2\pi\alpha_k m}
\tag{4.22}
$$

and let $\tilde{\mathbf{r}}$ denote the $Kp^2 \times 1$ vector composed of elements $\hat{R}_{ij,x}(\alpha_k; \tau_k)/\sqrt{\bar{\gamma}_{ij,x}(\alpha_k)}$ for all distinct triplets (i, j, k). Then by (4.16), we have $\lim_{M \to \infty} \sqrt{M}\tilde{\mathbf{r}} \stackrel{\mathcal{H}_0}{\sim} \mathcal{N}_c(0, \mathbf{I})$ leading to $2M\tilde{\mathbf{r}}^H\tilde{\mathbf{r}} \stackrel{\mathcal{H}_0}{\sim} \chi^2_{2Kp^2}$ where χ^2_n denotes the central chi-square distribution with n degrees of freedom (dof). Since $|R_{ij}(\alpha_k; \tau_k)| > 0$ for some i, j, k, we have $E\{\tilde{\mathbf{r}}^H\tilde{\mathbf{r}} \,|\, \mathcal{H}_1\} > E\{\tilde{\mathbf{r}}^H\tilde{\mathbf{r}} \,|\, \mathcal{H}_0\}$. Furthermore, since the true values $\bar{\gamma}_{ij,n}(\alpha_k)$, $(k = 1, 2, \cdots, K)$, are not available, we replace

them by estimates $\hat{\gamma}_{ij,x}(\alpha_k)$ and consider the following *ad hoc* test motivated by $2M\tilde{\mathbf{r}}^H\tilde{\mathbf{r}}$ and $E\{\tilde{\mathbf{r}}^H\tilde{\mathbf{r}}\,|\,\mathcal{H}_1\} > E\{\tilde{\mathbf{r}}^H\tilde{\mathbf{r}}\,|\,\mathcal{H}_0\}$:

$$\mathcal{T} := 2M\sum_{k=1}^{K}\sum_{i=1}^{p}\sum_{j=1}^{p}\frac{|\hat{R}_{ij,x}(\alpha_k;\tau_k)|^2}{\hat{\gamma}_{ij,x}(\alpha_k)}\overset{\mathcal{H}_1}{\underset{\mathcal{H}_0}{\gtrless}}\eta \qquad (4.23)$$

where

$$\hat{\gamma}_{ij,x}(\alpha_k) := \sum_{m=-L_n}^{L_n}\hat{R}_{ii,x}(-m)\hat{R}_{jj,x}(m)e^{-j2\pi\alpha_k m}, \qquad (4.24)$$

$$\hat{R}_{ii,x}(m) := \frac{1}{M-m}\sum_{k=1}^{M-m}x_i(k)x_i^*(k+m), \quad m \geq 0, \qquad (4.25)$$

$\hat{R}_{ii,x}(-m) = \hat{R}_{ii,x}^*(m)$, and the threshold η is picked to achieve a pre-specified probability of false alarm $P_{fa} = P\{\mathcal{T} \geq \eta\,|\,\mathcal{H}_0\}$. By the results of Sec. 4.3.1, we can find (shown next) asymptotic distribution of $\mathcal{T}$ under $\mathcal{H}_0$ and design a CFAR test. Such CFAR tests are not optimal in any sense but do yield a constant false-alarm rate, a desirable property, under model parameter uncertainties. CFAR tests have been used in radar and other problems under parameter uncertainty [61, Sec. 8.1].

We now turn to calculation of η. It follows from (4.16) that asymptotically (as $M \to \infty$),

$$2M\frac{|\hat{R}_{ij,x}(\alpha_k;\tau_k)|^2}{\bar{\gamma}_{ij,x}(\alpha_k)}\overset{\mathcal{H}_0}{\sim}\chi_2^2. \qquad (4.26)$$

Eqn. (4.14) applied to finite-memory colored Gaussian noise also implies that as $M \to \infty$, under $\mathcal{H}_0$, $\hat{R}_{ii,x}(m)$ converges in the mean-square sense, hence in probability (i.p.), to $R_{ii,x}(m)$ [70, Appendix B]. Together with (4.26) this results implies that asymptotically [70, Lemma B.4]

$$2M\frac{|\hat{R}_{ij,x}(\alpha;\tau)|^2}{\hat{\gamma}_{ij,x}(\alpha_k)}\overset{\mathcal{H}_0}{\sim}\chi_2^2. \qquad (4.27)$$

As noted in Sec. 4.3.1, any element of $\hat{\mathbf{R}}_{xx}(\alpha_k;\tau_k)$ is asymptotically independent of all other elements and the same holds true for distinct cycle frequencies, therefore, in (4.23) we have (asymptotically) mutually independent random variables for distinct (i,j,k) triples. Since

there are Kp^2 such terms in $\mathcal{T}$, asymptotically

$$\mathcal{T} \overset{\mathcal{H}_0}{\sim} \chi^2_{2Kp^2}. \tag{4.28}$$

4.4.2 Conjugate CAF: GMSK Signals

In this case too the binary hypothesis testing problem is formulated as (4.21) except that we use $R_{(*)ij,x}(\alpha_k;\tau_k)$ instead of $R_{ij,x}(\alpha_k;\tau_k)$ and we will take $\tau_k = 0 \; \forall k$ since that is where the GMSK CAF is the strongest [68]. Following Secs. 4.3.2 and 4.4.1, we propose the test statistic

$$\mathcal{T}_{conj} := 2M \sum_{k=1}^{K} \sum_{i=1}^{p} \sum_{j=i}^{p} \frac{|\hat{R}_{(*)ij,x}(\alpha_k;0)|^2}{\sum_{m=-L_n}^{L_n} (1+\delta_{i,j})\hat{R}_{ii,x}(m)\hat{R}_{jj,x}(m)e^{j2\pi\alpha_k m}} \overset{\mathcal{H}_1}{\underset{\mathcal{H}_0}{\gtrless}} \eta_{conj}. \tag{4.29}$$

Using the results of Sec. 4.3.2 and noting that there are $K(p^2+p)/2$ terms in the double summation in (4.29), it follows that

$$\mathcal{T}_{conj} \overset{\mathcal{H}_0}{\sim} \chi^2_{K(p^2+p)} \tag{4.30}$$

which allows us to calculate the test threshold η_{conj} corresponding to a specified P_{fa}.

4.4.3 Single Antenna Case: Nonconjugate CAF

Proposed Test

For $p = 1$ (single antenna), the proposed nonconjugate CAF test reduces to

$$2M \sum_{k=1}^{K} \frac{|\hat{R}_{11,x}(\alpha_k;\tau_k)|^2}{\sum_{m=-L_n}^{L_n} |\hat{R}_{11,x}(m)|^2 e^{-j2\pi\alpha_k m}} \overset{\mathcal{H}_1}{\underset{\mathcal{H}_0}{\gtrless}} \eta. \tag{4.31}$$

4.5 Detection Probability

In this section we derive the asymptotic distribution of the proposed test statistics of Sec. 4.4 under $\mathcal{H}_1$ for a specified PU signal. We will assume a non-random channel; for random channels, our results offer conditional detection probability conditioned on the channel.

4.5.1 Nonconjugate CAF

Under $\mathcal{H}_1$, we have $R_{ij,x}(\alpha_k;\tau_k) \neq 0$ for at least one pair (i,j) and $\forall k$. Let $\hat{\mathbf{r}}$ denote the $Kp^2 \times 1$ vector composed of elements $\tilde{R}_{ij,x}(\alpha_k;\tau_k) := \hat{R}_{ij,x}(\alpha_k;\tau_k)/\sqrt{\hat{\gamma}_{ij,x}(\alpha_k)}$ for all distinct triples (i,j,k), with $\mathbf{m}_1 := E\{\hat{\mathbf{r}}\}$ composed of elements $R_{ij,x}(\alpha_k;\tau_k)/\sqrt{\gamma_{ij}^{(1)}(\alpha_k)}$ (for large M, i.e. $M \uparrow \infty$) where $\gamma_{ij}^{(\ell)}(\alpha_k) := \sum_{m=-L_n}^{L_n} R_{ii,x}^{(\ell)}(-m)R_{jj,x}^{(\ell)}(m)e^{-j2\pi\alpha_k m}$ and $R_{ii,x}^{(\ell)}(m) := E\{x_i(t)x_i^*(t+m)\,|\,\mathcal{H}_\ell\}$, $\ell = 0$ or 1. Let $\hat{\mathbf{r}}_{re} = \mathrm{Re}(\hat{\mathbf{r}})$, $\hat{\mathbf{r}}_{im} = \mathrm{Im}(\hat{\mathbf{r}})$, $\hat{\mathbf{c}} = [\hat{\mathbf{r}}_{re}^T\ \hat{\mathbf{r}}_{im}^T]^T$ and $\mathbf{m}_c = [\mathrm{Re}(\mathbf{m}_1^T)\ \mathrm{Im}(\mathbf{m}_1^T)]^T$. Then invoking asymptotic Gaussianity [59, 67, 64], we have $\lim_{M\to\infty}\sqrt{M}\,(\hat{\mathbf{c}} - \mathbf{m}_c) \overset{\mathcal{H}_1}{\sim} \mathcal{N}_r(0,\Sigma_{c1})$ where $\Sigma_{c\ell} := \lim_{M\to\infty}(1/M)\mathrm{cov}(\hat{\mathbf{c}},\hat{\mathbf{c}}\,|\,\mathcal{H}_\ell) =$ conditional covariance, $\ell = 0$ or 1. Define

$$\mathrm{SNR} = \lim_{M\to\infty}(1/M)\sum_{k=1}^{M} E\{\|\mathbf{s}(k)\|^2\}[E\{\|\mathbf{n}(k)\|^2\}]^{-1}. \tag{4.32}$$

If SNR=0, then the hypothesis $\mathcal{H}_1$ reduces to $\mathcal{H}_0$, with $\mathbf{m}_1 = \mathbf{0} = \mathbf{m}_c$, $\gamma_{ij}^{(1)}(\alpha_k) = \gamma_{ij}^{(0)}(\alpha_k)$, and by (4.14)-(4.15), $\Sigma_{c0} = \mathbf{I}$. Furthermore $\lim_{\mathrm{SNR}\downarrow 0}\Sigma_{c1} = \Sigma_{c0} = \mathbf{I}$. Under $\mathcal{H}_0$, complex $\hat{\mathbf{r}}$ is a proper random vector, hence, $\Sigma_0 = \mathbf{I}$ where $\Sigma_\ell := \lim_{M\to\infty}(1/M)\mathrm{cov}(\hat{\mathbf{r}},\hat{\mathbf{r}}^*\,|\,\mathcal{H}_\ell) =$ conditional covariance, $\ell = 0$ or 1. Therefore, under $\mathcal{H}_1$,

$$\lim_{\mathrm{SNR}\downarrow 0}\lim_{M\uparrow\infty}(1/M)\mathrm{cov}(\hat{\mathbf{r}},\hat{\mathbf{r}}^*) = \lim_{\mathrm{SNR}\downarrow 0}\Sigma_1 = \Sigma_0 = \mathbf{I}. \tag{4.33}$$

Again invoking asymptotic Gaussianity [59, 67, 64], under $\mathcal{H}_1$ and for "low" SNRs (i.e. SNR $\downarrow 0$),

$$\lim_{M\to\infty}\sqrt{M}\,(\hat{\mathbf{r}} - \mathbf{m}_1) \overset{\mathcal{H}_1}{\sim} \mathcal{N}_c(0,\Sigma_1). \tag{4.34}$$

66

(Note that $\lim_{M\to\infty} M\mathrm{cov}\left(\hat{R}_{ij}(\alpha;\tau), \hat{R}_{ij}(\alpha;\tau)\right) \neq 0$ when the PU signal is present, hence $\hat{R}_{ij}(\alpha;\tau)$ is not proper, but is approximately proper for "low" SNRs.) Then for large M, i.e. $M\uparrow\infty$,

$$2M\hat{\mathbf{r}}^H\Sigma_1^{-1}\hat{\mathbf{r}} \overset{\mathcal{H}_1}{\sim} \chi^2_{2Kp^2}(\lambda_1), \tag{4.35}$$

where $\chi^2_n(\lambda)$ denotes noncentral chi-square distribution with n degrees of freedom and non-centrality parameter λ, and $\lambda_1 = 2M\mathbf{m}_1^H\Sigma_1^{-1}\mathbf{m}_1$. Under **low SNR**, $\Sigma_1 \approx \mathbf{I} \Rightarrow 2M\hat{\mathbf{r}}^H\Sigma_1^{-1}\hat{\mathbf{r}} \approx \mathcal{T}$ and $\lambda_1 \approx 2M\mathbf{m}_1^H\mathbf{m}_1$. Thus, asymptotically,

$$\mathcal{T} \overset{\mathcal{H}_1}{\sim} \chi^2_{2Kp^2}(\lambda_1), \tag{4.36}$$

where (assuming $\mathbf{s}(t) = \sum_{l=0}^{L_c} \mathbf{h}(l)s_{pu}(t-l)$)

$$\lambda_1 = 2M\sum_{i=1}^{p}\sum_{k=1}^{K}\sum_{j=1}^{p} \frac{|R_{ij,x}(\alpha_k;\tau_k)|^2}{\sum_{m=-L_n}^{L_n} R_{ii,x}^{(1)}(-m)R_{jj,x}^{(1)}(m)e^{-j2\pi\alpha_k m}}, \tag{4.37}$$

$$R_{ii,x}^{(1)}(m) = R_{ii,n}(m) + E\{s_i(t)s_i(t+m)\,|\,h_i(l),\ 0\le l\le L_c\}. \tag{4.38}$$

Therefore, given a specified false alarm probability P_{fa}, the threshold η satisfies $P_{fa} = \int_\eta^\infty f_{\mathcal{T}}(x)\,dx$ where $\mathcal{T} \sim \chi^2_{2Kp^2}$ and $f_{\mathcal{T}}$ is the probability density function of $\mathcal{T}$. The resultant probability of PU detection P_d is then $P_d = P\{\mathcal{T}\ge\eta\,|\,\mathcal{H}_1,\ \mathbf{h}(l),\ 0\le l\le L_c\} = \int_\eta^\infty f_{\mathcal{T}}(y)\,dy$ where $\mathcal{T} \sim \chi^2_{2Kp^2}(\lambda_1)$. Note that (4.34) is valid only as SNR $\downarrow 0$ since $\hat{R}_{ij}(\alpha;\tau)$ is not proper when PU signal is present; hence, our results may not be accurate for "high" SNRs. The simulation results in Sec. 4.7.2 show that the low SNR results are quite good for all SNRs for the presented example.

4.5.2 Conjugate CAF

We will follow the same line of arguments as in Sec. 4.5.1. Under $\mathcal{H}_1$, we have $R_{(*)ij,x}(\alpha_k;0) \neq 0$ for at least one pair (i,j) and $\forall k$. Let $\hat{\mathbf{r}}_{(*)}$ denote the $\frac{K(p^2+p)}{2} \times 1$ vector composed

of elements $\tilde{R}_{(*)ij,x}(\alpha_k; 0) := \hat{R}_{(*)ij,x}(\alpha_k; 0)/\sqrt{\sum_{m=-L_n}^{L_n}(1 + \delta_{i,j})\hat{R}_{ii,x}(m)\hat{R}_{jj,x}(m)e^{j2\pi\alpha_k m}}$ for $1 \leq i \leq j \leq p$, with $\mathbf{m}_2 := E\{\hat{\mathbf{r}}_{(*)}\}$ composed of elements $R_{(*)ij}(\alpha_k; 0)/\sqrt{\sum_{m=-L_n}^{L_n}(1 + \delta_{i,j})\theta_m}$ where $\theta_m = R_{ii}^{(1)}(m)R_{jj}^{(1)}(m)e^{j2\pi\alpha_k m}$(for large M). Let $\lim_{M\to\infty}(1/M)\mathrm{cov}(\hat{\mathbf{r}}_{(*)}, \hat{\mathbf{r}}_{(*)}^*) =: \Sigma_2$. Then invoking the asymptotic Gaussianity [59, 67, 64], under $\mathcal{H}_1$ and for low SNRs,

$$\lim_{M\to\infty} \sqrt{M}\left(\hat{\mathbf{r}}_{(*)} - \mathbf{m}_2\right) \sim \mathcal{N}_c\left(0, \Sigma_2\right). \tag{4.39}$$

(Note that, as in Sec. 4.5.1, $\lim_{M\to\infty} M\mathrm{cov}\left(\hat{R}_{(*)ij,x}(\alpha; 0), \hat{R}_{(*)ij,x}(\alpha; 0)\right) \neq 0$ when the PU signal is present, hence $\hat{R}_{(*)ij,x}(\alpha; 0)$ is not proper, but is approximately proper for "low" SNRs.) Then for large M,

$$2M\hat{\mathbf{r}}_{(*)}^H \Sigma_1^{-1} \hat{\mathbf{r}}_{(*)} \overset{\mathcal{H}_1}{\sim} \chi^2_{K(p^2+p)}(\lambda_2), \tag{4.40}$$

where $\lambda_2 = 2M\mathbf{m}_2^H \Sigma_2^{-1}\mathbf{m}_2$. Under **low SNR**, $\Sigma_2 \approx \mathbf{I} \Rightarrow 2M\hat{\mathbf{r}}_{(*)}^H \Sigma_2^{-1}\hat{\mathbf{r}}_{(*)} \approx \mathcal{T}_{conj}$ and $\lambda_2 \approx 2M\mathbf{m}_2^H\mathbf{m}_2$. Thus,

$$\mathcal{T}_{conj} \overset{\mathcal{H}_1}{\sim} \chi^2_{K(p^2+p)}(\lambda_2) \tag{4.41}$$

where

$$\lambda_2 = 2M\sum_{k=1}^{K}\sum_{i=1}^{p}\sum_{j=i}^{p} \frac{\left|R_{(*)ij,x}(\alpha_k; 0)\right|^2}{\sum_{m=-L_n}^{L_n}(1 + \delta_{i,j})R_{ii,x}^{(1)}(m)R_{jj,x}^{(1)}(m)e^{j2\pi\alpha_k m}}. \tag{4.42}$$

4.6 Computational Complexity

Here we will compare computational complexity of our proposed tests with that of [59] (used in the single antenna case ($p = 1$) for testing a single cycle frequency at a single lag in [67] and extended to multiple cycle frequencies in [64]), [73] (extension of [59] to the multiple antennas case ($p > 1$)), and [71]. We will express computational complexity in terms of number of complex multiplications needed to implement the various approaches; the respective counts for various approaches are listed in Table 4.1. Given an observation sample size of M samples, for computing the CAF at given τ and α, we need $2M$ multiplications. To

Table 4.1: Number of complex multiplications for M samples with colored Gaussian noise

	Proposed	[59, 64, 73]	Tani-Fantacci [71]
$p=1$, $K=1$	$2M + (L_n + 1)M$	$3M + \frac{M}{2}\log_2 M + 4L_w$	$3M$
nonconjugate CAF $p \geq 1$, $K \geq 1$	$2KMp^2 + p(L_n + 1)M$	$Kp^2\left(3M + \frac{M}{2}\log_2 M + 4L_w\right)$	
conjugate CAF $p \geq 1$, $K \geq 1$	$KMp(p+1) + p(L_n + 1)M$	$K\frac{p^2+p}{2}\left(3M + \frac{M}{2}\log_2 M + 4L_w\right)$	

compute the (stationary) autocorrelation at any lag we need M multiplications, and there are $L_n + 1$ lags to be considered. This yields a count of $2M + (L_n + 1)M$ multiplications for the proposed test (4.31) for single antenna and single pair (α, τ), and a count of $2MK + (L_n + 1)M$ for single antenna and K pairs (α_k, τ_k) (ignoring computations for (4.24) given estimates of correlations). For the proposed multi-antenna detectors (4.23) or (4.29) with p antennas, we have to calculate p^2 CAFs (cyclic auto- and cross-correlations) and p stationary autocorrelation functions at $L_n + 1$ lags, yielding a count of $KMp(2p) + p(L_n + 1)p$ complex multiplications for (4.23) and a count of $KMp(p+1) + p(L_n + 1)p$ multiplications for (4.29).

For the test of [59] described in Sec. 2.4, one needs $2M$ multiplications to calculate the CAF at given τ and α, $(M/2)\log_2(2M)$ multiplications for the FFT involved (to compute the cyclic periodogram), and $M + 4L_w$ multiplications for smoothing the two cyclic periodograms. This yields the number of complex multiplications needed as $3M + \frac{M}{2}\log_2 M + 4L_w$ for a single pair (α, τ). The extension to $p > 1$ given in [73] requires $p^2\left(3M + \frac{M}{2}\log_2 M + 4L_w\right)$ complex multiplications for nonconjugate CAF-based test and $\frac{p^2+p}{2}\left(3M + \frac{M}{2}\log_2 M + 4L_w\right)$ multiplications for conjugate CAF-based test for a single pair (α, τ); extension to K pairs (α_k, τ_k) increases the multiplication count by a factor of K. Using the results of [71, Sec. IV-C], the test (2.30) for a single pair (α, τ) requires $3M$ complex multiplications; its extension to K pairs (α_k, τ_k) is not available in [71, Sec. IV-C].

4.7 Simulation Examples

We now present some computer simulation examples using OFDM and GMSK signals to illustrate our detectors and to compare their performance and computational complexity

with some existing detectors. In all presented examples noise variance/correlation function is assumed to be unknown.

4.7.1 Example 1: Analytical Threshold Selection, $p = 1$, $K = 1$, Colored Gaussian Noise

The proposed test as well as tests of [59, 64] rely on asymptotic distribution of the test statistic under $\mathcal{H}_0$ in order to calculate the test threshold for a specified false-alarm probability P_{fa}. How accurate is this distribution for finite data lengths? Parameters (L, β) of the smoothing Kaiser window (see Sec. 2.4) have a strong influence on this distribution (whereas there is no such issue with our approach). Ref. [64] has extensively used $(L, \beta) = (2049, 10)$ and it is claimed therein that for $M \geq 1000$, it is quite accurate. We generated scalar ($p = 1$) colored Gaussian noise by passing white zero-mean circularly symmetric complex-Gaussian noise through a 3-tap linear filter with coefficients $\{0.3, 1, 0.3\}$. Fig. 4.1(a) with $(L, \beta) = (2049, 1)$ and Fig. 4.1(b) with $(L, \beta) = (65, 1)$ show the actual and design P_{fa}'s based on $M = 2000$ and 2000 Monte Carlo runs where the thresholds were based on χ_2^2 distribution of the respective test statistics. It is seen that for [59, 64], $(L, \beta) = (65, 1)$ works much better than the other choice; the choice $(L, \beta) = (2049, 10)$ was poor also (not shown). On the other hand the proposed approach needs no such parameters but needs L_n which was picked to be 5, and works quite well.

4.7.2 Example 2: Single Antenna Receiver, Colored Gaussian Noise, $K =$1 or 4, OFDM PU signal (IEEE 802.11a/g)

The primary signal is an OFDM signal satisfying IEEE 802.11a/g WLAN standard with number of subcarriers $N_c = 64$ and cyclic prefix of length $N_{cp} = 16$. The number of OFDM symbols were taken to be $N_{ofdm} = 50$ or 250 with the corresponding observation size of $M = N_{ofdm}(N_c + N_{cp}) = 4000$ or 20000. The subcarrier modulation was 64-QAM. The false alarm probability is 0.01 and all results are averaged over 2000 Monte Carlo runs. For PU signal detection we picked either $K = 1$ with $\alpha = 1/(N_c + N_{cp})$ and $\tau = N_c$, or $K = 4$ with

$\alpha = 1/N, 2/N$, and $\tau = \pm N_c$. We used colored Gaussian noise as in Example 1. The OFDM signal was passed through a constant gain channel. In applying the proposed test we set $L_n = 5$. In Fig. 4.2 we compare the theoretical performance based on (4.28) and (4.36) with the simulations-based performance for the proposed detector when $p = 1$ and the channel is unit gain. It is seen that the agreement between theory and simulations is excellent.

4.7.3 Example 3: Multi-antenna Receiver ($p = 1, 2, 4, 8$), OFDM PU signal (IEEE 802.11a/g), Colored Gaussian Noise, Rayleigh flat-fading channel, $K = 1, 2, 4$

We consider the example of Sec. 4.7.2 (64 subcarrier OFDM signal from IEEE 80211a/g WLAN standard) except with variable number of antennas (p), Rayleigh flat-fading sub-channels and independent colored Gaussian noise at each antenna. For PU signal detection we picked either $K = 1$ with $\alpha = 1/(N_c + N_{cp})$ and $\tau = N_c$, or $K = 4$ with $\alpha = 1/N, 2/N$ and $\tau = \pm N_c$, or $K = 2$ with two different combinations of cycle frequency and lags: $(\alpha, \tau) = (1/N, N_c), (2/N, N_c)$ or $(\alpha, \tau) = (1/N, N_c), (1/N, -N_c)$. In Figs. 4.3 and 4.4 we compare our proposed approach ($L_n = 5$) with that of [59], [64] or [73] (modified to handle nonconjugate CAFs, an extension of [59] to multiple antenna receiver) via simulations for $M = 20000$ (250 OFDM symbols) based on 2000 runs; for [59, 64, 73], we used a Kaiser smoothing window with parameters $(L_w, \beta) = (65, 1)$. It is seen in Figs. 4.3 and 4.4 that for $K = 4$ and any value of p, the approaches of [59, 64, 73] yield a much larger value of P_d than the design value 0.01 of P_{fa} at very low SNRs (-30 dB) whereas there is no such problem with our proposed approach; as SNR $\downarrow 0$, $\mathcal{H}_1$ becomes $\mathcal{H}_0$. This reflects the discussion of Sec. 4.7.1 regarding analytical threshold selection: our proposed detector does a much better job of yielding the design P_{fa} compared to the approaches of [59, 64, 73]. It is seen from Figs. 4.3 and 4.4 that the proposed approach is slightly superior (higher P_d for a given SNR) to [59, 64, 73] for every value of p and $K = 1$ and 2, discounting $K = 4$ for which P_{fa} is not maintained by [59, 64, 73]. Note also that there is an SNR advantage of about 2 dB (same P_d with a 2dB smaller SNR) in using $K = 4$ over $K = 1$, and about 1 dB in using $K = 2$

over $K = 1$, when $p = 1$, and a somewhat smaller advantage when p is larger. On the other hand, for a fixed value of K, each increase in the value of p by a factor of 2 (i.e. p from 1 to 2, or from 2 to 4, etc.), yields an SNR advantage of about 2dB.

Using the results of Table 4.1, we find that the approaches of [59, 64, 73] need 2.54, 3.05, 3.63 and 4.16 times more complex multiplications than the proposed approach for $p =$1, 2, 4 and 8, respectively, when $K = 1$, and 2.54, 3.05, 3.63 and 4.16 times more complex multiplications for $p =$1, 2, 4 and 8, respectively, when $K = 4$.

In Fig. 4.5 we compare our proposed detector with that of [76] under the same conditions as for Fig. 4.4(a). We implemented the detector of [76, Secs. III, V] and for our approach, we used a single lag and cycle frequency pair at $(\alpha, \tau) = (1/N, N_c)$. The test threshold for the detector of [76] was computed via simulations (based on 50000 runs) to achieve $P_{fa} = 0.01$. It is seen from Fig. 4.5 that the proposed approach significantly outperforms [76].

4.7.4 Example 4: Single Antenna Receiver, Colored Gaussian Noise, $K =$1, OFDM PU signal (WiMAX)

We now turn to comparison with the Tani-Fantacci test (2.30) [71]. Here we used an OFDM PU signal (similar to examples in [71]) satisfying WiMAX standard with QPSK subcarrier modulation, $N_c = 256$, $N_{cp} = 64$, $M = (N_c + N_{cp})256 = 81920$, $L = N_{cp} + 2$, $\alpha = 1/N$, $\tau = N_c$, $S_{bin} = 4$ (see Sec. 2.4); for shorter observation lengths (such as $M = 2000$), performance of [71] is erratic and poor, and is not shown here. In Fig. 4.6 we compare P_d performance (as a function of SNR for $P_{fa} = 0.05$) of the proposed test (4.31) with the Tani-Fantacci test (2.30) [71] under colored Gaussian noise (chosen as in Sec. 4.7.1). It is seen from Fig. 4.6 that the Tani-Fantacci test (2.30) yields a much lower actual P_{fa} than the design value of 0.05 when the theoretical expression provided in [71] is used; this results in a poorer P_d performance. We also selected the test threshold based on simulations (10000 Monte Carlo runs). This leads to an improved performance but it is still inferior to our

proposed test (about 3-4 dB SNR penalty to achieve the same performance). Simulation-based threshold selection for colored Gaussian noise is not practical since the noise correlation will not be known in practice and since the distribution of the test statistic is dependent upon the noise correlation (even asymptotically). Note that the analysis in [71] assumes white Gaussian noise.

4.7.5 Example 5: Multi-Antenna Receiver ($p = 4$), GSM GMSK PU signal, colored Gaussian Noise, $K = 1$

Now we consider a GMSK PU signal (GSM standard) with $N=2$ samples per symbol. We seek to detect the PU signal using conjugate CAF at the normalized cycle frequency $\alpha = \frac{1}{4}$ and lag $\tau = 0$. The channel was flat Rayleigh fading, with circularly symmetric complex Gaussian additive noise. Fig. 4.7 shows the P_d performance (as a function of SNR for $P_{fa} = 0.01$) of our proposed approach and that of [73] for Rayleigh fading channel based on 2000 runs when number of antennas $p = 4$ and $M=540$ (1 ms duration). For the approach of [73], we used Kaiser window with parameters $(\beta, L_w) = (1,65)$. As seen from Fig. 4.7, the performance of our proposed detector is slightly better than that of [73]. Using the results of Table 4.1 for conjugate CAFs, we find that the [73] needs 1.82 times more complex multiplications than the proposed approach for $M =540$; thus the proposed approach is to be preferred when both performance and computational complexity are considered.

4.7.6 Example 6: Computational Complexity

Here we compare computational complexity of various schemes using the analysis of Sec. 4.6. The complex multiplications counts are shown in Fig. 4.8 for varying sizes of observation length M when nonconjugate CAFs are used. It is seen that the computational complexity of the proposed approach is lower than that of [59, 64] in the single antenna case, and that of [73] for multiple antennas ($p=4$), by a factor of 2.0 to 6. (The length L of the frequency-domain Kaiser smoothing window needed in [59, 67, 64] was picked to be $L = 65$ whereas in

[64] it has been picked to be $L = 2049$ regardless of the sample size M which would result in still larger computational load for the approaches of [59, 64, 73].)

4.8   Conclusions

Detection of cyclostationary PU signals in colored Gaussian noise for cognitive radio systems was considered based on looking for single or multiple cycle frequencies at single or multiple time lags in the CAF of the noisy PU signal. We explicitly exploit the knowledge that under the null hypothesis of PU signal absent, the measurements originate from colored Gaussian noise with possibly unknown correlation. Our formulation allows us to simplify the spectrum sensing detector, and obviates the need for estimating an unwieldy covariance matrix needed in the Dandawate-Giannakis [59, 64] and related approaches. We considered both single and multiple antenna receivers and both nonconjugate and conjugate CAFs. A performance analysis of the proposed detectors was carried out. Supporting simulation examples were presented to compare our detectors with those of [59], [73], [64] and [71]. Our proposed approaches are computationally cheaper than the Dandawate-Giannakis and related approaches [59], [64], [73] while having quite similar detection performance for a fixed false alarm rate. Our proposed approach significantly outperforms [71].

(a)

(b)

Figure 4.1: Example 1. Analytical threshold selection performance: colored Gaussian noise, $M = 2000$, 2000 Monte Carlo runs. The approach labeled "Dandawate-Giannakis" is used in [59, 67, 64].
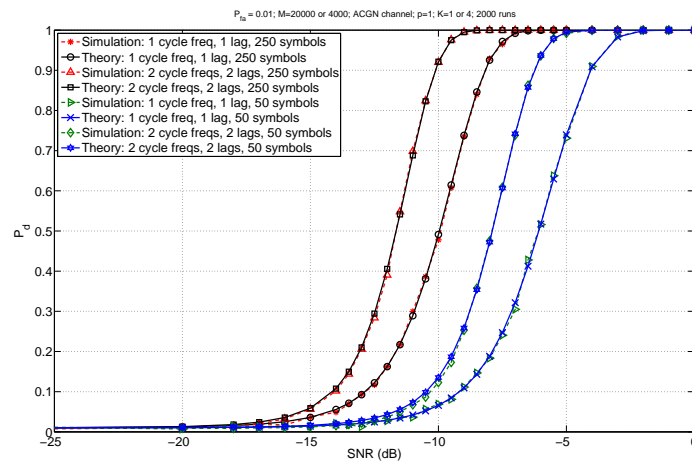
Figure 4.2: Example 2: Performance analysis: theoretical and simulation-based performance comparison of probability of detection P_d versus SNR for the proposed single-antenna spectrum sensing: OFDM signal, non-random channel with unit gain, 2000 runs, $P_{fa} = 0.01$, $p = 1$, $K = 1$ or 4, colored Gaussian noise, $M = 4000$ or 20000.
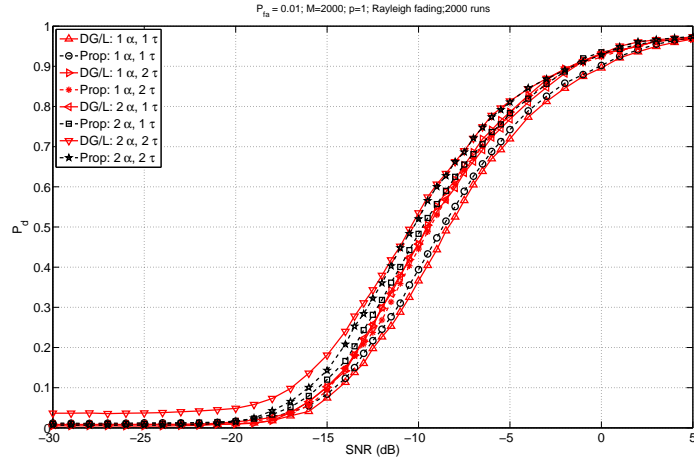
(a)
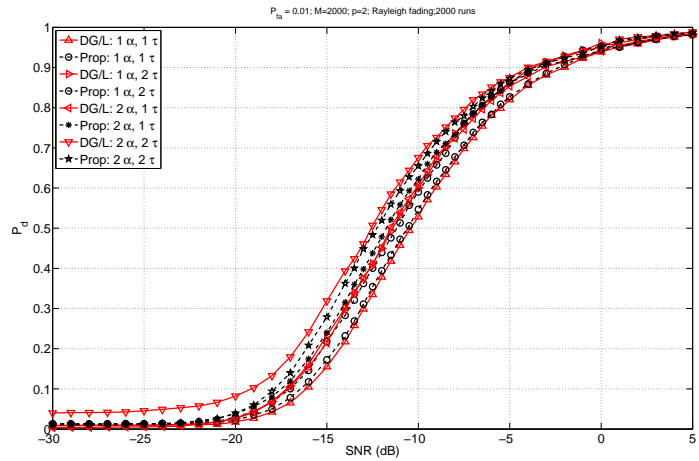
(b)

Figure 4.3: Example 3: Simulation-based comparison of P_d versus SNR with variable number of antennas: OFDM signal, $M = 20000$ (250 OFDM symbols), Rayleigh flat-fading channel, 2000 runs, $P_{fa} = 0.01$, $p = 1$ in (a) and $p = 2$ in (b), $K = 1$, 2 or 4, colored Gaussian noise. The approach labeled "DG/L" refers to the ones based on [59, 64, 73] and that labeled "prop" refers to our proposed detector. the labels "α" and "τ" refer to cycle frequency and lag, respectively.
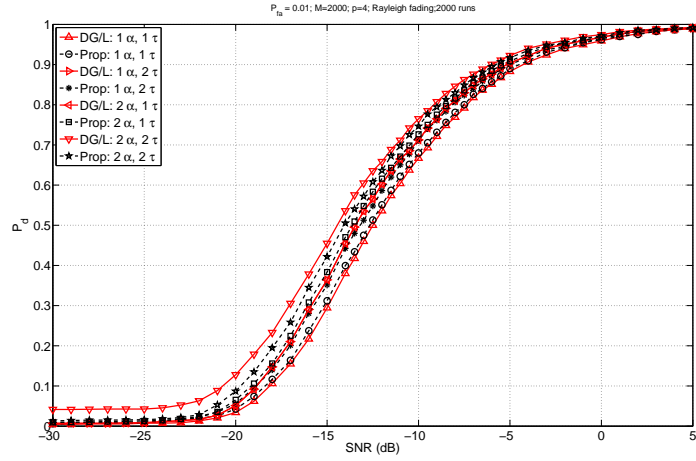
(a)
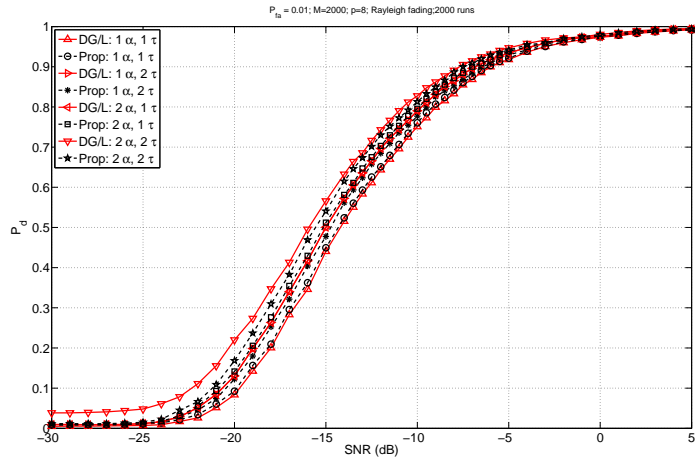
(b)

Figure 4.4: Example 3: Simulation-based comparison of P_d versus SNR with variable number of antennas: OFDM signal, $M = 20000$ (250 OFDM symbols), Rayleigh flat-fading channel, 2000 runs, $P_{fa} = 0.01$, $p = 4$ in (a) and $p = 8$ in (b), $K = 1$, 2 or 4, colored Gaussian noise. The approach labeled "DG/L" refers to the ones based on [59, 64, 73] and that labeled "Proposed" refers to our proposed detector.
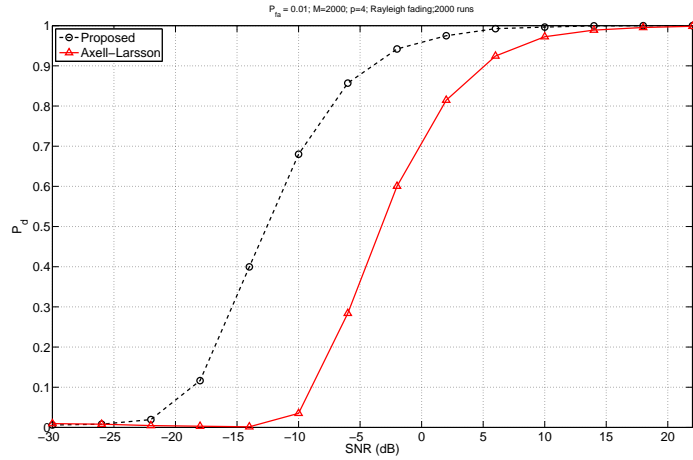
Figure 4.5: Example 3: Simulation-based comparison of P_d versus SNR with four antennas: OFDM signal, $M = 20000$ (250 OFDM symbols), Rayleigh flat-fading channel, 2000 runs, $P_{fa} = 0.01$. The approach labeled "Axell-Larsson" is from [76] and that labeled "Proposed" refers to our proposed detector.
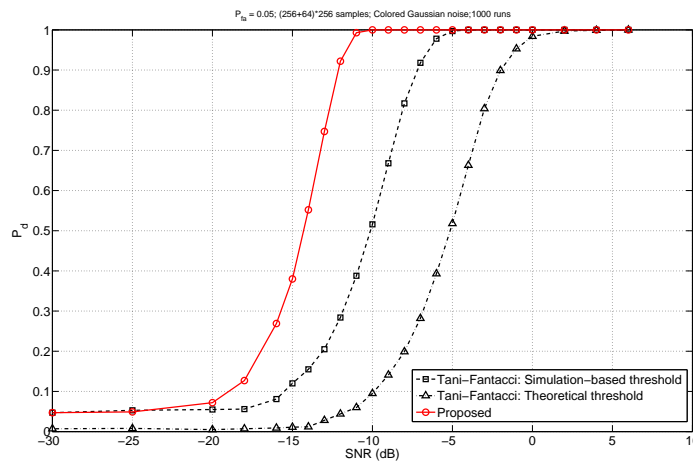
Figure 4.6: Example 4: Simulation-based comparison of P_d versus SNR with single antenna under non-random channel with constant gain: $P_{fa} = 0.05$, $p = 1$, $K = 1$, $M = 81920$, 2000 Monte Carlo runs, OFDM signal (number of subcarriers $N_c = 256$, cyclic prefix length $N_{cp} = 64$), colored Gaussian noise. The approach labeled "Tani-Fantacci" is that of [71].
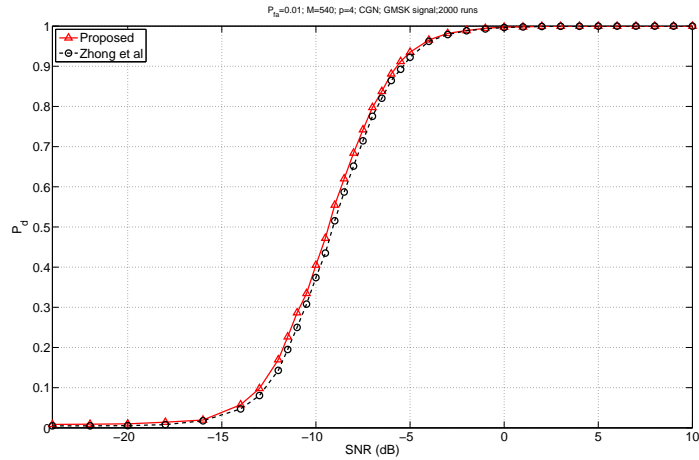
Figure 4.7: Example 4: Simulation-based comparison of probability of detection versus SNR for GMSK signal with 2 samples per symbol, with $p = 4$ antennas under Rayleigh flat-fading, colored Gaussian noise and $M = 540$: $P_{fa} = 0.01$, 2000 runs. The approach labeled "Zhong et al" is from [73].
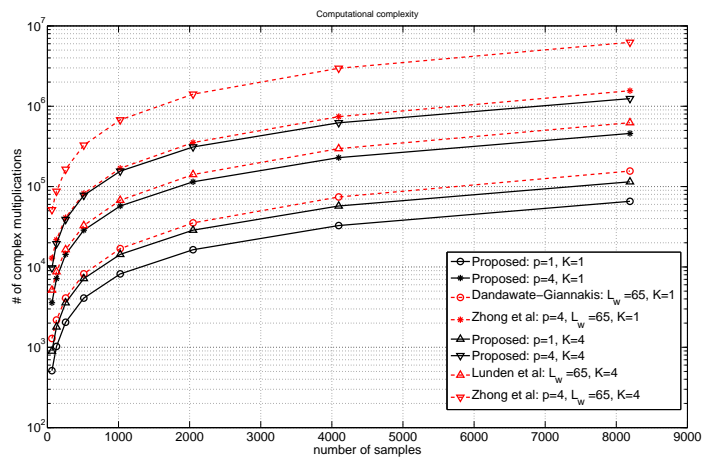
Figure 4.8: Example 5: Computational complexity of different spectrum sensing algorithms for varying sizes of observation length M, $(L, \beta) = (65, 1)$ when nonconjugate CAFs are used.

Chapter 5

Design of Sensing and Power Allocation Strategies for Energy Aware Multi-Channel

Cognitive Radio Networks

Frequency spectrum and energy are two key resources of green cognitive radio networks with battery-powered wireless terminals. The issues of how to utilize sparse frequency spectrum and limited energy resource pose challenges to the design of sensing and power allocation strategies that affect both throughput and energy consumption. In this chapter, we first construct an utility function that incorporates throughput as reward and energy consumption as cost for a time slotted multi-channel cognitive radio network. An optimization problem to maximize the utility function is formulated involving optimization of both sensing parameters (sensing duration, local test threshold) and power allocation strategy. The problem is non-convex, however, we decouple it into two separate convex problems and propose an iterative algorithm to obtain a suboptimal solution. The simulation results show that our iterative algorithm converges fast and performs better than a "only power allocation optimization" approach and an existing approach that ignores energy efficiency.

5.1   Introduction

The goal of cognitive radio is to alleviate the shortage of frequency spectrum for emerging wireless communication applications. To maximize spectrum utilization while maintaining an upper bound on the interference to licensed users, spectrum sensing is a key step of cognitive radio network (CRN) that identifies spectrum opportunity. Existing spectrum sensing techniques [56] include matched filter, energy detector [22] and feature detector [74]. On the other side, energy efficiency is an objective of green cognitive radio networks with battery for power supply [77] and has recently attracted more attention than before.

However, most current research on CRN focuses on sensing accuracy and maximization of throughput [56, 22, 78, 79]. This motivates the need for designing advanced power-aware spectrum sensing, MAC protocols and cross layer approaches such as PHY-MAC design.

In recent years, energy-aware spectrum sensing and access related research has been gaining importance when power limitation becomes a key feature of green CRN. In [80, 81], energy efficient sequential sensing is studied for multi-channel PU (primary user) networks. However, since SU (secondary user) can only sense and transmit on a single PU channel at a time, power allocation issues are not involved. An energy efficient power allocation and transmission duration design is proposed in [82] for multi-channel simultaneous transmission. It is assumed that the activity states (active or idle, ON or OFF) of slotted PU channels are independent and identically distributed. However, perfect sensing is assumed in [82], thus spectrum sensing optimization is not involved.

In [22], using periodic sensing, a sensing-throughput trade off optimization problem is formulated and the optimal sensing duration is proven to exist based on energy detection. Joint optimization of soft-decision cooperative spectrum sensing, channel access strategy and power allocation is proposed in [79] for an overlay multichannel cognitive radio networks. The optimization aims to maximize the secondary users' sum instantaneous throughput with constraints on interference to primary users. Ref. [78] investigates a single SU and multiple channel CRN where the SU can sense and access multiple PU channels simultaneously. To maximize the overall throughput, an optimization problem involving joint optimization of sensing duration, sensing detector threshold and transmit power allocation is formulated under constraints on interference to the PU network and total transmit power over multiple channels. However, energy consumption is considered in none of [22, 79, 78].

Energy consumption is considered as a constraint in constrained throughput optimization in [80, 83]. In [80], a limited energy budget is allocated to sensing, probing for channel quality and data transmission, and the variables associated with these factors are then jointly optimized to maximize the achievable average throughput of the secondary users in a

CRN composed of multiple PU channels. In [83] distributed sensing and access strategies for opportunistic spectrum access under constraints on energy consumption by the SUs and interference probability to the PU, is formulated as a sequential decision making problem in the framework of partially observable Markov decision processes for a slotted PU network. However, the sensing duration optimization and power allocation are not discussed in [80, 83].

Energy consumption is incorporated into the optimization problems in [84, 82, 85, 81]. Ref. [84] considers designing optimal sensing policy to maximize the expected reward that rewards potential transmission throughput and penalizes energy consumption in sensing and transmission. The optimization problem is formulated under a partially observable Markov decision process formulation, but power allocation for SU transmission is not considered in [84]. An energy efficient power allocation and transmission duration optimization is proposed in [82] for multi-channel simultaneous transmission in a slotted CRN. However, perfect sensing is assumed in [82], thus spectrum sensing optimization is not involved. Ref. [85] studies how to choose sensing duration to balance energy consumption and system throughput. An utility function incorporating throughput as reward and energy consumption as penalty is formulated to find optimal sensing duration under a collision probability constraint for PU protection. However, only single PU channel is considered and power allocation issues are omitted. Maximizing energy efficiency is considered in [81] for a CRN in which a secondary user sequentially senses multiple licensed PU channels before it transmits on one idle PU channel. Energy consumption includes consumption during sensing and transmission. Sensing strategy deciding when to stop sensing and transmitting, and power level allocation for transmission are jointly considered. The optimization problem is formulated as a sequential decision-making problem. An alternative parametric formulation of the original optimization problem is proposed to solve the posed problem, which rewards throughput and penalizes

energy consumption. However, the sensing duration and sensing test threshold are not optimized. Moreover, power allocation for multiple channel simultaneous transmission is not considered as the SU is allowed to transmit only over one channel.

For balancing throughput maximization and energy consumption minimization in multiple channels CRN, joint design of spectrum sensing and power allocation has rarely been explored in the literature; this is the topic of this chapter. Based (partially) on the approaches of [85, 81] and [82], we consider both sensing and power allocation optimization for simultaneous multiple channel sensing and transmission. We aim to design spectrum sensing parameters (sensing duration, local test threshold) and power allocation strategy to balance throughput and energy consumption.

In this chapter, we consider a CRN composed of a single SU and multiple PU channels. We assume that the primary users access the PU channels in a synchronous time slot structure [86, 87]. The activity states of the PU channels are independent from each other and are constant during one slot. One SU can sense all PU channels simultaneously with wide-band spectrum sensor at the beginning of each slot. Then the SU can access multiple idle PU channels using advanced spectrum access technology such as OFDM.

Sensing duration, local test threshold and power allocation will affect both throughput and energy consumption. Long sensing duration means high detection accuracy, thus probability of collision with PU and related energy consumption for collided transmission are reduced. However, longer sensing duration also means shorter potential transmission time for SU. How to balance power allocation among different idle PU channels determines how effectively the temporal transmission opportunity and limited power budget is exploited. By treating effective throughput as reward and energy consumption as cost, we first propose an utility function that incorporates throughput and energy consumption with a price weight. The energy consumption includes sensing and transmission energy consumption where we only consider effective transmission throughput without collision with PU. The sensing duration, local test threshold and power allocation strategy are the optimization parameters to

maximize the utility function. The utility function is non-convex, however, we decouple it into two separate convex problems and propose an iterative algorithm to obtain suboptimal solutions. Both sensing parameters (sensing duration, local test threshold) and power allocation are optimized under flat fading channel condition, total transmission power constraint and interference constraint to protect PU activity.

Notation: Complex scalar h_{pm} denotes the flat fading coefficient of subchannel m from the PU on subchannel m (if active) to the SU sensing subchannel m while h_{sm} is the flat fading coefficient of subchannel m from the SU transmitter to SU receiver on subchannel m. In the following h_{pm} and h_{sm} are assumed to be known before the SU senses subchannel m. $\sigma_{x_m}^2$ is the power of received PU signal on subchannel m. σ^2 is the noise power on each subchannel. σ^2 and $\sigma_{x_m}^2$ are assumed to be perfectly known a priori. Nonnegative real ρ denotes the energy price and $[x]^+ := max(x, 0)$. x^* is the optimal value for x optimizing some function of x. P_{tot} is the total transmit power constraint. $P_{d_{min}}$ denotes the minimum detection probability requirement and $P_{f_{max}}$ denotes the maximum allowable false alarm probability for spectrum sensing. $T_{s_{min}}$ is the lower bound on sensing duration T_s. $P\{\cdot\}$ denotes probability of an event $\{\cdot\}$.

5.2 System Model

In this chapter, we consider a CRN composed of single SU and M_p PU channels. We assume the primary users access the PU channels in a synchronous time slotted structure of duration T [86]. The activities of PU on each channels stay either idle or busy during one slot, and are independent from each other. The SU senses and accesses PU channels in a slotted manner synchronized to the PU network. We assume the maximum allowable sensing duration is $T/2$, which is reasonable considering sparsity of transmission duration for SU. At the beginning of each slot, SU senses all M_p PU channels with duration T_s. If the sensing result shows the channel is idle, SU will access the channel in the rest of the slot and the transmission time is $T - T_s$. If the sensing result shows the channel is busy, SU will not

access the channel in this slot and will wait for the next slot to sense again. All the channel gains either between PU and SU or between SU transmitter and receiver pair are assumed to be known a priori. Knowledge of the average noise power and signal power of PU on each PU channel is assumed to be available.

5.2.1 Primary network

Consider a cognitive radio network consisting of M_p PU channels. For simplicity we assume that all channels have the same bandwidth (this assumption is not essential) and each of them occupies a bandwidth of B Hz. The primary users access these channels in a synchronized slotted manner, each slot of duration T. Assume that the activity states of PU on each channel stays constant, either idle or busy, and are independent on different PU channels and time slots. Let $S = [s_1, s_2, ..., s_{M_p}]$ denote the channel activity state vector, of which s_m is the state of mth PU channel on a single slot; $s_m = 0$ and $s_m = 1$ denote mth channel is idle or busy, respectively. Let π_{0m} and π_{1m} be the stationary probabilities that the mth channel is idle and busy, respectively:

$$\pi_{0m} = P\{s_m = 0\},$$
$$\pi_{1m} = P\{s_m = 1\}. \tag{5.1}$$

5.2.2 Spectrum Sensing

Similar to [78], with wide-band spectrum sensing, there are N (time-)samples for each PU channel. Let $y_m[n]$ be the received signal at mth ($1 \leq m \leq M_p$) PU channel at the nth ($1 \leq n \leq N$) sampling instant. A binary hypothesis test is performed by the SU to decide whether any PU activity is present

$$H_{1m}: \quad y_m[n] = h_{pm}x_m[n] + w_m[n],$$
$$H_{0m}: \quad y_m[n] = w_m[n]. \tag{5.2}$$

H_{1m} and H_{0m} denote hypotheses that the activity state of PU at the mth channel is $s_m = 1$ and $s_m = 0$, respectively. $x_m[n]$ is the PU signal at mth channel and nth sampling instant, which is assume to be i.i.d. white with mean zero and variance $\sigma_{x_m}^2$. The noise $w_m[n]$ is assumed to be circularly symmetric complex Gaussian distributed with zero mean and variance σ^2, for all M_p PU channels. Complex-valued flat channel fading coefficient h_{pm} stays constant during the entire slot. The average SNR of PU signal on mth channel received by SU during one slot is deduced as $\gamma_m = \frac{|h_{pm}|^2 \sigma_{x_m}^2}{\sigma^2}$.

With energy detector [22], the sensing test statistic L_m is defined as

$$L_m = \frac{1}{N} \sum_{n=1}^{N} |y_m[n]|^2. \tag{5.3}$$

Suppose the sensing frequency (number of samples per second) is f_s. Based on [22], the false alarm probability P_{f_m} and detection probability P_{d_m} are given by

$$P_{f_m} = Q\left(\left(\frac{\varepsilon_m}{\sigma^2} - 1 \right) \sqrt{T_s f_s} \right), \tag{5.4}$$

$$P_{d_m} = Q\left(\left(\frac{\varepsilon_m}{\sigma^2} - \gamma_m - 1 \right) \sqrt{\frac{T_s f_s}{2\gamma_m + 1}} \right) \tag{5.5}$$

where ε_m is local test threshold at mth channel detector and $Q(x) = \frac{1}{\sqrt{2\pi}} \int_x^\infty e^{-\frac{t^2}{2}} dt$. Based on (5.4) and (5.5), we can express P_{f_m} as a function of T_s and P_{d_m} as

$$P_{f_m} = Q\left(\sqrt{2\gamma_m + 1} Q^{-1}(P_{d_m}) + \gamma_m \sqrt{T_s f_s} \right). \tag{5.6}$$

Based on the energy detector's result, we acquire the estimated channel states as $\hat{S} = [\hat{s}_1, \hat{s}_2, \ldots, \hat{s}_{M_p}]$, of which $\hat{s}_m = 0$ and $\hat{s}_m = 1$ represent the event mth PU channel is detected

as idle or busy, respectively. The relation between s_m and $\hat{s}_m$ is given by

$$P\{\hat{s}_m = 0 | s_m = 0\} = 1 - P_{f_m}, \ \ P\{\hat{s}_m = 1 | s_m = 0\} = P_{f_m}, \tag{5.7}$$

$$P\{\hat{s}_m = 0 | s_m = 1\} = 1 - P_{d_m}, \ \ P\{\hat{s}_m = 1 | s_m = 1\} = P_{d_m}. \tag{5.8}$$

For protection of PU at each PU channel, the detection probability at the SU is required to have a lower bound $P_{d_{min}}$. Similarly, we impose an upper bound $P_{f_{max}}$ on the false alarm probability. In a realistic CRN scenario, it is required that $P_{f_{max}} \le 0.5$ and (hopefully) $P_{d_{min}} \ge 0.9$. In this chapter, we assume that the spectrum sensing detector is designed is to keep the detection probability to be equal to the minimum requirement $P_{d_{min}}$ in order to protect PU activities, resulting in an upper bound of $1 - P_{d_{min}}$ on the collision probability (both SU and PU transmit simultaneously). On the other hand, we aim to minimize the false alarm probability P_{f_m} with the upper bound $P_{f_{max}}$ to obtain more transmission opportunity for SU when PU is inactive on mth channel. Therefore, the relevant constraints are as follows

$$P_{d_m} = P_{d_{min}} \ \text{and} \ P_{f_m} \le P_{f_{max}} \tag{5.9}$$

where $m = 1, 2, \ldots, M_p$.

We first clarify the range of sensing duration T_s. First we need to demonstrate that $Q(x)$ is a monotonically decreasing function with $Q(0) = 0.5$. With a fixed $P_{d_{min}}$, it follows from (5.6) that the constraint $P_{f_m} \le P_{f_{max}} < 0.5$ implies

$$\gamma_m \sqrt{T_s f_s} + Q^{-1}(P_{d_{min}})\sqrt{2\gamma_m + 1} > 0, \quad m = 1, \ldots, M_p. \tag{5.10}$$

The minimum sensing duration $T_{s_{m,min}}$ for the mth PU channel that satisfies (5.9) is given by

$$T_{s_{m,min}} = (Q^{-1}(P_{d_{min}}))^2 \frac{2\gamma_m + 1}{(\gamma_m)^2 f_s}, \quad m = 1, 2, \ldots, M_p. \tag{5.11}$$

As noted earlier in the chapter, the upper bound on T_s is $T/2$. For those PU channels that need $T_{s_{m,min}} > T/2$, we would not transmit and allocate any power to them since their sensing requirement can not be met within the $T/2$ sensing duration. Let the set $\mathcal{O}$ denote the set of PU channels for which $T_{s_{m,min}} \leq T/2$, and let the size (number of elements) of $\mathcal{O}$ be M. For convenience, we (re-)index the PU channels in $\mathcal{O}$ as ranging over $1, 2, \ldots, M$. Consequently, the lower bound for T_s is deduced as

$$T_{s_{min}} = \max_{1 \leq m \leq M}(T_{s_{m,min}}). \tag{5.12}$$

with T_s picked to be $T_s \in (T_{s_{min}}, \frac{T}{2}]$.

5.2.3 Spectrum Access

The access strategy is that the SU will only transmit on the mth PU channel that is detected as idle ($1 \leq m \leq M$), and the SU's transmission on this channel is allocated transmit power $P_m \geq 0$. Under the channel gain $|h_{sm}|^2$ and channel noise with power σ^2, the potential achievable rate R_m bps/Hz (instantaneous capacity) on the mth idle PU channel is given by

$$R_m = B \log_2(1 + \frac{|h_{sm}|^2 P_m}{\sigma^2}). \tag{5.13}$$

The sum of SU's transmission power over various channels has an upper bound of P_{tot}. Let P_m denote the power allocated to the mth PU channel for SU's transmission. Then we must have

$$\sum_{m=1}^{M} P_m \leq P_{tot}. \tag{5.14}$$

5.3 Problem Formulation

5.3.1 Throughput and Energy Consumption

In this chapter, we consider energy consumed during sensing and transmission, and the effective throughput when a PU's absence on the mth channel is correctly detected. Since PU's activity on M channels are independent, we analyze the energy consumption and throughput on the mth PU channel under the following four cases. Assume the power consumed during sensing is P_s.

- **Case 1** $(s_m, \hat{s}_m) = (0, 0)$: Under hypothesis H_0, PU is detected as absent, and the SU data is successfully transmitted after sensing. The throughput is $(T - T_s)R_m$. The energy consumed due to sensing is $P_s T_s$ and energy consumed during transmission is $P_m(T - T_s)$. The probability for this case is $\pi_{0m}(1 - P_{f_m})$.

- **Case 2** $(s_m, \hat{s}_m) = (0, 1)$: Under hypothesis H_0, PU is detected as present due to false alarm. Based on the spectrum access policy, there would be no SU transmission. As a result the effective throughput and energy consumed during transmission are both 0. The energy consumed during sensing is $P_s T_s$, and the probability for this case is $\pi_{0m}P_{f_m}$.

- **Case 3** $(s_m, \hat{s}_m) = (1, 0)$: Under hypothesis H_1, PU is detected as absent (inactive). The SU would transmit data but it would collide with the PU signal. We assume the SU receiver can not correctly decode the collided data, so there is no effective throughput. The energy consumed during sensing and collided transmission is $P_s T_s$ and $P_m(T - T_s)$, respectively. The probability for this case is $\pi_{1m}(1 - P_{d_m})$.

- **Case 4** $(s_m, \hat{s}_m) = (1, 1)$: Under hypothesis H_1, PU is detected as present (active). Thus no SU data is transmitted after sensing. The throughput and energy consumed are the same as in *case 2*. The probability for this case is $\pi_{1m}P_{d_m}$.

Based on the above four cases, the achievable throughput during one slot duration is given by

$$C = \sum_{m=1}^{M} R_m(T - T_s)\pi_{0m}(1 - P_{f_m}) \tag{5.15}$$

and the potential energy consumption during one slot is deduced as

$$E = P_s T_s + \sum_{m=1}^{M} P_m(T - T_s)[\pi_{0m}(1 - P_{f_m}) + \pi_{1m}(1 - P_{d_m})]. \tag{5.16}$$

We are interested in choosing $T_s, \{\varepsilon_m\}, \{P_m\}$ to balance throughput C maximization and energy consumption E minimization. Inspired by [84, 85, 81], we aim to formulate an utility function that incorporates throughput as reward and energy consumption as cost. Assuming an unit energy price ρ, the energy consumption cost is given by ρE while the throughput reward is C. With high energy price ρ, energy consumption minimization gains more importance than throughput, wheres with low ρ, we pay more attention to throughput maximization while reducing the importance of energy consumption. To balance the throughput and energy consumption, we define an utility function $U_G(T_s, \{\varepsilon_m\}, \{P_m\}) = C - \rho E$, which should be maximized to balance throughput maximization and energy consumption minimization:

$$\begin{aligned} U_G&(T_s, \{\varepsilon_m\}, \{P_m\}) \\ &= \sum_{m=1}^{M} \Big[(B \log_2\Big(1 + \frac{|h_{sm}|^2 P_m}{\sigma^2}\Big) - \rho P_m)\pi_{0m}(1 - P_{f_m}) \\ &\quad - \rho P_m \pi_{1m}(1 - P_{d_m}) \Big](T - T_s) - \rho P_s T_s. \end{aligned} \tag{5.17}$$

We wish to find optimal energy-aware sensing parameters and power allocation set $(T_s, \{\varepsilon_m\}, \{P_m\})$ to maximize the utility function subject to (s.t.) all relevant constraints. This

optimization problem is

$$\textbf{Problem P1:} \quad \max_{T_s, \{\varepsilon_m\}, \{P_m\}} U_G(T_s, \{\varepsilon_m\}, \{P_m\})$$

$$s.t. \quad P_{d_m} = P_{d_{min}} \; \forall m$$

$$P_{f_m} \le P_{f_{max}} \; \forall m$$

$$P_m \ge 0 \; \forall m$$

$$\Sigma_{m=1}^{M} P_m \le P_{tot}. \tag{5.18}$$

[We note that this is the parametric formulation in [81] where the ultimate goal is to maximize energy efficiency defined as bits per sec per Joule. In this chapter we use $U_G(T_s, \{\varepsilon_m\}, \{P_m\})$ as defined above to retain more flexibility compared to [81] where an unique price ρ leads to maximization of their energy efficiency metric.] This utility function is non-convex in $T_s, \{\varepsilon_m\}, \{P_m\}$, thus an optimal set $(T_s, \{\varepsilon_m\}, \{P_m\})$ may exist but there is no obvious effective way to find it. However, we can decouple this problem into two separate optimization problems each one of them is convex. Based on the separate convex problems, we propose an iterative optimization approach to find locally optimal solution $(T_s, \{\varepsilon_m\}, \{P_m\})$. The two optimization problems are detailed in the following section.

5.4 Iterative Algorithm for optimizing Sensing Parameters and Power Allocation

5.4.1 Power Allocation Optimization

With a fixed $(T_s, \{\varepsilon_m\})$ satisfying $P_{d_m} = P_{d_{min}}$ and $P_{f_m} \le P_{f_{max}}$, it is easy to prove that $U_G(T_s, \{\varepsilon_m\}, \{P_m\})$ is strictly convex in $\{P_m\}$ ($m = 1, \ldots, M$. With fixed P_s, T_s, ρ and T, the term $-\rho P_s T_s$ and the coefficient $T - T_s$ in $U_G(T_s, \{\varepsilon_m\}, \{P_m\})$ are both constants. Ignoring the fixed terms, we only consider the remaining part $U_P(\{P_m\})$ of the original utility

function, defined as

$$U_P(\{P_m\}) = \sum_{m=1}^{M} \Big[(B \log_2(1 + \frac{|h_{sm}|^2 P_m}{\sigma^2}) - \rho P_m) \pi_{0m}(1$$

$$- P_{f_m}) - \rho P_m \pi_{1m}(1 - P_{d_m}) \Big]. \tag{5.19}$$

The corresponding optimization problem is reformulated as

$$\textbf{Problem P2:} \quad \max_{P_m} \quad U_P(\{P_m\}) \tag{5.20}$$

$$s.t. \quad P_m \geq 0,$$

$$\sum_{m=1}^{M} P_m \leq P_{tot}$$

With λ denoting the (non-negative) Lagrange multiplier, the Lagrangian function $\mathcal{L}(\lambda)$ to be minimized is given by

$$\mathcal{L}(\lambda) = \sum_{m=1}^{M} \Big[\Big(\rho P_m - B \log_2(1 + \frac{|h_{sm}|^2 P_m}{\sigma^2}) \Big) \pi_{0m}(1 - P_{f_m})$$

$$+ \rho P_m \pi_{1m}(1 - P_{d_m}) \Big] + \lambda \Big(\sum_{m=1}^{M} P_m - P_{tot} \Big). \tag{5.21}$$

The second-order partial derivatives of the objective function are given by

$$\frac{\partial^2 U_P(\{P_m\})}{\partial P_m^2} = \frac{-B \pi_{0m}(1 - P_{f_m})}{\Big(\frac{\sigma^2}{|h_{sm}|^2} + P_m \Big)^2 \ln 2}, \tag{5.22}$$

$$\frac{\partial^2 U_P(\{P_m\})}{\partial P_{m_1} \partial P_{m_2}} = 0 \quad \forall m_1 \neq m_2 \tag{5.23}$$

where $1 \leq m, m_1, m_2 \leq M$. Since $P_{f_m} \leq P_{f_{max}} < 1$, it follows that the Hessian $\nabla^2 U_P(\{P_m\})$ is negative-definite, implying that $U_P(\{P_m\})$ is concave in $\{P_m\}$ [88].

With a fixed λ, the optimal power allocation is obtained by solving $\frac{\partial \mathcal{L}}{\partial P_m} = 0$ to obtain

$$P_m = \left[\frac{B\pi_{0m}(1 - P_{f_m})}{\{\rho[\pi_{0m}(1 - P_{f_m}) + \pi_{1m}(1 - P_{d_m})] + \lambda\} \ln 2} - \frac{\sigma^2}{|h_{sm}|^2} \right]^+, \quad \forall m = 1, \ldots, M. \tag{5.24}$$

Let $\{P_m^*\}$ and λ^* denote the optimal power allocation and optimal value of the Lagrange multiplier λ. then the optimal solution must satisfy the Karush-Kuhn-Tucker (KKT) conditions [88]

$$\sum_{m=1}^{M} P_m^* - P_{tot} \leq 0, \tag{5.25}$$

$$\lambda^* \geq 0, \tag{5.26}$$

$$\lambda^* (\sum_{m=1}^{M} P_m^* - P_{tot}) = 0, \tag{5.27}$$

$$\left[\rho - \frac{B}{(\sigma^2/|h_{sm}|^2 + P_m^*) \ln 2} \right] \pi_{0m}(1 - P_{f_m})$$

$$+ \rho\pi_{1m}(1 - P_{d_m}) + \lambda^* = 0 \tag{5.28}$$

where $m = 1, \ldots, M$.

The "maximum" power allocation is $\{P_m^*\}|_{\lambda^*=0}$ (P_m^* is P_m given by (5.24) with λ replaced with λ^*), which is the optimal solution for problem **P2** without any transmit power constraints. As a result, when the total power constraint P_{tot} is not less than $\Sigma_{m=1}^{M} P_m^*|_{\lambda^*=0}$, based on (5.27) and (5.26), $\lambda^* = 0$ and the resulting optimal power allocation is $\{P_m^*\}|_{\lambda^*=0}$. When $P_{tot} < \Sigma_{m=1}^{M} P_m^*|_{\lambda^*=0}$, based on (5.25), (5.26) and (5.27), the optimal $\lambda^* > 0$ implying that $\Sigma_{m=1}^{M} P_m^* - P_{tot} = 0$. Note that $\Sigma_{m=1}^{M} P_m^* - P_{tot}$ is a subgradient of $\mathcal{L}$ w.r.t. λ, $\partial_\lambda \mathcal{L} = \Sigma_{m=1}^{M} P_m - P_{tot}$, evaluated at $P_m = P_m^*$. Since the optimal λ^* minimizes the Lagrange dual function, we must have $\partial_\lambda \mathcal{L}|_{\lambda=\lambda^*, P_m=P_m^*} = 0$. Since there is only single Lagrange multiplier λ, we use line search for the optimal λ^* that satisfies $\partial_\lambda \mathcal{L}|_{\lambda=\lambda^*, P_m=P_m^*} = 0$. The transmit

power P_m is related to λ via (5.24). The lower limit for the line search is $\lambda = 0$ such that $\partial_\lambda \mathcal{L} > 0$ and the upper-limit is any positive value for which $\partial_\lambda \mathcal{L} < 0$.

5.4.2 Optimization of Sensing Parameters T_s and ε_m

With fixed power allocation P_m $(m = 1, \ldots, M)$ that satisfies $\sum P_m \leq P_{tot}$ and $P_m \geq 0$, we aim to find optimal sensing parameters T_s and $\{\varepsilon_m\}$. Since our sensing policy is to keep detection probability $P_{d_m} = P_{d_{min}} \geq 0.9$ and minimize false alarm probability $P_{f_m} \leq P_{f_{max}} < 0.5$, the local test threshold $\{\varepsilon_m\}$ is a function of T_s and $P_{d_{min}}$, based on (5.5). As a result, we just have to optimize w.r.t. sensing duration T_s.

Set $P_{d_m} = P_{d_{min}}$ into $U_G(T_s, \{\varepsilon_m\}, \{P_m\})$ in problem **P1** and reformulate it as below

$$
\begin{aligned}
U_G&(T_s, \{\varepsilon_m\}, \{P_m\}) \\
&= \sum_{m=1}^{M} \left[\left(B \log_2(1 + \frac{|h_{sm}|^2 P_m}{\sigma^2}) - \rho P_m \right) \right. \\
&\quad \times \pi_{0m}(1 - P_{f_m})(T - T_s) \\
&\quad \left. - \rho P_m \pi_{1m}(1 - P_{d_{min}})(T - T_s) - \rho \frac{P_s}{M} T_s \right]
\end{aligned}
\tag{5.29}
$$

where P_{f_m} is defined in (5.6). With a fixed power allocation $\{P_m\}$, energy price ρ, stationary channel state distribution $\{\pi_{0m}\}, \{\pi_{1m}\}$ and channel noise power σ^2, we define the following constants for convenience to formulate the optimization problem for T_s:

$$
c_{1m} \quad := \left[B \log_2 \left(1 + \frac{|h_{sm}|^2 P_m}{\sigma^2} \right) - \rho P_m \right] \pi_{0m},
\tag{5.30}
$$

$$
c_{2m} \quad := \rho P_m \pi_{1m}(1 - P_{d_{min}}),
\tag{5.31}
$$

$$
c_3 \quad := \rho \frac{P_s}{M}.
\tag{5.32}
$$

Obviously, $\{c_{2m}\}$ and c_3 are all positive. We will assume that the value of ρ is such that $\{c_{1m}\}$ is positive for all m. We need this condition for Lemma 1 to hold true. Intuitively,

if this condition is not satisfied, then we lose any rationale for SU transmission because c_{1m} represents the reward we obtain from balancing throughput and energy consumption during transmission on the mth PU channel.

While $\{\varepsilon_m\}$ can be expressed as a function of T_s and $P_{d_{min}}$ based on (5.5), we transform optimization in problem **P1** into optimization of $U_s(T_s)$ that only relies on T_s, as follows:

$$\textbf{Problem P3:} \; \max_{T_s} U_s(T_s) = \sum_{m=1}^{M}[c_{1m}(T-T_s)(1-P_{f_m})$$

$$- c_{2m}(T-T_s) - c_3 T_s] \tag{5.33}$$

$$s.t. \quad P_{f_m} \leq P_{f_{max}}$$

$$P_{d_m} = P_{d_{min}}$$

where $m = 1, 2, \ldots, M$ and P_{f_m} is a function of T_s with fixed $P_{d_{min}}$ as in (5.6).

Now we prove that $U_s(T_s)$ is a concave function in T_s in its range $(T_{s_{min}}, T/2]$. First, we define u_m as the utility function for the mth PU channel

$$u_m = c_{1m}(T-T_s)(1-P_{f_m}) - c_{2m}(T-T_s) - c_3 T_s. \tag{5.34}$$

Lemma 1 . The utility function u_m is a concave function in $T_s \in (T_{s_{min}}, \frac{T}{2}]$.

Proof: Based on [22], P_{f_m} in (5.6) is decreasing and convex in $T_s \in (T_{s_{min}}, \frac{T}{2}]$ when $P_{f_m} \leq P_{f_{max}} < 0.5$. We calculate the second partial derivative of u_m w.r.t. T_s as

$$\frac{\partial^2 u_m}{\partial T_s^2} = 2c_{1m}\frac{\partial P_{f_m}}{\partial T_s} - c_{1m}(T-T_s)\frac{\partial^2 P_{f_m}}{\partial T_s^2}. \tag{5.35}$$

Since $c_{1m} > 0$ and P_{f_m} is decreasing and convex in T_s, we have

$$\frac{\partial^2 u_m}{\partial T_s^2} < 0. \tag{5.36}$$

Thus u_m is concave in $T_s \in [T_{s_{min}}, \frac{T}{2}]$ $\quad \square$

Since sum of concave functions is concave [88] and $U_s(T_s) = \sum_{m=1}^{M} u_m$, it follows that $U_s(T_s)$ is concave in T_s. Then we can use line search on $[T_{s_{min}}, \frac{T}{2}]$ to obtain the optimal T_s and corresponding $\{\varepsilon_m\}$ that satisfies $P_{d_m}|_{T_s, \varepsilon_m} = P_{d_{min}}$.

5.4.3 Iterative algorithm for power allocation and sensing parameters optimization

First we use an initial sensing duration and test threshold set that satisfies the interference constraints $P_{d_m} = P_{d_{min}}$ and $P_{f_m} < P_{f_{max}}$. Then we use the Lagrange optimization method to obtain the optimal power allocation. Second, based on power allocation results, we further optimize T_s and ε_m using convex optimization. Repeat these two steps until maximum iteration number or the improvement is below a predefined threshold. First choose a random initial $T_s \in (T_{s_{min}}, \frac{T}{2}]$, then choose initial local test threshold ε_m that satisfies $P_{d_m} = P_{d_{min}}$. The initial power allocation strategy is an equal allocation such that $P_m = \frac{P_{tot}}{M}$ with $m = 1, 2, \ldots, M$. Let i denote step sequence number; $(T_{s,i}, \{\varepsilon_{m,i}\}, \{P_{m,i}\})$ denote the optimal spectrum sensing parameters set in ith step. The iterative optimization algorithm is detailed below.

ITERATIVE OPTIMIZATION ALGORITHM

1) Set $i = 0$ and initialize $(T_{s,i}, \{\varepsilon_{m,i}\}, \{P_{m,i}\})$.

2) Use the Lagrange optimization method to solve the convex optimization problem **P2** for optimal power allocation $\{P_m^*\}$ based on $(T_{s,i}, \{\varepsilon_{m,i}\})$.

3) For the fixed power allocation $\{P_m^*\}$, apply the convex optimization method of Sec. 5.4.2 to find a stationary point T_s^* and ε_m^* to maximize the utility function $U_s(T_s)$ in problem **P3**.

4) Set $(T_{s,i+1}, \{\varepsilon_{m,i+1}\}, \{P_{m,i+1}\})=(T_s^*, \{\varepsilon_m^*\}, \{P_m^*\})$. If the improvement of utility function $U_G(T_{s,i+1}, \{\varepsilon_{m,i+1}\}, \{P_{m,i+1}\})$ compared with $U_G(T_{s,i}, \{\varepsilon_{m,i}\}, \{P_{m,i}\})$ in problem **P1** is less than a predefined threshold or if the algorithm reaches a maximum number of iterations, then stop, else go back to step 2.

5.5 Simulation Examples

Consider a wideband CRN composed of $M_p = 8$ "narrowband" PU channels. The slot in the slotted system has a fixed length $T = 100$ms. Assume the primary user idle probabilities on each channel are $\pi_0 = [0.7, 0.5, 0.8, 0.7, 0.6, 0.9, 0.5, 0.7]$. The sampling rate of energy detection is $f_s = 6$M samples/s. The noise power is $\sigma^2 = -40$dBW. The minimum required detection probability is $P_{d_{min}} = 0.9$ and maximum false alarm probability is $P_{f_{max}} < 0.5$. The channel power gains $|h_{sm}|^2$ and $|h_{pm}|^2$ are all ergodic, stationary and exponentially distributed with mean of 1, but they are independent from each other. The average SNR vector of the primary users' signal on each channel is $\{\gamma_m\} = [-21.5 - 21 - 20.5 - 20 - 19.5 - 19 - 18.5 - 18]$dB with mean $|h_{pm}|^2 = 1$. We use 10000 slots simulation runs with the channel power gains picked independently over different slots.

5.5.1 Utility function versus total power constraint

The average utility function U_G versus total power constraint P_{tot} is shown in Figs. 5.1 and 5.2 on a per slot basis for two different values of energy price ρ (=10 and 150, respectively). In these figures the approach labeled "Only power allocation" is the utility function value with a random T_s located in $(T_{s_{min}}, T/2]$ and only power allocation optimization, and

the approach of [5] corresponds to our approach with $\rho = 0$. It is seen that the iterative algorithm converges quickly and outperforms the case where only power allocation is optimized. Fig. 5.2 shows that in the low P_{tot} region, utility increases as P_{tot} increases. However, when P_{tot} becomes larger than approximately -12dBW, the utility function plateaus out; this phenomenon is not present in Fig. 5.1. The reason for this leveling off is the increase in energy price which discourages higher transmit power even when the transmit power constraint P_{tot} is increased. Compared with the throughput maximization scheme of [78] that does not consider energy consumption, our proposed iterative algorithm can achieve larger utility value, especially with high P_{tot}.
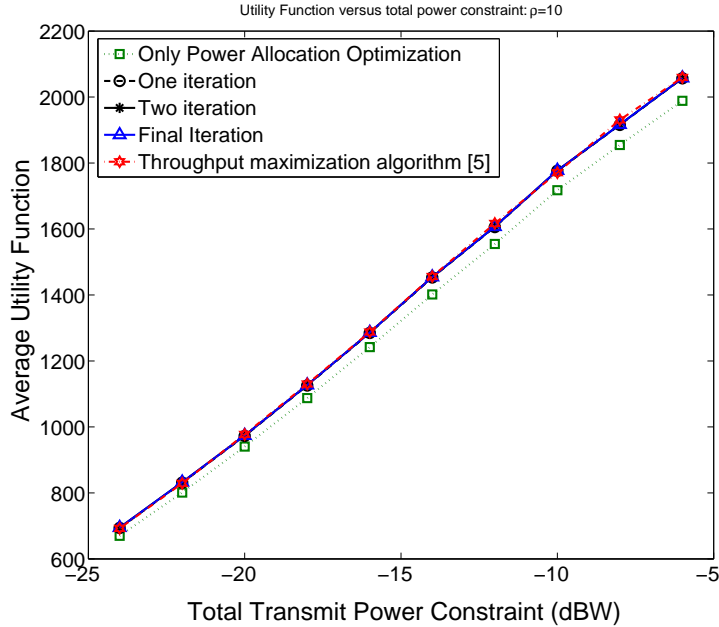
Figure 5.1: Utility function versus the total power constraint, when the minimum required detection probability is fixed at 0.9, energy price $\rho = 10$. The final iteration denotes the result obtained after 10 iterations. The "Only power allocation" is the utility function value with a random T_s located in $(T_{s_{min}}, T/2]$ and only power allocation optimization. The approach of [5] corresponds to our approach with $\rho = 0$.

5.5.2   Energy Efficiency versus energy price ρ

We define energy efficiency as the ratio of throughput and energy consumption, and further define normalized energy efficiency as energy efficiency normalized to have a peak
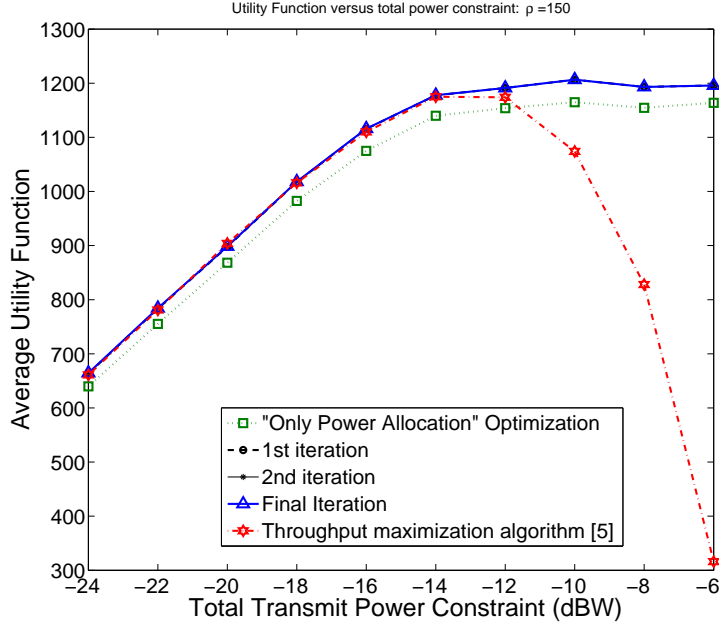
Figure 5.2: Utility function versus the total power constraint, when the minimum required detection probability is fixed at 0.9, energy price $\rho = 150$. The final iteration denotes the result obtained after 10 iterations. The "Only power allocation" is the utility function value with a random T_s located in $(T_{s_{min}}, T/2]$ and only power allocation optimization. The approach of [5] corresponds to our approach with $\rho = 0$.

value of one. In a similar fashion we also define normalized energy consumption per slot and normalized throughput per slot. Fig. 5.3 shows the normalized energy efficiency, normalized energy consumption and normalized throughput versus price of energy ρ. The variation of ρ will affect throughput and energy consumption in two ways. First, for small values of ρ, throughput is more important than the energy consumption. As energy price ρ increases, energy consumption begins to become a significant factor, finally outweighing throughput. As a result, as ρ increases, the throughput decreases to save energy. There exists a "balance" point at which normalized energy efficiency is maximized.

5.6 Conclusions

In this chapter we studied how to balance throughput and energy consumption for a slotted multi-channel CRN. An optimization problem involving sensing parameters (sensing
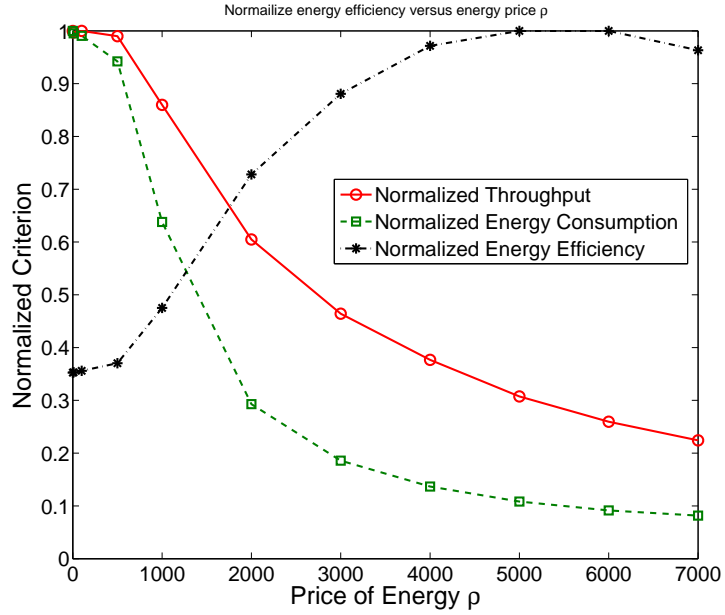
Figure 5.3: Normalized criteria versus the price of energy ρ, when the total power constraint is fixed at -20dBW.

duration and local test threshold) and power allocation was formulated to maximize a utility function that rewards throughput but penalizes energy consumption. To obtain (locally) optimal sensing parameters and power allocation, an iterative algorithm was proposed. Numerical simulations demonstrate that the iterative algorithm converges fast. It performs better than a "only power allocation optimization" approach and an existing approach [78] that ignores energy efficiency.

Chapter 6

On Energy Efficient MIMO-Assisted Spectrum Sharing for Cognitive Radio Networks

We formulate the design of energy efficiency maximization for a single secondary link in an underlay spectrum sharing cognitive radio network under an SU (secondary user) transmit-power constraint and an upperbound on the interference power at the PU (primary user). We propose energy efficient precoding (beamforming) for the SU transmitter to maximize energy efficiency defined as the transmission rate to power ratio, when the terminals in the system are equipped with multiple antennas. The underlying channels are assumed to be known at the SU transmitter. The nonlinear optimization (fractional programming) problem is transformed into a parametrized convex optimization problem and the corresponding solution is discussed. Computer simulation examples are provided to illustrate the proposed approach and to explore the trade-off between energy efficiency and spectrum efficiency.

6.1 Introduction

Cognitive radio techniques aim to alleviate the shortage of frequency spectrum as wireless communication applications proliferate dramatically. Spectrum sharing is central to cognitive radio which permits (unlicensed) secondary users (SUs) to access the licensed spectrum as long as the interference to (licensed) primary users (PUs) is tolerable. There are two popular spectrum sharing schemes. The first one (spectrum underlay) is to allow primary and secondary users access to the same channel simultaneously while constraining the transmitted power of secondary users so that it can be treated as background noise at primary users without exceeding the primary users noise floor. In the second scheme (spectrum overlay) secondary users need to detect spectrum holes and then access spectrum white space in an nonintrusive way [98]. This chapter is concerned with underlay systems.

102

To enhance spectrum utilization, MIMO (multiple-input multiple-output) techniques have been employed in [97] for a single secondary link transmission in underlay CRNs (cognitive radio networks).

Besides the capacity/transmission rate issues, energy consumption is a critical factor that deserves attention. For mobile terminals with battery for power supply, the energy consumption issues are more serious because development of battery technology lags behind the development of wireless communication technologies. Energy efficiency and related aspects for wireless communication systems and networks have recently been reviewed in [94, 93]. An energy efficient design aims to enhance energy efficiency of the transmitter defined as the transmission rate to power ratio.

In this chapter, we aim to optimize the transmit signal covariance matrix (precoding matrix) to maximize the energy efficiency for the SU transmission in an MIMO-based underlay CRN. Our work is inspired by [89] where energy efficient MIMO precoding is investigated for point-to-point MIMO wireless communications. Optimal energy efficient precoding strategies are proposed for both static and fast-fading MIMO channels to maximize the energy efficiency defined as the transmission rate to power ratio. However, cognitive radio network aspects requiring limiting interference to PUs and circuit power consumption are not considered in [89, 92].

Recently, several investigations on energy efficient MIMO CRNs have been reported in [92, 90, 95]. Minimization of total transmission energy consumption for point-to-point MIMO transmission is studied in [92] under sum rate constraint; however, [92] does not consider the interference power constraint to PU. For a TDMA-based cognitive radio MIMO multiuser multiple access network, [90] studies how to optimize time allocation and beamforming among SU transmitters to minimize total transmission energy consumption while guaranteeing the SUs' rate requirement and the interference power constraints. However, the focus of [92, 90] is minimization of energy consumption rather than maximization of energy efficiency. A Stackelberg game theory based power control involving both SU and PU is considered in

103

[95] to maximize the long-term energy efficiency. However, the energy efficiency is defined as an utility function rather than the more commonly accepted and utilized definition of the transmission rate to power ratio (see [89] and references therein). Moreover, MIMO related transmission is not involved in [95]. In addition, circuit power issues are also not considered in [92, 90, 95].

In this chapter, we optimize the transmit signal covariance matrix (precoding matrix) to maximize the energy efficiency for the SU transmission in an MIMO-based underlay CRN. We construct an energy efficiency function that incorporates both transmission and circuit power consumption. Then an energy efficiency maximization problem is formulated for a single secondary link in a CRN under SU transmit-power and PU interference power constraints. It turns out to be a fractional programming problem that is iteratively solved via a parametrized convex optimization problem formulation.

In Sec. II, the system model is introduced and the problem formulation is presented. A fractional programming based iterative semidefinite programming (SDP) algorithm is proposed and analyzed in Sec. III. In Sec. IV we present a multichannel formulation. Computer simulations are presented in Sec. V to illustrate the proposed approaches.

Notation: The determinant of the square matrix $\mathbf{S}$ is denoted by $|\mathbf{S}|$ and $\mathbf{S} \succeq 0$ denotes that $\mathbf{S}$ is a positive semi-definite matrix. The notation $\mathbf{M}^\dagger$ denotes the conjugate transpose of a matrix $\mathbf{M}$ and $\mathbb{E}\{\cdot\}$ denotes the statistical expectation. The space of $n \times m$ matrices with complex entries is denoted by $\mathbb{C}^{m \times n}$. For circularly symmetric complex Gaussian vector $\mathbf{x}$ with mean vector μ and the covariance matrix $\mathbf{\Sigma}$, the probability distribution is denoted as $\mathbf{x} \sim \mathcal{CN}(\mu, \mathbf{\Sigma})$. The notation $tr(\mathbf{S})$ denotes the trace of square matrix $\mathbf{S}$, $\mathbf{I}_M$ denotes the $M \times M$ identity matrix, and $\mathbf{x}^*$ denotes the optimal solution with respect to (w.r.t.) $\mathbf{x}$ of some objective function $g(\mathbf{x})$.

6.2 System Model and Problem Formulation

6.2.1 System Model

In this chapter, we consider a CRN composed of a single SU transmitter and receiver pair that shares the same bandwidth for transmission with a PU receiver. Assume multiple antennas are employed by SU and PU such that the SU transmitter has $N_{t,s}$ antennas, the SU receiver has $N_{r,s}$ antennas, and the PU receiver has $N_{r,p}$ antennas. We consider a block channel fading model such that the channel state would be constant in the frame duration. The frame duration is assumed to be long enough to allow us to adapt the transmit signal covariance matrix so as to maximize the energy efficiency of secondary link while keeping the interference power measured at PU below a predefined threshold. It is assumed that the channel state information from the SU transmitter to the SU receiver and to the PU receiver are precisely known at the SU transmitter.

Let n denote the time index. The complex baseband received signal $\mathbf{y}[n]$ at the SU receiver is given by

$$\mathbf{y}[n] = \mathbf{H}_s \mathbf{x}[n] + \mathbf{z}[n] \tag{6.1}$$

where $\mathbf{y}[n] \in \mathbb{C}^{N_{r,s} \times 1}$, $\mathbf{x}[n] \in \mathbb{C}^{N_{t,s} \times 1}$ is the transmitted signal from the SU, $\mathbf{H}_s \in \mathbb{C}^{N_{r,s} \times N_{t,s}}$ is the channel matrix from the SU transmitter to the SU receiver, and $\mathbf{z}[n] \in \mathbb{C}^{N_{r,s} \times 1}$ is additive white noise assumed to be complex Gaussian with zero mean and covariance matrix $\sigma_z^2 \mathbf{I}_{N_{r,s}}$. Assume that the elements of $\mathbf{H}_s$ are mutually independent and identically distributed as $\mathcal{CN}(0, \sigma_{H_s}^2)$.

Let $\mathbf{Q} = \mathbb{E}\{\mathbf{x}[n]\mathbf{x}^\dagger[n]\}$ denote the transmit covariance matrix (precoding matrix) of the SU transmitter. Assume that an ideal Gaussian code-book with infinitely large number of codeword symbols is used at the SU transmitter such that $\mathbf{x}[n] \sim \mathcal{CN}(0, \mathbf{Q})$. Assume that the rank of $\mathbf{Q}$ is d. Then the eigenvalue decomposition of $\mathbf{Q}$ is

$$\mathbf{Q} = \mathbf{V}\Sigma\mathbf{V}^\dagger \tag{6.2}$$

where $\mathbf{V} \in \mathbb{C}^{N_{t,s} \times d}$ contains the orthonormal eigenvectors of $\mathbf{Q}$ as its columns so that $\mathbf{V}^\dagger \mathbf{V} = \mathbf{I}_d$ and $\Sigma = \mathrm{diag}\{\sigma_1^2,\ \sigma_2^2,\ \cdots,\sigma_d^2\}$ is the $d \times d$ diagonal matrix with the eigenvalues σ_i^2 ($1 \leq i \leq d$) of $\mathbf{Q}$ along its diagonal. Each column of $\mathbf{V}$ is the precoding vector for one transmit data stream of the SU transmitter where $d \leq N_{t,s}$ denotes the degree of spatial multiplexing. The transmit power is given by $tr(\mathbf{Q}) = \sum_{i=1}^{d} \sigma_i^2$. Clearly $\mathbf{Q} \succeq 0$ since it is a covariance matrix. We assume that the transmit power for SU has an upper bound P_t such that $tr(\mathbf{Q}) \leq P_t$. The corresponding achievable rate for the SU transmission link (when $\mathbf{Q}$ and $\mathbf{H}_s$ are known to the transmitter) is given by [96, Chap. 8]

$$C(\mathbf{Q}) = \log_2 |\mathbf{I}_{N_{r,s}} + \rho \mathbf{H}_s \mathbf{Q} \mathbf{H}_s^\dagger| \text{ bps/Hz where } \rho = \frac{1}{\sigma_z^2}. \tag{6.3}$$

Let $\mathbf{H}_p \in \mathbb{C}^{N_{r,p} \times N_{t,s}}$ denote the channel fading coefficients from the SU transmitter to the PU receiver. For the PU receiver, with $N_{r,p}$ receive antennas, the interference power constraint is given by

$$tr(\mathbf{H}_p \mathbf{Q} \mathbf{H}_p^\dagger) \leq \beta \tag{6.4}$$

where β is a predefined interference power upperbound.

6.2.2 Energy Model

It is shown in [93] that besides transmit power consumption, the circuit power consumption is another factor that affects the energy efficiency of the system. Consequently, we consider both transmit power and circuit power consumption as parts of our energy consumption model. In this chapter the circuit power is taken to be a constant P_c regardless of transmit power. The overall power consumption at the SU transmitter is then given by

$$P(\mathbf{Q}) = \eta \, tr(\mathbf{Q}) + P_c \tag{6.5}$$

where η is the reciprocal of the drain efficiency of the power amplifier [92].

6.2.3 Problem Formulation

As in [89] and others, we consider bits per Joule as the metric for energy efficiency. The energy efficiency is defined as the ratio of transmission rate to energy (power) consumption, denoted by $\Psi(\mathbf{Q})$. The goal of this chapter is to optimize transit signal covariance matrix (the precoding matrix) $\mathbf{Q}$ to maximize $\Psi(\mathbf{Q})$ under SU transmit power constraint and PU interference power constraints. The optimization problem is then given by

$$P1: \quad \max_{\mathbf{Q} \succeq 0} \quad \Psi(\mathbf{Q}) = \frac{\log_2 |\mathbf{I}_{N_{r,s}} + \rho \mathbf{H}_s \mathbf{Q} \mathbf{H}_s^\dagger|}{\eta \ tr(\mathbf{Q}) + P_c} \tag{6.6}$$

$$s.t. \quad tr(\mathbf{Q}) \le P_t \tag{6.7}$$

$$tr(\mathbf{H}_p \mathbf{Q} \mathbf{H}_p^\dagger) \le \beta \tag{6.8}$$

$$\mathbf{Q} \succeq 0. \tag{6.9}$$

6.3 Solutions based on Concave Fractional Program and Related Parametric Problem

The problem P1 is nonlinear in $\mathbf{Q}$ and it is not clear how to obtain an explicit solution. However, it will be shown to be a concave fractional program [105], which can then be solved with an equivalent parametric formulation resulting in a concave optimization problem.

Lemma 1. The optimization problem P1 is a concave fractional program.   •

Proof: Concave fractional programming problems are very briefly reviewed in the Appendix C following [105]. Since the numerator and the denominator of $\Psi(\mathbf{Q})$ in problem **P1** are concave and affine, respectively, in $\mathbf{Q}$, problem P1 is a concave fractional program [105]. □

Consider a parameter $\alpha \in \mathbb{R}$. Following [105], problem P1 transformed to the following parametrized concave objective function

$$F(\mathbf{Q}, \alpha) = \log_2 |\mathbf{I}_{N_{r,s}} + \rho \mathbf{H}_s \mathbf{Q} \mathbf{H}_s^\dagger| - \alpha \left(\eta \ tr(\mathbf{Q}) + P_c \right) \tag{6.10}$$

with the corresponding optimization problem **P2**, given by

$$\mathbf{P2}: \quad \max_{\mathbf{Q} \succeq 0} \quad F(\mathbf{Q}, \alpha)$$

$$s.t. \quad tr(\mathbf{Q}) \leq P_t \tag{6.11}$$

$$tr(\mathbf{H}_p \mathbf{Q} \mathbf{H}_p^\dagger) \leq \beta \tag{6.12}$$

$$\mathbf{Q} \succeq 0. \tag{6.13}$$

Since problem **P1** is a concave fractional program, problem **P2** is a parametric concave program. The problem **P2** is more tractable than problem **P1** because of its simpler structure in which the numerator and denominator of $\Psi(\mathbf{Q})$ are separated in $(\mathbf{Q}, \alpha)$ with the help of α. Since $\mathbf{Q}$ is semi-definite, the concave optimization problem **P2** can be solved by utilizing mature SDP (Semidefinite Program) software. In this chapter, we employ SeDuMi that is embedded in the CVX Matlab software package [91].

We would like to show that the optimal solution to problem **P1** can be obtained from the optimal solution(s) to the parametrized problem **P2**. Define

$$\Theta(\alpha) = F(\mathbf{Q}^*(\alpha), \alpha) \tag{6.14}$$

where

$$\mathbf{Q}^*(\alpha) = \arg \left\{ \max_{\mathbf{Q} \succeq 0} \quad F(\mathbf{Q}, \alpha) \right\} \tag{6.15}$$

satisfying the constraints (6.11)-(6.13), that is, $\Theta(\alpha)$ denotes the optimal objective function value for problem **P2** for a given α. Then we have the following theorem to demonstrate the relation between optimal solutions of **P1** and **P2**.

Theorem 1: Let Q^* be the optimal feasible transmit covariance matrix that achieves the optimal energy efficiency, that is, the maximum value of the concave fractional program in **P1** subject to all constraints. Then we have $\Psi(\mathbf{Q}^*) = \alpha^*$ if and only if $\Theta(\alpha^*) = F(\mathbf{Q}^*(\alpha^*), \alpha^*) = \max_{\mathbf{Q} \succeq 0} F(\mathbf{Q}, \alpha^*) = 0.$ •

Proof: Based on the inequality constraints of **P1**, dom$\{\Psi\}$ is compact. Let $\mathbf{Q}^*$ be an optimal solution of **P1** and let $\alpha^* = \Psi(\mathbf{Q}^*) = C(\mathbf{Q}^*)/P(\mathbf{Q}^*)$. When $\Psi(\mathbf{Q}^*) = \alpha^*$, we have

$$\Psi(\mathbf{Q}) = \frac{\log_2|\mathbf{I}_{N_{r,s}} + \rho\mathbf{H}_s\mathbf{Q}\mathbf{H}_s^\dagger|}{\eta\ tr(\mathbf{Q}) + P_c} \leq \alpha^*$$

and

$$\Psi(\mathbf{Q}^*) = \frac{\log_2|\mathbf{I}_{N_{r,s}} + \rho\mathbf{H}_s\mathbf{Q}^*\mathbf{H}_s^\dagger|}{\eta\ tr(\mathbf{Q}^*) + P_c} = \alpha^*.$$

Since $\eta\ tr(\mathbf{Q}) + P_c > 0$, it follows that $F(\mathbf{Q}, \alpha^*) \leq 0$ and $F(\mathbf{Q}^*(\alpha^*), \alpha^*) = 0$. Conversely, when $\Theta(\alpha^*) = F(\mathbf{Q}^*(\alpha^*), \alpha^*) = 0$, we have $\Psi(\mathbf{Q}^*) = \alpha^*$ and also $F(\mathbf{Q}, \alpha^*) \leq 0$ implying $\Psi(\mathbf{Q}) \leq \alpha^*$. Thus Q^* "solves" problem **P1**. $\square$

It follows from [105] that $\Theta(\alpha)$ has the following properties:

$$\Theta(\alpha) > 0 \text{ iff } \alpha < \alpha^* \tag{6.16}$$

$$\Theta(\alpha) = 0 \text{ iff } \alpha = \alpha^* \tag{6.17}$$

$$\Theta(\alpha) < 0 \text{ iff } \alpha > \alpha^* \tag{6.18}$$

Furthermore, the optimal solution of problem **P1** is equivalent to the optimal solution of problem **P2** with parameter $\alpha = \alpha^*$. Consequently, seeking the root of the nonlinear equation $\Theta(\alpha) = 0$ is the key to solving **P1**. It turns out [105] that $\Theta(\alpha)$ is convex, continuous and strictly decreasing in α with $\lim_{\alpha \to \infty} \Theta(\alpha) = \infty$ and $\lim_{\alpha \to -\infty} \Theta(\alpha) = -\infty$. Finally, there exists an unique solution $\alpha = \alpha^*$ for $\Theta(\alpha) = 0$.

The subgradient of $\Theta(\alpha)$ can also be obtained through solving problem **P2**. With optimal solution Q^* of problem **P2** with $\alpha = \alpha^*$, the following value

$$\log_2|\mathbf{I}_{N_{r,s}} + \rho\mathbf{H}_s\mathbf{Q}^*\mathbf{H}_s^\dagger| - \alpha(\eta\ tr(\mathbf{Q}^*) + P_c) \tag{6.19}$$

is a tangent to $\Theta(\alpha)|_{\alpha=\alpha^*}$, which means that $-(\eta \; tr(\mathbf{Q}^*) + P_c)$ is a subgradient of $\Theta(\alpha)$ at α^* (that is also the derivative if $\Theta(\alpha)$ is differentiable at α^*).

With these characteristics of **P1**, a bisection method can be employed for solving the nonlinear equation $\Theta(\alpha) = 0$. One can search for the optimal α^* over an interval $[\alpha_{min} \; \alpha_{max}]$ which is known to contain the optimal value α^*. Since $\Psi(\mathbf{Q})$ is always positive, the possible $\alpha^* = \Psi(\mathbf{Q}^*)$ is positive too. Thus we initially set $\alpha_{min} = 0$. The upperboundα_{max} is an arbitrary value such that $\Theta(\alpha_{max})$ in **P2** is negative. During the iterative bisection algorithm, we first solve the concave optimization problem **P2** at the midpoint $\alpha = \frac{\alpha_{min}+\alpha_{max}}{2}$. Depending on the feasibility of **P2**, we determine whether the optimal value is located in the lower or upper half of the interval, then update the interval accordingly. This would generate a new search interval that is half of the former one. The iteration would continue until the width of the interval is small enough: $\alpha_{max} - \alpha_{min} \leq \epsilon$ where ϵ is the tolerance to control the accuracy of the algorithm. The iterative bisection algorithm is summarized below:

BISECTION ALGORITHM FOR PARAMETRIC OPTIMIZATION

1) Given $\alpha_{min} = 0$ and $\alpha_{max} \; (\geq \alpha^*)$, tolerance $\epsilon > 0$.

2) Set $\alpha = \frac{\alpha_{min}+\alpha_{max}}{2}$. Solve the concave optimization problem **P2**.

3) If $\Theta(\alpha) > 0$ then $\alpha_{min} = \alpha$, else if $\Theta(\alpha) < 0$, then $\alpha_{max} := \alpha$.

4) If $\Theta(\alpha) = 0$ or $\alpha_{max} - \alpha_{min} \leq \epsilon$, stop; otherwise go to step 2.

6.4 Multichannel Energy Efficient Precoding

In this subsection, we consider a general multichannel cognitive radio network where both secondary and primary users transmit on multiple parallel subchannels with multiple antennas. This scenario can be viewed as that of MIMO-OFDMA in which multiple

subcarriers are utilized. Assume that there are K parallel OFDM subcarrier tones. Let $\mathbf{H}_{s_k} \in \mathbb{C}^{N_{r,s} \times N_{t,s}}$ and $\mathbf{H}_{p_k} \in \mathbb{C}^{N_{r,p} \times N_{t,s}}$ denote the channel matrices for the kth subchannel ($1 \leq k \leq K$) from the SU transmitter to the SU and PU receivers, respectively. Let $\mathbf{Q}_k \in \mathbb{C}^{N_{r,s} \times N_{t,s}}$ denote the signal covariance matrix (precoding matrix) on the kth subchannel. Suppose that each subchannel has the same bandwidth BHz. The transmit power and interference power constraints on each subchannel are identical and are the same as in the single-channel case discussed in Sec. III. The achievable transmission rate for the SU on the kth channel is

$$R_{s_k} = B \log_2 |\mathbf{I}_{N_{r,s}} + \rho \mathbf{H}_{s_k} \mathbf{Q} \mathbf{H}_{s_k}^\dagger| \quad \text{bps.} \tag{6.20}$$

Let w_k denote a predefined nonnegative priority weight for transmission over the kth channel ($1 \leq k \leq K$) and $\Sigma_{k=1}^K w_k = K$. Then the weighted sum rate is given by

$$C(\{\mathbf{Q}_k\}_{k=1}^K) = \sum_{k=1}^K w_k B \log_2 |\mathbf{I}_{N_{r,s}} + \rho \mathbf{H}_{s_k} \mathbf{Q} \mathbf{H}_{s_k}^\dagger|. \tag{6.21}$$

The total power consumption at the SU is given by

$$P(\{\mathbf{Q}_k\}_{k=1}^K) = \eta \sum_{k=1}^K \text{tr}(\mathbf{Q}_k) + K P_c. \tag{6.22}$$

The corresponding energy efficiency, defined by $\Psi(\{\mathbf{Q}_k\}_{k=1}^K) = C(\{\mathbf{Q}_k\}_{k=1}^K)/P(\{\mathbf{Q}_k\}_{k=1}^K)$, is given by

$$\Psi(\{\mathbf{Q}_k\}_{k=1}^K) = \frac{\sum_{k=1}^K w_k B \log_2 |\mathbf{I}_{N_{r,s}} + \rho \mathbf{H}_{s_k} \mathbf{Q} \mathbf{H}_{s_k}^\dagger|}{\eta \sum_{k=1}^K \text{tr}(\mathbf{Q}_k) + K P_c}. \tag{6.23}$$

The transmit and interference power constraints are given by

$$\text{tr}(\mathbf{Q}_k) \leq P_t \qquad\qquad \forall k \tag{6.24}$$

$$\text{tr}(\mathbf{H}_{p_k} \mathbf{Q}_k \mathbf{H}_{p_k}^\dagger) \leq \beta \qquad\qquad \forall k \tag{6.25}$$

$$\mathbf{Q}_k \succeq 0 \qquad\qquad \forall k \tag{6.26}$$

The overall optimization problem can be formulated as

$$\mathbf{P3}: \max_{\{\mathbf{Q}_k\}_{k=1}^K} \quad \Psi(\{\mathbf{Q}_k\}_{k=1}^K)$$

$$s.t. \quad tr(\mathbf{Q}_k) \leq P_t \qquad\qquad \forall k \qquad\qquad (6.27)$$

$$tr(\mathbf{H}_{p_k}\mathbf{Q}_k\mathbf{H}_{p_k}^\dagger) \leq \beta \qquad\qquad \forall k \qquad\qquad (6.28)$$

$$\mathbf{Q}_k \succeq 0 \qquad\qquad \forall k. \qquad\qquad (6.29)$$

The corresponding parametric objective function is given by

$$F(\{\mathbf{Q}_k\}_{k=1}^K, \alpha) = \sum_{k=1}^K w_k B \log_2 |\mathbf{I}_{N_{r,s}} + \rho \mathbf{H}_{s_k}\mathbf{Q}\mathbf{H}_{s_k}^\dagger|$$

$$- \alpha \left(\eta \sum_{k=1}^K tr(\mathbf{Q}_k) + KP_c \right). \qquad (6.30)$$

Consequently, we consider the following parametric problem associated with **P3**:

$$\mathbf{P4}: \max_{\{\mathbf{Q}_k\}_{k=1}^K \succeq 0} \quad F(\{\mathbf{Q}_k\}_{k=1}^K, \alpha)$$

$$s.t. \quad tr(\mathbf{Q}_k) \leq P_t \quad \forall k \qquad\qquad (6.31)$$

$$tr(\mathbf{H}_{p_k}\mathbf{Q}_k\mathbf{H}_{p_k}^\dagger) \leq \beta \forall k \qquad\qquad (6.32)$$

$$\mathbf{Q}_k \succeq 0 \quad \forall k. \qquad\qquad (6.33)$$

Define

$$F(\{\mathbf{Q}_k\}, \alpha) = w_k B \log_2 |\mathbf{I}_{N_{r,s}} + \rho \mathbf{H}_{s_k}\mathbf{Q}\mathbf{H}_{s_k}^\dagger| - \alpha(\eta tr(\mathbf{Q}_k) + P_c). \qquad (6.34)$$

Then it follows that

$$F(\{\mathbf{Q}_k\}_{k=1}^K, \alpha) = \sum_{k=1}^K F(\{\mathbf{Q}_k\}, \alpha). \qquad (6.35)$$

Notice that the constraints in the problem **P4** is separable. Therefore, the solution to problem **P4** is equivalent to solutions to the following K subproblems:

$$\textbf{P5}: \quad \max_{\mathbf{Q}_k \succeq 0} \quad F(\{\mathbf{Q}_k\}, \alpha)$$

$$s.t. \quad tr(\mathbf{Q}_k) \leq P_t \tag{6.36}$$

$$tr(\mathbf{H}_{p_k} \mathbf{Q}_k \mathbf{H}_{p_k}^{\dagger}) \leq \beta \tag{6.37}$$

$$\mathbf{Q}_k \succeq 0. \tag{6.38}$$

The solution algorithm for problem **P5** is similar to that for the problem **P2**.

6.5 Simulation Examples

It is assumed that the SU transmitter is equipped with $N_{t,s} = 2$ or 3 antennas and both SU and PU receivers have 1, 2 or 3 antennas. The elements of the channel fading matrices $\mathbf{H}_p$ and $\mathbf{H}_s$ from the SU transmitter to the primary and secondary receivers are both mutually independent complex Gaussian random variables distributed as $\mathcal{CN}(0, \ 0.1)$ and $\mathcal{CN}(0, 1)$, respectively. It is assumed that the power amplifier efficiency is 38% for the secondary transmitter, leading to $\eta = 1/0.38$ in (6.5). The static circuit power consumption is $P_c = 20$mW. At the PU receiver, the maximum interference power constraint is $\beta = 1$mW . The noise power is assumed to be $\sigma_z^2 = 1$mW (=0 dBm). The reported results are based on 1000 Monte Carlo runs with 1000 randomly generated channel states $\mathbf{H}_p$ and $\mathbf{H}_s$.

6.5.1 Energy Efficiency and Capacity Comparisons

Figs. 6.1 and 6.2 show the capacity and energy efficiency, respectively, of the secondary link under two cases of energy efficiency maximization as discussed in Sec. III and spectral efficiency (capacity) maximization without any consideration of power consumption, as discussed in [97]. Three different antenna settings were considered: 2×1 MISO with $N_{t,s} = 2$, $N_{r,s} = 1$ and $N_{r,p} = 1$, 2×2 MIMO with $N_{t,s} = 2$, $N_{r,s} = 2$ and $N_{r,p} = 2$ and 3×3

MIMO with $N_{t,s} = 3$, $N_{r,s} = 3$ and $N_{r,p} = 3$. The transmit power constraint P_t for the SU transmitter was varied from 0dBm to 22dBm. It is seen that compared with the conventional spectrum efficiency maximization design, the energy efficient design can enhance energy efficiency dramatically, particularly in the higher transmit power range but at the cost of smaller throughput. In addition, more receive antennas result in higher energy efficiency and capacity because spatial diversity is utilized.
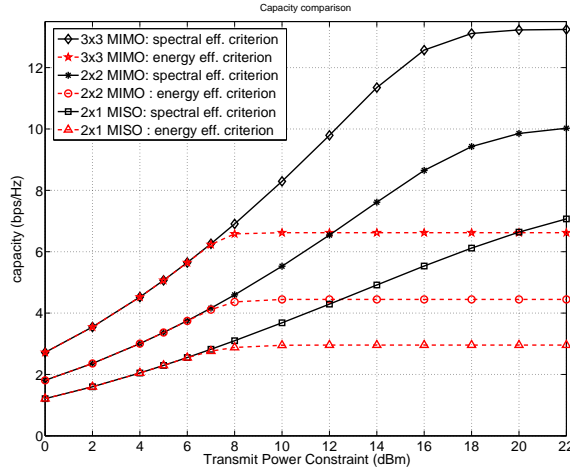
Figure 6.1: Capacity comparison: In the energy efficiency criterion we maximize energy efficiency $\Psi(\mathbf{Q})$ as in problem **P1** whereas in the spectral efficiency criterion we maximize the channel capacity as in [97]. In 2×1 MISO system we used $N_{t,s} = 2$, $N_{r,s} = 1$ and $N_{r,p} = 1$, the 2×2 MIMO system had $N_{t,s} = 2$, $N_{r,s} = 2$ and $N_{r,p} = 2$, and the 3×3 MIMO system had $N_{t,s} = 3$, $N_{r,s} = 3$ and $N_{r,p} = 3$.

6.5.2 Multichannel Energy Efficient MIMO Transmission

In this case, two subchannels are utilized and each subchannel has independent and identically distributed channel gain matrix. Furthermore, each subchannel has independent transmit power and interference power constraints for which the parameter settings are the same as for the single channel scenario discussed in Sec. V-A. The priority weights of the two channels are 0.6 and 1.4, respectively. The bandwidth B is assumed to be 1 Hz. Figs. 6.3 and 6.4 show the capacity and energy efficiency, respectively, of the secondary link under two cases of energy efficiency maximization as discussed in Sec. IV and spectral efficiency
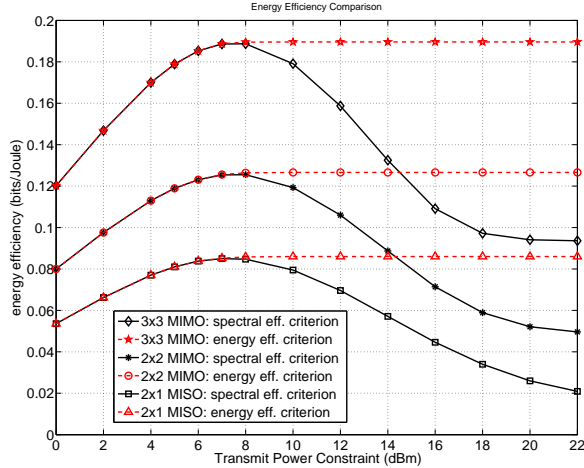
Figure 6.2: Energy efficiency comparison: In the energy efficiency criterion we maximize energy efficiency $\Psi(\mathbf{Q})$ as in problem $\mathbf{P1}$ whereas in the spectral efficiency criterion we maximize the channel capacity as in [97]. In 2×1 MISO system we used $N_{t,s} = 2$, $N_{r,s} = 1$ and $N_{r,p} = 1$, the 2×2 MIMO system had $N_{t,s} = 2$, $N_{r,s} = 2$ and $N_{r,p} = 2$, and the 3×3 MIMO system had $N_{t,s} = 3$, $N_{r,s} = 3$ and $N_{r,p} = 3$.

(capacity) maximization without any consideration of power consumption. We used two MIMO antenna configurations: the 2×2 MIMO system with $N_{t,s} = 2$, $N_{r,s} = 2$ and $N_{r,p} = 2$, and the 3×3 MIMO system with $N_{t,s} = 3$, $N_{r,s} = 3$ and $N_{r,p} = 3$. The conclusions drawn in Sec. V-A apply here too.

6.6 Conclusions

In this chapter, we proposed an energy-efficient transmit covariance matrix (precoder) design for spectrum sharing underlay cognitive radio networks when multiple antennas are employed at the secondary user transmitter. We constructed an energy efficiency function that incorporates both transmission and circuit power consumption. Then an energy efficiency maximization problem was formulated for a single secondary link in a CRN under SU transmit-power and PU interference power constraints. It turned out to be a fractional programming problem that was iteratively solved via a parametrized convex optimization problem formulation. A multichannel extension of the problem was also investigated. The

Figure 6.3: Capacity comparison for the multichannel case with $K = 2$: In the energy efficiency criterion we maximize energy efficiency $\Psi(\{\mathbf{Q}_k\}_{k=1}^K)$ as in problem **P3** whereas in the spectral efficiency criterion we maximize the channel capacity as in [97]. We used two MIMO systems: the 2×2 MIMO system with $N_{t,s} = 2$, $N_{r,s} = 2$ and the 3×3 MIMO system with $N_{r,p} = 2$, and $N_{t,s} = 3$, $N_{r,s} = 3$ and $N_{r,p} = 3$.

trade-off between energy efficiency and spectrum efficiency was explored via computer simulations.
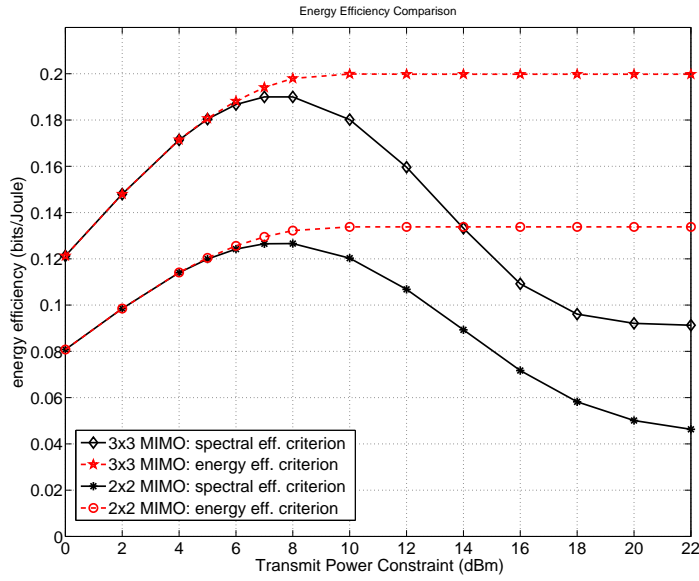
Figure 6.4: Energy efficiency comparison for the multichannel case with $K = 2$: In the energy efficiency criterion we maximize energy efficiency $\Psi(\{\mathbf{Q}_k\}_{k=1}^K)$ as in problem **P3** whereas in the spectral efficiency criterion we maximize the channel capacity as in [97]. We used two MIMO systems: the 2×2 MIMO system with $N_{t,s} = 2$, $N_{r,s} = 2$ and the 3×3 MIMO system with $N_{r,p} = 2$, and $N_{t,s} = 3$, $N_{r,s} = 3$ and $N_{r,p} = 3$.

Chapter 7

On Precoding for Maximum Weighted Energy Efficiency of MIMO Cognitive Multiple

Access Channels

We study weighted energy efficiency maximization for multiple-input multiple-output cognitive multiple access channels under both secondary user transmit power constraint and primary user interference power constraint. Energy efficiency is defined as the ratio of weighted sum rate and energy consumption including both transmission and circuit energy consumption. The nonlinear (fractional programming) energy efficiency optimization problem is transformed into a series of parametrized convex optimization problems. A combination of bisection search method and cyclic coordinate ascent-based iterative water-filling algorithm is proposed to solve the parametrized problem. Computer simulation examples are provided to illustrate the proposed approach and to explore the trade-off between energy efficiency and spectrum efficiency.

7.1 Introduction

Cognitive radio techniques aim to alleviate the shortage of frequency spectrum as wireless communication applications proliferate dramatically. Spectrum sharing is central to cognitive radio which permits (unlicensed) secondary users (SUs) to access the licensed spectrum as long as the interference to (licensed) primary users (PUs) is tolerable. There are two popular spectrum sharing schemes. The first one (spectrum underlay) is to allow primary and secondary users access to the same channel simultaneously while constraining the transmitted power of secondary users so that the interference power received at primary users should be below the predefined interference threshold [24]. In the second scheme (spectrum overlay) secondary users need to detect spectrum holes and then access spectrum white

space in an nonintrusive way [24]. This chapter is concerned with energy efficient precoding for cognitive multiple access in spectrum underlay cognitive radio networks.

Current research on wireless communication channel precoding mainly focuses on optimizing transmit signal covariance matrix (precoding) to maximize spectral efficiency (capacity) [106, 107, 100, 101] where MIMO (multiple-input multiple-output) techniques have been employed to enhance spectrum utilization. The water filling algorithm for Gaussian multiple access channel under individual transmit power constraint was first proposed in [106]. Ref. [100] further proposed a sum power iterative water-filling for multiantenna Gaussian broadcast channel (BC) based on [106], which solves an equivalent dual MAC (multiple access channel) capacity maximization with sum power constraint. A similar problem as [100] was solved alternatively with a dual decomposition method by [107] with the same system model as [100]. For weighted sum rate maximization of the Gaussian BC channel under sum power constraint, the iterative water filling algorithm in [100] was extended to solve dual MAC capacity maximization under sum power constraint based on BC-MAC duality [101]. For cognitive MAC with multiple antennas, in [99] maximization of the weighted sum rate under weighted sum power constraint (interference power to PU) was solved with a dual decomposition algorithm [107]. However, none of the algorithms proposed in [106, 107, 100, 101, 99] consider energy efficiency (i.e. they omit any consideration of power consumption).

Besides the capacity/transmission rate issues, energy consumption is a critical factor that deserves attention. For mobile terminals with battery for power supply, the energy consumption issues are more serious because development of battery technology lags behind the development of wireless communication technologies. Energy efficiency and related aspects for wireless communication systems and networks have recently been reviewed in [93, 111]. An energy efficient design aims to enhance energy efficiency of the transmitter defined as the transmission rate to power ratio. Energy efficient precoding has been considered in [89, 108]. The energy efficient precoding for point to point MIMO wireless communication was first studied in [89]. For multiuser BC, an energy efficient precoding scheme was proposed [108].

However, cognitive radio network aspects requiring limiting interference to PUs and circuit power consumption are not considered in [89] and [108].

In this chapter, we optimize the transmit signal covariance matrix (precoding matrix) to maximize the energy efficiency for a MIMO cognitive multiple access channel (C-MAC). The secondary BS is informed of the channel states from SUs to both secondary BS and PU; SUs are assumed to obtain the optimal power allocation information from BS via an additional control channel. To our best knowledge, there is currently no paper on energy efficient precoding for MIMO C-MAC. We formulate a weighted energy efficiency (EE) optimization problem under transmit power constraint and interference power constraint for MIMO cognitive MAC channels. EE is defined as the ratio of weighted sum capacity and energy consumption that includes both transmission power and static circuit power consumption. With circuit power consumption, the energy efficiency versus transmission power is a bell shape function [111], such that the maximal energy efficiency can be achieved in moderate transmission rate. This is different from the conclusion that energy efficiency is maximized at very low or even minimum transmit power when only transmission power consumption is considered [89]. The EE objective function is nonlinear but quasi-convex, which can be transformed into a series of parametrized concave energy-aware utility functions, following [105]. We prove that such transformation guarantees that the optimal energy efficient power allocation is obtained; a similar proof can also be found in [110]. A combination of bisection search method and cyclic coordinate ascent-based iterative water-filling algorithm is proposed to solve the parametrized problem. Computer simulation examples are provided to illustrate the proposed approach and to explore the trade-off between energy efficiency and spectrum efficiency.

In Sec. II, the system model is introduced and the problem formulation is presented. A fractional programming based bisection search algorithm is proposed in Sec. III. In Sec. IV we present a cyclic coordinate ascent based semidefinite programming (SDP) algorithm to

optimize transmit covariance matrix iteratively. Computer simulations are presented in Sec. V to illustrate the proposed approaches.

Notation: We use bold letters $\mathbf{x}$ to denote vectors and bold capital letters $\mathbf{H}$ to denote matrices. $\text{tr}\{\mathbf{H}\}$ denotes the trace of matrix $\mathbf{H}$. $\mathbf{x} \geq 0$ denotes that $\mathbf{x}$ is a non-negative vector (all elements are non-negative). $|\mathbf{S}|$ denotes the determinant of the general matrix $\mathbf{S}$. $\mathbf{S} \succeq 0$ denotes $\mathbf{S}$ is positive semidefinite matrix. The notation $\mathbf{M}^{\dagger}$ denotes the conjugate transpose of a matrix $\mathbf{M}$. The space of $m \times n$ matrices with complex entries is denoted by $\mathbb{C}^{m \times n}$. Let $\mathbb{R}^{+}$ denote the field of positive real numbers. For circularly symmetric complex Gaussian vector $\mathbf{x}$ with mean vector μ and the covariance matrix $\boldsymbol{\Sigma}$, the probability distribution is denoted as $\mathbf{x} \sim \mathcal{CN}(\mu, \boldsymbol{\Sigma})$. $\mathbf{I}_M$ denotes the $M \times M$ identity matrix. $\mathbf{x}^*$ denotes the optimal solution with respect to (w.r.t) $\mathbf{x}$ of some objective function $g(\mathbf{x})$. "Subject to" is abbreviated as s.t.

7.2 System Model and Problem Formulation

7.2.1 System Model

We consider an MIMO cognitive multiple access channel where K secondary users with $N_{t,s}$ transmit antennas communicate with a secondary BS with $N_{r,s}$ receiver antennas. The K SUs and the secondary BS share spectrum with a primary user with $N_{p,r}$ receive antennas. We consider a block channel fading model where the channel state is constant during the frame duration which is assumed to be long enough to allow us to adapt the transmit signal covariance matrix (precoding matrix) so as to maximize the energy efficiency of cognitive MAC while keeping the interference power measured at PU below a predefined threshold. It is assumed that the channel state information from the SU transmitter to the secondary BS and to the PU receiver is precisely known at the secondary BS. The K SUs can communicate simultaneously to the secondary BS where successive interference cancellation (SIC) technique [104] is used to decode the received K SUs' signal.

The secondary BS's complex baseband received signal at time n, denoted $\mathbf{y}[n]$, is modeled as

$$\mathbf{y}[n] = \sum_{k=1}^{K} \mathbf{H}_{k,s} \mathbf{x}_k[n] + \mathbf{z}[n] \tag{7.1}$$

where $\mathbf{y}[n] \in \mathbb{C}^{N_{r,s} \times 1}$ denotes received signal vector, $\mathbf{x}_k[n] \in \mathbb{C}^{N_{t,s} \times 1}$ denotes transmitted signal from the kth SU, $\mathbf{H}_{k,s} \in \mathbb{C}^{N_{r,s} \times N_{t,s}}$ denotes channel matrix from the kth SU transmitter to secondary BS, and noise $\mathbf{z}[n] \in \mathbb{C}^{N_{r,s} \times 1}$ is distributed as $\mathcal{CN}(0, \sigma_z^2 \mathbf{I}_{N_{r,s}})$. Let $\mathbf{H}_{k,p} \in \mathbb{C}^{N_{r,p} \times N_{t,s}}$ denote the channel matrix from kth SU to PU. Let $\mathbf{Q}_k = \mathbb{E}\{\mathbf{x}_k[n]\mathbf{x}_k^{\dagger}[n]\}$ denote the transmit covariance matrix (precoding matrix) of the kth SU transmitter. Assume that an ideal Gaussian code-book with infinitely large number of codeword symbols is used at the SU transmitter such that $\mathbf{x}_k[n] \sim \mathcal{CN}(0, \mathbf{Q}_k)$. Assume that the rank of $\mathbf{Q}_k$ is d_k. Then the eigenvalue decomposition of $\mathbf{Q}_k$ is

$$\mathbf{Q}_k = \mathbf{V}_k \Sigma_k \mathbf{V}_k^{\dagger} \tag{7.2}$$

where $\mathbf{V}_k \in \mathbb{C}^{N_{t,s} \times d_k}$ contains the orthonormal eigenvectors of $\mathbf{Q}_k$ as its columns so that $\mathbf{V}_k^{\dagger} \mathbf{V}_k = \mathbf{I}_{d_k}$ and $\Sigma_k = \text{diag}\left\{\sigma_1^2, \sigma_2^2, \cdots, \sigma_{d_k}^2\right\}$ is the $d_k \times d_k$ diagonal matrix with the eigenvalues σ_i^2 $(1 \leq i \leq d_k)$ of $\mathbf{Q}_k$ along its diagonal. Each column of $\mathbf{V}_k$ is the precoding vector for one transmit data stream of the kth SU transmitter where $d_k \leq N_{t,s}$ denotes the degree of spatial multiplexing. The transmit power is given by $\text{tr}(\mathbf{Q}_k) = \sum_{i=1}^{d_k} \sigma_i^2$. Clearly $\mathbf{Q}_k \succeq 0$ since it is a covariance matrix. We assume that the transmit power for kth SU has an upper bound $\text{tr}\{\mathbf{Q}_k\} \leq P_{st}$. Under the spectrum sharing scenario, the interference power to PU has an upperbound β such that $\Sigma_{k=1}^{K} \text{tr}\{\mathbf{H}_{k,p} \mathbf{Q}_k \mathbf{H}_{k,p}^{\dagger}\} \leq \beta$. For the channel matrices $\mathbf{H}_{k,s}$ and $\mathbf{H}_{k,p}$, we consider a block fading model where $\mathbf{H}_{k,s}$ and $\mathbf{H}_{k,p}$ keep constant for one block and are independently distributed among the blocks. Moreover, $\mathbf{H}_{k,s}$ and $\mathbf{H}_{k,p}$ are perfectly known to the secondary BS.

It is assumed each SU k has a priority weight w_k [104, 101, 99]. With successive interference cancellation (SIC) [104], the received K SU signals are decoded successively. The

corresponding achievable rate is given by [99, Eqn. 5]

$$R_{\pi_k} = B \log_2 \frac{|\mathbf{I}_{N_{r,s}} + \rho \sum_{j=1}^{k} \mathbf{H}_{\pi_j,s} \mathbf{Q}_j \mathbf{H}_{\pi_j,s}^{\dagger}|}{|\mathbf{I}_{N_{r,s}} + \rho \sum_{j=1}^{k-1} \mathbf{H}_{\pi_j,s} \mathbf{Q}_j \mathbf{H}_{\pi_j,s}^{\dagger}|} \text{ bps }, \forall k \tag{7.3}$$

where $\rho = \frac{1}{\sigma_z^2}$ (σ_z^2 is the noise power), B is the bandwidth and $\pi_1, \ldots, \pi_K$, a permutation of $(1, \ldots, K)$, represents a decoding order (π_K is decoded first and π_1 is decoded last).

According to [104], the optimal decoding order for SIC is obtained by sorting priority weights in a non-increasing order as $w_{\pi_1} \geq w_{\pi_2} \geq \cdots \geq w_{\pi_K}$. Consequently, without loss of generality the optimal decoding order is assumed to be $\pi_k = k$ [101, 99]. The weighted sum rate for all K users is given by

$$C(\{\mathbf{Q}_k\}_{k=1}^{K}) = \sum_{k=1}^{K} \Delta_k B \log_2 |\mathbf{I}_{N_{r,s}} + \rho \Sigma_{j=1}^{k} \mathbf{H}_{j,s} \mathbf{Q}_j \mathbf{H}_{j,s}^{\dagger}| \tag{7.4}$$

where $\Delta_k = w_k - w_{k+1}$, and $w_{K+1} = 0$.

As demonstrated in [93], both transmission and circuit energy consumption contribute to total energy efficiency. The circuit power is treated as a constant P_c. Power amplifier efficiency is considered for SU's transmission power. The overall power consumption of K SUs is given by

$$E(\{\mathbf{Q}_k\}_{k=1}^{K}) = \eta \sum_{k=1}^{K} \text{tr}\{\mathbf{Q}_k\} + K P_c \tag{7.5}$$

where η is the reciprocal of the drain efficiency of the power amplifier.

Similar to [89], the energy efficiency denoted as $\Psi(\{\mathbf{Q}_k\}_{k=1}^{K})$, is defined as the ratio of weighted sum rate and energy consumption, with units bits per Joule. We aim to optimize transmit covariance matrices $\{\mathbf{Q}_k\}_{k=1}^{K}$ to maximize $\Psi(\{\mathbf{Q}_k\}_{k=1}^{K})$ under both transmit power

constraint and interference power constraint to PU, which is given by

$$P1: \quad \max_{\{\mathbf{Q}_k\}_{k=1}^{K}} \Psi(\{\mathbf{Q}_k\}_{k=1}^{K}) = \frac{C(\{\mathbf{Q}_k\}_{k=1}^{K})}{E(\{\mathbf{Q}_k\}_{k=1}^{K})} \qquad (7.6)$$

$$s.t. \quad \mathrm{tr}\{\mathbf{Q}_k\} \leq P_{st} \text{ and } \mathbf{Q}_k \succeq 0, \ \forall k \qquad (7.7)$$

$$\sum_{k=1}^{K} \mathrm{tr}\{\mathbf{H}_{k,p}\mathbf{Q}_k\mathbf{H}_{k,p}^{\dagger}\} \leq \beta. \qquad (7.8)$$

7.3 Solutions: Concave Fractional Program and Related Parametrized Problem

The problem P1 is nonlinear and it is hard to obtain explicit solution directly. However, it turns out to be a concave fractional program which can be solved with an equivalent parametrized program.

Lemma 1. The optimization problem P1 is a concave fractional program. ●

Proof: Since the numerator and denominator of $\Psi(\{\mathbf{Q}_k\}_{k=1}^{K})$ in problem P1 are concave and affine, problem P1 is a concave fractional program based on the definition and property of concave fractional program [105]. □

Consider a parameter $\alpha \in \mathbb{R}$. Following [105] problem P1 is related to the following concave objective function

$$\Phi(\{\mathbf{Q}_k\}_{k=1}^{K}, \alpha) = \sum_{k=1}^{K} \Delta_k B \log_2 |\mathbf{I}_{N_{r,s}} + \rho \Sigma_{j=1}^{k} \mathbf{H}_{j,s} \mathbf{Q}_j \mathbf{H}_{j,s}^{\dagger}| - \alpha \left(\eta \sum_{k=1}^{K} \mathrm{tr}\{\mathbf{Q}_k\} + KP_c \right) \quad (7.9)$$

and the corresponding optimization problem P2

$$P2: \quad \max_{\{\mathbf{Q}_k\}_{k=1}^{K}} \quad \Phi(\{\mathbf{Q}_k\}_{k=1}^{K}, \alpha) \qquad (7.10)$$

subject to (7.7)-(7.8). Since P1 is a concave fractional program, P2 is a parametrized concave program [105]. P2 is more tractable than P1 because of its simpler structure where the numerator and denominator are separated with the help of α.

We now show that the optimal solution to P1 can be obtained from the optimal solution to P2. Define

$$\Theta(\alpha) = \Phi(\{\mathbf{Q}_k^*(\alpha)\}_{k=1}^K, \alpha) \tag{7.11}$$

where

$$\{\mathbf{Q}_k^*(\alpha)\}_{k=1}^K = \arg\left\{ \max_{\{\mathbf{Q}_k \succeq 0\}_{k=1}^K} \Phi(\{\mathbf{Q}_k\}_{k=1}^K, \alpha) \right\} \tag{7.12}$$

satisfying (7.7)-(7.8). Then we have the following theorem linking the optimal solutions of problems P1 and P2.

Theorem 1: Let $\{\mathbf{Q}_k^*\}_{k=1}^K$ be the optimal feasible transmit covariance matrix that achieves the optimal energy efficiency, that is, the maximum value of the concave fractional program in $P1$ subject to all constraints. Then we have $\Psi(\{\mathbf{Q}_k^*\}_{k=1}^K) = \alpha^*$ if and only if $\Theta(\alpha^*) = \Phi(\{\mathbf{Q}_k^*(\alpha^*)\}_{k=1}^K, \alpha^*) = \max_{\{\mathbf{Q}_k \succeq 0\}_{k=1}^K} \Phi(\{\mathbf{Q}_k\}_{k=1}^K, \alpha^*) = 0$.   ●

Proof: Based on the inequality constraints of $P1$, dom$\{\Psi\}$ is compact. Let $\{\mathbf{Q}_k^*\}_{k=1}^K$ be an optimal solution of $P1$ and let $\alpha^* = \Psi(\{\mathbf{Q}_k^*\}_{k=1}^K) = C(\{\mathbf{Q}_k^*\}_{k=1}^K)/E(\{\mathbf{Q}_k^*\}_{k=1}^K)$. When $\Psi(\{\mathbf{Q}_k^*\}_{k=1}^K) = \alpha^*$, we have

$$\Psi(\{\mathbf{Q}_k\}_{k=1}^K) = \frac{\sum_{k=1}^K \Delta_k B \log_2 |\mathbf{I}_{N_{r,s}} + \rho\Sigma_{j=1}^k \mathbf{H}_{j,s}\mathbf{Q}_j\mathbf{H}_{j,s}^\dagger|}{\eta \sum_{k=1}^K \text{tr}\{\mathbf{Q}_k\} + KP_c} \leq \alpha^* \tag{7.13}$$

and

$$\Psi(\{\mathbf{Q}_k^*\}_{k=1}^K) = \frac{\sum_{k=1}^K \Delta_k B \log_2 |\mathbf{I}_{N_{r,s}} + \rho\Sigma_{j=1}^k \mathbf{H}_{j,s}\mathbf{Q}_j^*\mathbf{H}_{j,s}^\dagger|}{\eta \sum_{k=1}^K \text{tr}\{\mathbf{Q}_k^*\} + KP_c} = \alpha^*. \tag{7.14}$$

Since $\eta \sum_{k=1}^K \text{tr}\{\mathbf{Q}_k\} + KP_c > 0$, it follows that $\Phi(\{\mathbf{Q}_k\}_{k=1}^K, \alpha^*) \leq 0$ and $\Phi(\{\mathbf{Q}_k^*(\alpha^*)\}_{k=1}^K, \alpha^*) = 0$. Conversely, when $\Theta(\alpha^*) = \Phi(\{\mathbf{Q}_k^*(\alpha^*)\}_{k=1}^K, \alpha^*) = 0$, we have $\Psi(\{\mathbf{Q}_k^*\}_{k=1}^K) = \alpha^*$ and also $\Phi(\{\mathbf{Q}_k\}_{k=1}^K, \alpha^*) \leq 0$ implying $\Psi(\{\mathbf{Q}_k\}_{k=1}^K) \leq \alpha^*$. Thus Q^* "solves" problem $P1$.   □

It follows from [105, Sec. 2.2.4] that $\Theta(\alpha)$ has the following properties: $\Theta(\alpha) > 0$ iff $\alpha < \alpha^*$, $\Theta(\alpha) = 0$ iff $\alpha = \alpha^*$ and $\Theta(\alpha) < 0$ iff $\alpha > \alpha^*$. Moreover, the optimal solution of P1 is equivalent to the optimal solution of P2 with parameter $\alpha = \alpha^*$. Consequently, seeking the root of the nonlinear equation $\Theta(\alpha) = 0$ is the key to solving P1. It turns out [105]

that $\Theta(\alpha)$ is convex, continuous and strictly decreasing in α with $\lim_{\alpha \to \infty} \Theta(\alpha) = \infty$ and $\lim_{\alpha \to -\infty} \Theta(\alpha) = -\infty$. Finally, there exists an unique solution $\alpha = \alpha^*$ for $\Theta(\alpha) = 0$.

With these characteristics of P1, a bisection method can be employed for solving the nonlinear equation $\Theta(\alpha) = 0$. The optimal α^* can be searched over the interval $[\alpha_{min} \ \alpha_{max}]$ which is known to contain α^*. Since $\Psi(\{\mathbf{Q}_k\}_{k=1}^K)$ is always positive, the possible $\alpha^* = \Psi(\{\mathbf{Q}_k^*\}_{k=1}^K)$ is positive too. Thus we initially set $\alpha_{min} = 0$. The upperbound α_{max} is an arbitrary value satisfying $\Theta(\alpha_{max}) < 0$. The iteration would continue until the algorithm accuracy is reached such that $\alpha_{max} - \alpha_{min} \leq \epsilon$ (ϵ is accuracy tolerance) [105]. The iterative bisection algorithm is summarized below:

Bisection Algorithm for Parametrized Optimization

1) Given $\alpha_{min} = 0$, $\alpha_{max} \geq \alpha^*$, tolerance $\epsilon > 0$.

2) Set $\alpha = \frac{\alpha_{min} + \alpha_{max}}{2}$. Solve the concave optimization problem P2.

3) If $\Theta(\alpha) > 0$ then $\alpha_{min} = \alpha$;, else if $\Theta(\alpha) < 0$ $\alpha_{max} := \alpha$.

4) If $\Theta(\alpha) = 0$ or $\alpha_{max} - \alpha_{min} \leq \epsilon$, stop; otherwise go to step 2.

7.4 SDP-based Cyclic Coordinate Ascent for Problem P2

Due to convexity of $\Phi(\{\mathbf{Q}_k\}_{k=1}^K, \alpha)$, problem P2 can be solved by standard interior point algorithms that unfortunately suffer from high computational complexity. Utilizing the inherent structural properties of $\Phi(\{\mathbf{Q}_k\}_{k=1}^K, \alpha)$, we now propose a simple iterative water-filling algorithm. It is a generalization of the cyclic coordinate ascent algorithm proposed in [100] for optimizing transmit covariance matrix with sum power constraint in broadcast channels. Due to the coupled interference power constraint involving all K SUs' transmit covariance matrices $\{\mathbf{Q}_k\}_{k=1}^K$, the classical water-filling [106] for individual power constraint cannot be

directly used here. Due to coupled power constraint, all K SUs need to do water-filling simultaneously with the same water level. On the other hand, the objective function in problem P2 is also coupled on all K transmit covariance matrices $\{\mathbf{Q}_k\}_{k=1}^K$, therefore, an equivalent Lagrangian problem based on gradient methods cannot be directly applied. The reason is that all $\{\mathbf{Q}_k\}_{k=1}^K$ are correlated with each other in their Lagrangian primal-dual solution. In our proposed generalized iterative water-filling algorithm, we first use cyclic coordinate ascent algorithm to decompose the coupled objective function into a sum of K non-coupled functions involving only individual $\mathbf{Q}_k$'s. The other transmit covariance matrices are treated as interference and all $\mathbf{Q}_k$'s are simultaneously updated based on results from the previous iteration. The Lagrangian primal-dual method is used to solve the optimization problem in each step (iteration) which decomposes weighted interference power constraint into separable constraints. Finally, we decompose the optimization problem with separable objective functions and constraints into K individual semi-definite programming (SDP) problems. We first describe the cyclic coordinate ascent algorithm that decomposes coupled objective function in problem P2 into separable functions.

Cyclic Coordinate Ascent Based Iterative Water-Filling

1) Initialize $\mathbf{Q}_k^{(0)} = \mathbf{I}_{N_{t,s}} \quad \forall k$

2) At iteration m, compute for $k = 1, \ldots, K$ and $i \geq k$ the noise and interference matrix coefficients

$$\boldsymbol{\Sigma}_{k,i}^{(m)} = \mathbf{I}_{N_{r,s}} + \rho \sum_{j=1,j\neq k}^{i} \mathbf{H}_{j,s} \mathbf{Q}_j^{(m-1)} \mathbf{H}_{j,s}^\dagger \tag{7.15}$$

and the sum power of all other users except user k

$$\delta_k = \sum_{i=1,i\neq k}^{K} \text{tr}\{\mathbf{Q}_i^{(m-1)}\} \tag{7.16}$$

3) **Water-filling step**: Treat the matrices $\mathbf{\Sigma}_{k,i}^{(m)}$ and variables δ_k as parallel, noninterfering ones and obtain the new transmit covariance matrix $\{\mathbf{S}_k\}_{k=1}^K$ by water-filling under interference power constraint $\Sigma_{k=1}^K \text{tr}\{\mathbf{H}_{k,p}\mathbf{S}_k\mathbf{H}_{k,p}^\dagger\} \leq \beta$, as described next. Define intermediate variable $\Gamma(\{\mathbf{S}_k\}_{k=1}^K)$ as below

$$\Gamma(\{\mathbf{S}_k\}_{k=1}^K) = \sum_{k=1}^K \{\sum_{i=k}^K \Delta_i B \log_2 |\rho \mathbf{H}_{k,s}\mathbf{S}_k\mathbf{H}_{k,s}^\dagger + \mathbf{\Sigma}_{k,i}^{(m)}|$$
$$- \alpha\left(\eta(\text{tr}\{\mathbf{S}_k\} + \delta_k) + KP_c\right)\}. \tag{7.17}$$

Let $\{\mathbf{S}_k^{(m)}\}_{k=1}^K$ be the solution of

$$\{\mathbf{S}_k^{(m)}\}_{k=1}^K = \arg \max_{\substack{\mathbf{S}_k \succeq 0, \text{tr}\{\mathbf{S}_k\} \leq P_{st} \\ \sum_{k=1}^K \text{tr}\{\mathbf{H}_{k,p}\mathbf{S}_k\mathbf{H}_{k,p}^\dagger\} \leq \beta}} \Gamma(\{\mathbf{S}_k\}_{k=1}^K). \tag{7.18}$$

4) Update transmit covariance matrices as
$\mathbf{Q}_k^{(m)} = \frac{1}{K}\mathbf{S}_k^{(m)} + \frac{K-1}{K}\mathbf{Q}_k^{(m-1)}, \quad k = 1, \ldots, K.$

The proof of convergence of the proposed iterative water-filling algorithm is similar to that in [100, 101] and is omitted. Owing to the convexity of $\Gamma(\{\mathbf{S}_k\}_{k=1}^K)$, the "water-filling step" is a convex optimization problem that has a unique solution. We first consider the Karush-Kuhn-Tucker (KKT) conditions for the problem in (7.18). The Lagrangian function [88] is given by

$$\mathcal{L}(\{\mathbf{S}_k\}_{k=1}^K, \lambda) = \Gamma(\{\mathbf{S}_k\}_{k=1}^K) - \lambda(\sum_{k=1}^K \text{tr}\{\mathbf{H}_{k,p}\mathbf{S}_k\mathbf{H}_{k,p}^\dagger\} - \beta) \tag{7.19}$$

$$s.t. \quad \mathbf{S}_k \succeq 0, \quad \text{tr}\{\mathbf{S}_k\} \leq P_{st}, \quad \forall k \tag{7.20}$$

where λ is the dual variable. By the KKT conditions for (7.18)

$$\sum_{k=1}^{K} \text{tr}\{\mathbf{H}_{k,p}\mathbf{S}_k\mathbf{H}_{k,p}^{\dagger}\} - \beta \leq 0 \tag{7.21}$$

$$\lambda(\sum_{k=1}^{K} \text{tr}\{\mathbf{H}_{k,p}\mathbf{S}_k\mathbf{H}_{k,p}^{\dagger}\} - \beta) = 0 \tag{7.22}$$

$$\lambda \geq 0 \tag{7.23}$$

$$\partial\Gamma(\{\mathbf{S}_k\}_{k=1}^{K})/\partial\mathbf{S}_k - \lambda\mathbf{H}_{k,p}^{\dagger}\mathbf{H}_{k,p} = 0, \quad 1 \leq k \leq K \tag{7.24}$$

where

$$\frac{\partial\Gamma(\{\mathbf{S}_k\}_{k=1}^{K})}{\partial\mathbf{S}_k} = \sum_{i=k}^{K} \Delta_i B\mathbf{H}_{k,s}^{\dagger}(\rho\mathbf{H}_{k,s}\mathbf{S}_k\mathbf{H}_{k,s} + \mathbf{\Sigma}_{k,i}^{(m)})^{-1}\mathbf{H}_{k,s} - \alpha\eta\mathbf{I}_{N_{t,s}} \tag{7.25}$$

The dual function of (7.18) is problem $P3$

$$P3: \quad g(\lambda) = \max_{\substack{\{\mathbf{S}_k\}_{k=1}^{K}:\mathbf{S}_k \succeq 0 \\ \text{tr}\{\mathbf{S}_k\} \leq P_{st}}} \mathcal{L}(\{\mathbf{S}_k\}_{k=1}^{K}, \lambda) \tag{7.26}$$

Because the problem in (7.18) is convex, it is equivalent to the following minimization problem

$$\min_{\lambda} g(\lambda), \quad s.t. \ \lambda \geq 0 \tag{7.27}$$

We choose initial λ, calculate $\mathbf{S}_k(\lambda)$ and resulting $g(\lambda)$, and then update λ according to the descent direction of $g(\lambda)$. This process repeats until the algorithm converges.

Since $g(\lambda)$ may not be differentiable, we use subgradient direction to update λ. The subgradient is $\beta - \sum_{k=1}^{K} \text{tr}\{\mathbf{H}_{k,p}\mathbf{S}_k\mathbf{H}_{k,p}^{\dagger}\}$. When $\sum_{k=1}^{K} \text{tr}\{\mathbf{H}_{k,p}\mathbf{S}_k\mathbf{H}_{k,p}^{\dagger}\} > \beta$, increase λ and vice versa. With a fixed λ, the optimal transmit covariance matrices $\{\mathbf{S}_k\}_{k=1}^{K}$ can be obtained by solving problem $P3$. We reformulate the objective function in $P3$ as

$$\mathcal{L}(\{\mathbf{S}_k\}_{k=1}^{K}, \lambda) = \sum_{k=1}^{K}\{\sum_{i=k}^{K} \Delta_i B\log_2 |\rho\mathbf{H}_{k,s}\mathbf{S}_k\mathbf{H}_{k,s}^{\dagger} + \mathbf{\Sigma}_{k,i}^{(m)}| - \alpha\left(\eta(\text{tr}\{\mathbf{S}_k\} + \delta_k) + KP_c\right)$$

$$-\lambda(\text{tr}\{\mathbf{H}_{k,p}\mathbf{S}_k\mathbf{H}_{k,p}^\dagger\} - \frac{1}{K}\beta)\}. \tag{7.28}$$

Let $\mathcal{L}'(\mathbf{S}_k, \lambda)$ denote kth "element" in $\mathcal{L}(\{\mathbf{S}_k\}_{k=1}^K, \lambda)$:

$$\mathcal{L}'(\mathbf{S}_k, \lambda) = \sum_{i=k}^K \Delta_i B \log_2 |\rho\mathbf{H}_{k,s}\mathbf{S}_k\mathbf{H}_{k,s}^\dagger + \mathbf{\Sigma}_{k,i}^{(m)}| - \alpha\left(\eta(\text{tr}\{\mathbf{S}_k\} + \delta_k) + KP_c\right)$$
$$- \lambda(\text{tr}\{\mathbf{H}_{k,p}\mathbf{S}_k\mathbf{H}_{k,p}^\dagger\} - \frac{1}{K}\beta). \tag{7.29}$$

It is clear that objective function as well as the constraints in $P3$ are separable. Therefore, the solution to problem $P3$ is equivalent to solutions to the following K subproblems:

$$P4: \quad \max_{\substack{\mathbf{S}_k \succeq 0 \\ \text{tr}\{\mathbf{S}_k\} \leq P_{st}}} \mathcal{L}'(\mathbf{S}_k, \lambda). \tag{7.30}$$

The objective $\mathcal{L}'(\mathbf{S}_k, \lambda)$ is a linear combination of concave functions on $\mathbf{S}_k$ and the constraints on $\mathbf{S}_k$ are also convex. Based on [88], problem $P4$ is a concave optimization problem in positive semidefinite matrix $\mathbf{S}_k$. In a realistic MAC scenario, it is reasonable to assume that the BS has more antennas than the SUs. Consequently, the possible MAC channel models include SISO, SIMO and MIMO models. For SISO and SIMO models, an SU has just one transmitter antenna and only the transmit power s_k needs to be optimized; however, it is hard to get an explicit solution for s_k using a gradient method directly [99, 101]. Due to convexity of $\mathcal{L}'(\mathbf{S}_k, \lambda)$, s_k can be obtained using a simple line search in range $(0, P_{st})$. For general MAC with multiple antennas at both transmitter and receiver, we need to optimize transmit covariance matrix $\mathbf{S}_k$. However, the solution for $\mathbf{S}_k$ cannot utilize a water-filling algorithm as in [106, 100, 108] because $\mathbf{S}_k$ cannot be diagonalized. Fortunately, $\mathbf{S}_k$ is a positive semi-definite matrix, therefore the concave optimization problem $P4$ can be solved by utilizing the SDP software, in particular, SeDuMi embedded in the CVX Matlab software package.

Let $\{\mathbf{S}_k^*\}_{k=1}^K$ and λ^* denote the optimal energy efficient power allocation and optimal value of the Lagrange multiplier λ. Then $\{\mathbf{S}_k^*\}_{k=1}^K$ and λ^* satisfy the KKT conditions.

7.5 Simulation Examples

We consider a C-MAC composed of a single PU, 2 SUs with multiple transmit antennas and a single secondary BS with multiple antennas. The priority weights for two SUs are fixed at (w_1, w_2)=(1.4, 0.6). The bandwidth B is normalized to be 1. The elements of the channel fading matrices $\{\mathbf{H}_{k,p}\}_{k=1}^2$ and $\{\mathbf{H}_{k,s}\}_{k=1}^2$ from the SU transmitter to the primary and secondary receivers are both mutually independent complex Gaussian random variables distributed as $\mathcal{CN}(0,\ 0.1)$ and $\mathcal{CN}(0,1)$, respectively. It is assumed the power amplifier efficiency is 38% for the secondary transmitter's RF amplifier, leading to $\eta = 1/0.38$ in (7.5). The static circuit power is assumed to be 100 mW. The value of interference power constraint on PU is $\beta = 1$ mW. The background white Gaussian noise power is assumed to be 1 mW (0dBm). The reported results are based on 100 Monte Carlo runs with 100 randomly generated $\{\mathbf{H}_{k,p}\}_{k=1}^2$ and $\{\mathbf{H}_{k,s}\}_{k=1}^2$.

Figs. 7.1 and 7.2 show the capacity and energy efficiency, respectively, of the cognitive MAC channel under two cases of energy efficiency maximization as discussed in Sec. III and spectral efficiency (capacity) maximization without any consideration of power consumption, as discussed in [99]. Our proposed scheme and the spectral efficiency maximization of [99] are denoted as "EE Max" and "SE Max" respectively in these figures. Three different antenna settings were considered: 1×1 SISO with $N_{t,s} = 1$, $N_{r,s} = 1$ and $N_{r,p} = 1$, 1×2 SIMO with $N_{t,s} = 1$, $N_{r,s} = 2$ and $N_{r,p} = 2$ and 2×2 MIMO with $N_{t,s} = 2$, $N_{r,s} = 2$ and $N_{r,p} = 2$. The transmit power constraint P_{st} for the SU transmitter was varied from 0 mW to 150 mW. It is seen that compared with the conventional spectrum efficiency maximization design for multiple access channel, the energy efficient design can enhance energy efficiency dramatically, particularly in the higher transmit power range but at the cost of smaller

throughput. In addition, more receive antennas result in higher energy efficiency and capacity because spatial diversity is utilized.

7.6 Conclusions

In this chapter, we proposed an energy-efficient transmit covariance matrix (precoder) design for MIMO based cognitive multiple access channel in spectrum sharing underlay cognitive radio networks. We constructed an energy efficiency function that incorporates both transmission and circuit power consumption. Then an energy efficiency maximization problem was formulated for C-MAC under individual SU transmit-power and PU interference power constraints. It turned out to be a fractional programming problem that was iteratively solved via a parametrized convex optimization problem formulation. We further decompose the coupled parametrized convex optimization into K parallel non-interfering sub convex optimization problem solved by simple line search or mature SDP algorithm. Compared with existing spectrum efficiency maximization [99], our proposed energy efficient scheme can enhance energy efficiency significantly under different receiver antenna number. The trade-off between energy efficiency and spectrum efficiency was explored via computer simulations.
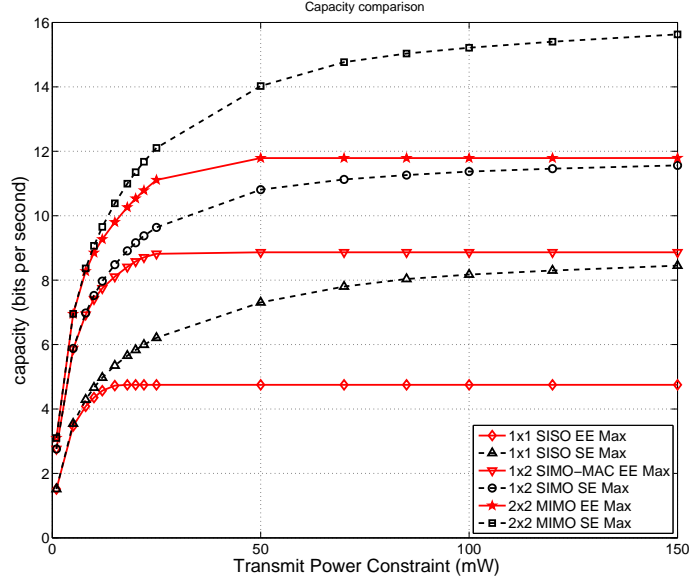
Figure 7.1: Capacity comparison: In the energy efficiency criterion we maximize energy efficiency $\Psi(\{\mathbf{Q}_k\}_{k=1}^{K})$ as in problem $P1$ whereas in the spectral efficiency criterion we maximize the channel capacity as in [99]. In 1×1 SISO system we used $N_{t,s} = 1$, $N_{r,s} = 1$ and $N_{r,p} = 1$, the 1×2 SIMO system had $N_{t,s} = 1$, $N_{r,s} = 2$ and $N_{r,p} = 2$, and the 2×2 MIMO system had $N_{t,s} = 2$, $N_{r,s} = 2$ and $N_{r,p} = 2$.
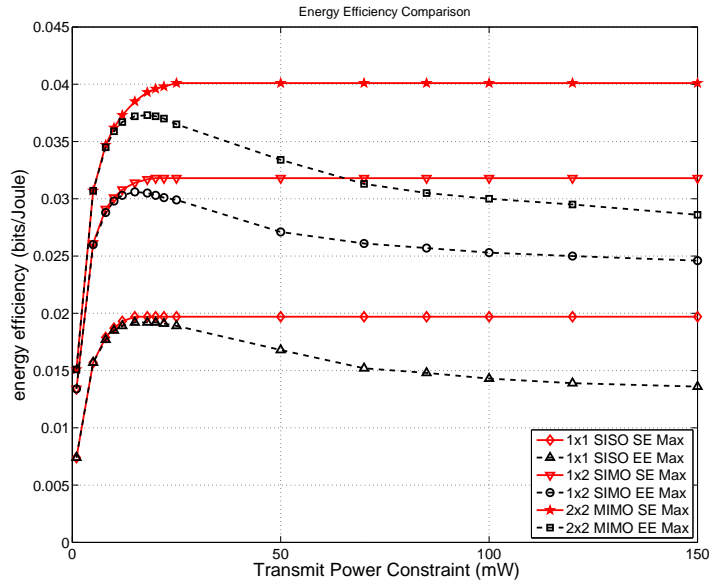
Figure 7.2: Energy efficiency comparison: In the energy efficiency criterion we maximize energy efficiency $\Psi(\{\mathbf{Q}_k\}_{k=1}^{K})$ as in problem $P1$ whereas in the spectral efficiency criterion we maximize the channel capacity as in [99]. In 1×1 SISO system we used $N_{t,s} = 1$, $N_{r,s} = 1$ and $N_{r,p} = 1$, the 1×2 SIMO system had $N_{t,s} = 1$, $N_{r,s} = 2$ and $N_{r,p} = 2$, and the 2×2 MIMO system had $N_{t,s} = 2$, $N_{r,s} = 2$ and $N_{r,p} = 2$.

133

Chapter 8

Conclusion and Future Work

8.1 Conclusion

This dissertation covers two main topics: 1) low complexity cyclostationary spectrum sensing, and 2) energy efficient resource allocation for cognitive radio network.

In Chapter 2 through Chapter 5, secondary users need to first sense the activities of primary users and then decide whether to transmit or not based on presence or absence of primary users. This secondary access scheme is called overlay spectrum sharing for cognitive radio network. Low-complexity cyclostationary spectrum sensing under white Gaussian noise and colored Gaussian noise are studied in Chapter 3 and Chapter 4, respectively. In addition to sensing complexity, energy efficiency has become a "hot" research topic due to the trend of sustainable energy and green wireless communication and networks. A joint energy efficient sensing and transmission for multichannel based cognitive radio works is proposed in Chapter 5. The energy efficient resource allocation is also studied under another spectrum sharing cognitive radio network named underlay CRN in Chapter 6 and Chapter 7. With underlay access, secondary users can transmit simultaneously with primary users under limited interference power constraint to primary users. To utilize spatial diversity and multiplexing, MIMO-assisted transmission is incorporated into transmission scheme. We design optimal transmit power allocation for energy efficiency maximization in single secondary link and multi secondary links based cognitive radio network.

In Chapter 3, detection of cyclostationary primary user (PU) signals in white Gaussian noise for cognitive radio systems was considered based on looking for a cycle frequency at a particular time lag in the cyclic autocorrelation function (CAF) of the noisy PU signal. We explicitly exploit the knowledge that under the null hypothesis of PU signal absent,

the measurements originate from white Gaussian noise with possibly unknown variance. Our formulation allows us to simplify the spectrum sensing detector, and obviates the need for estimating an unwieldy covariance matrix needed in the Dandawate-Giannakis [59] and related approaches. We considered both single and multiple antenna receivers and both nonconjugate and conjugate CAFs. A performance analysis of the proposed detectors was carried out. Supporting simulation examples were presented to compare our detectors with those of [59], [73], [63] and [71], and to demonstrate the capability to discriminate among signals exhibiting cyclostationarity at different cycle frequencies and/or time lags. Our proposed approaches are computationally cheaper than the Dandawate-Giannakis and related approaches [59], [73] while having quite similar detection performance. Our proposed approach significantly outperforms [71] while having same computational complexity. In white noise channels, the single-antenna detector of [63] has a 3dB SNR advantage for achieving a detection probability of 0.9 over our proposed detector but requires five times more complex multiplications. Also, Jallon's test [63] fails to reject a class of cyclostationary interfering signals whereas our proposed detector is successful.

In Chapter 4, detection of cyclostationary PU signals in colored Gaussian noise for cognitive radio systems was considered based on looking for single or multiple cycle frequencies at single or multiple time lags in the CAF of the noisy PU signal. We explicitly exploit the knowledge that under the null hypothesis of PU signal absent, the measurements originate from colored Gaussian noise with possibly unknown correlation. Our formulation allows us to simplify the spectrum sensing detector, and obviates the need for estimating an unwieldy covariance matrix needed in the Dandawate-Giannakis [59, 64] and related approaches. We considered both single and multiple antenna receivers and both nonconjugate and conjugate CAFs. A performance analysis of the proposed detectors was carried out. Supporting simulation examples were presented to compare our detectors with those of [59], [73], [64] and [71]. Our proposed approaches are computationally cheaper than the Dandawate-Giannakis

and related approaches [59], [64], [73] while having quite similar detection performance for a fixed false alarm rate. Our proposed approach significantly outperforms [71].

In Chapter 5, we studied how to balance throughput and energy consumption for a slotted multi-channel CRN. An optimization problem involving sensing parameters (sensing duration and local test threshold) and power allocation was formulated to maximize a utility function that rewards throughput but penalizes energy consumption. To obtain (locally) optimal sensing parameters and power allocation, an iterative algorithm was proposed. Numerical simulations demonstrate that the iterative algorithm converges fast. It performs better than a "only power allocation optimization" approach and an existing approach [78] that ignores energy efficiency.

In Chapter 6, we proposed an energy-efficient transmit covariance matrix (precoder) design for spectrum sharing underlay cognitive radio networks when multiple antennas are employed at the secondary user transmitter. We constructed an energy efficiency function that incorporates both transmission and circuit power consumption. Then an energy efficiency maximization problem was formulated for a single secondary link in a CRN under SU transmit-power and PU interference power constraints. It turned out to be a fractional programming problem that was iteratively solved via a parametrized convex optimization problem formulation. A multichannel extension of the problem was also investigated. The trade-off between energy efficiency and spectrum efficiency was explored via computer simulations.

In Chapter 7, we proposed an energy-efficient transmit covariance matrix (precoder) design for MIMO based cognitive multiple access channel in spectrum sharing underlay cognitive radio networks. We constructed an energy efficiency function that incorporates both transmission and circuit power consumption. Then an energy efficiency maximization problem was formulated for C-MAC under individual SU transmit power and PU interference power constraints. It turned out to be a fractional programming problem that was iteratively solved via a parametrized convex optimization problem formulation. We further decompose

136

the coupled parametrized convex optimization into K parallel non-interfering sub convex optimization problem solved by simple line search or mature SDP algorithm. Compared with existing spectrum efficiency maximization [99], our proposed energy efficient scheme can enhance energy efficiency significantly under different receiver antenna number. The trade-off between energy efficiency and spectrum efficiency was explored via computer simulations.

8.2 Future Work

The research work on energy efficient precoding in underlay MIMO single secondary link and power allocation in SIMO cognitive MAC is an initial step of our research on energy efficient resource allocation in CRN. There are still future research topics that merit study:

- **On Robust Energy Efficient MIMO-Assisted Spectrum Sharing**

  In Chapter 6, we proposed energy efficient transmit covariance matrix (precoder) for MIMO-assisted single secondary link. However, our algorithm requires exact channel state information (CSI) from secondary transmitter to both secondary receiver and primary receiver. Due to channel noise, fading and/or shortage of feedback between transmitter and receiver, CSI may be partially known or even unknown. This brings challenge to our proposed algorithm in Chapter 6 and inspires us to design robust energy efficient precoding (beamforming) for the SU transmitter to maximize energy efficiency when CSI is not perfectly known.

- **On Energy Efficient MIMO Broadcast (BC) in Underlay Cognitive Radio Networks**

  In underlay broadcast channel, how to optimize the transmit signal covariance matrix at the base station (BS) for multiple secondary user receivers to maximize capacity have attracted attention and efforts from academia. However, how to design energy efficient broadcast (BC) has received less attention. We aim to enhance energy efficiency of BC transmission by optimizing transmit signal covariance matrix at BS.

The secondary users is equipped with either single or multiple antennas. Moreover, different secondary receivers have different nonnegative priority weights, thus the total BC capacity is a weighted sum. Consequently, the final energy efficiency is defined as a weighted capacity versus energy consumption. The BC transmission is constrained by the interference power upper bound to the primary users.

Bibliography

[1] FCC, "Spectrum policy task force report," FCC, Washington, D.C., ET Docket 02-155, Nov. 2002.

[2] J. Mitola and G. Q. Maguire, "Cognitive radio: Making software radios more personal," *IEEE Pers. Commun*, vol. 6, pp. 13–18, Aug. 1999.

[3] FCC, "Notice of proposed rule making and order: facilitating opportunities for flexible, efficient, and reliable spectrum use employing cognitive radio technologies," FCC, Washington, D.C., *ET Docket 03-108*, Feb. 2005.

[4] FCC, "Second report and order and memorandum opinion and order," FCC, Washington, D.C., *ET Docket No. 08-260*, Nov. 2008.

[5] A. Sahai, N. Hoven, and R. Tandra, "Some fundamental limits on cognitive radio," in *Proc. Allerton Conf. Commun., Contr., Comput.*, Univ. of Illinois, Urbana-Champaign, IL, 2004.

[6] A. Ghasemi and E. Sousa, "Spectrum sensing in cognitive radio networks: Requirements, challenges and design trade-offs," *IEEE Commun. Mag.* , vol. 46, pp. 32–39, Apr. 2008.

[7] B. Wang and K. J. Ray Liu, "Advances in cognitive radio networks: A survey," *IEEE J. Sel. Areas Commun.*, vol. 5, pp. 5–23, Feb. 2011.

[8] K. G. Shin, H. Kim, A. W. Min, and A. Kumar, "Cognitive radios for dynamic spectrum access: From concept to reality," *IEEE Wireless Commun.*, vol. 17, pp. 64–74, Dec. 2010.

[9] S. Filin, H. Harada, H. Murakami, and K. Ishizu, "International standardization of cognitive radio systems," *IEEE Commun. Mag.* , vol. 49, pp. 82–89, Mar. 2011.

[10] J. Wang, M. Ghosh, and K. Challapali, "Emerging cognitive radio applications: A survey," *IEEE Commun. Mag.*, vol. 49, pp. 74–81, May. 2011

[11] Ofcom, "A statement on our approach to awarding the digital dividend," Ofcom, London, UK, *Digital Dividend Review*, Dec. 2007.

[12] H. R. Karimi, M. Fenton, G. Lapierre, and E. Fournier, "European harmonized technical conditions and band plans for broadband wireless access in the 790-862 MHz digital dividend spectrum," in *Proc. IEEE Symp. New Frontiers Dynamics Spectrum Access Networks(DySPAN)*, Singapore, 2010.

[13] OET, "Evaluation of the performance of prototype TV-band white space devices phase II," FCC, Washington, D.C., *OET Report FCC/OET 08-TR-1005*, Oct. 2008.

[14] Spectrum Bridge. (2009, Oct.). The nation's first white spaces network: Press release [Online]. Available: http://spectrumbridge.com/web/images/pdfs/ PRclaudville-whitespaceprojectpressrelease.pdf

[15] Spectrum Bridge. (2010, May.). TV white spaces powering smart city services [Online]. Available: http://spectrumbridge.com/web/images/pdfs/smartcityspectrumbridge.pdf

[16] T. Yucek and H. Arslan, "A survey of spectrum sensing algorithms for cognitive radio applications," *IEEE Commun. Surveys Tuts.*, vol. 11, pp. 116–130, First Quarter. 2009.

[17] B. Wild and K. Ramchandran, "Detecting primary receivers for cognitve radio applications," in *Proc. IEEE Symp. New Frontiers Dynamics Spectrum Access Networks(DySPAN)*, Baltimore, MD, 2005.

[18] G. J. Buchwald, S. L. Juffner, L. M. Ecklund, M. Brown, and E. H. Callaway, "The design and operation of the IEEE 802.22 disabling beacon for the protection of TV whitespace incumbents," in *Proc. IEEE Symp. New Frontiers Dynamics Spectrum Access Networks(DySPAN)*, Chicago, IL, 2008.

[19] D. Gurney, G. Buchwald, L. Ecklund, S. L. Kuffner, and J. Grosspietsch, "GEO-location database techniques for incumbent protection in the TV white space," in *Proc. IEEE Symp. New Frontiers Dynamics Spectrum Access Networks(DySPAN)*, Chicago, IL, 2008.

[20] D. Chen, S. Yin, Q. Zhang, M. Liu, and S. Li, "Mining spectrum usage data: a large-scale spectrum measurement study," in *Proc. The 15th Annu. Int. Conf. Mobile Computing and Networking(MobiCom)*, Beijing, China, 2009.

[21] H. Kim and K. G. Shin, "Efficient discovery of spectrum opportunisties with MAC-layer sensing in cognitive radio networks," *IEEE Trans. Mobile Comput.*, vol. 7, pp. 533–545, May. 2008.

[22] Y. C. Liang, Y. Zeng, E. C. Y. Peh, and A. T. Hoang, "Sensing throughput tradeoff for cognitive radio networks," *Trans. Wireless Commun.*, vol. 7, pp. 1326–1337, Apr. 2008.

[23] W. Zhang and K. Letaief, "Cooperative spectrum sensing with transmit and relay diversity in cognitive radio networks," *Trans. Wireless Commun.*, vol. 7, pp. 4761–4766, Dec. 2008.

[24] Q. Zhao and B. M. Sadler, "A survey of dynamic spectrum access," *IEEE Signal Process. Mag.*, May. 2007.

[25] L. Gao, X. Wang, Y. Xu, and Q. Zhang, "Spectrum trading in cognitive radio networks: A contract-theoretic modeling approach," *IEEE J. Sel. Areas Commun.*, vol. 29, pp. 843–855, Apr. 2011.

[26] O. Simeone, Y. Bar-Ness, and U. Spagnolini, "Stable throughput of cognitive radio radios with and without relaying capability," *IEEE Trans. Commun.*, vol. 55, pp. 2351–2360, Dec. 2007.

[27] S. Srinivasa and S. A. Jafar, "Cognitive radios for dynamic spectrum access - the throughput potential of cognitive radio: A theoretical perspective," *IEEE Commun. Mag.*, vol. 45, pp. 73–79, May. 2007.

[28] V. K. Tumuluru, P. Wang, and D. Niyato, "A novel spectrum scheduling scheme for multi-channel cognitive radio network and performance analysis," *IEEE Trans. Veh. Technol.*, vol. 60, pp. 1849–1858, May. 2011.

[29] Y. Chen, Q. Zhao, and A. Swami, "Joint design and separation principle for opportunistic spectrum access in the presence of sensing errors," *IEEE Trans. Inform. Theory*, vol. 54, pp. 2053–2071, May. 2008.

[30] H. Su and X. Zhang, "Cross-layered based oportunistic MAC protocols for QoS provisioning over cognitive radio wireless networks," *IEEE J. Sel. Areas Commun.*, vol. 26, pp. 118–129, Jan. 2008.

[31] Y. T. Hou, Y. Shi, and H. D. Sherali, "Spectrum sharing for multi-hop networking with cognitive radios," *J. Sel. Areas Commun.*, vol. 26, pp. 146–155, Jan. 2008.

[32] I. F. Akyildiz, W. Y. Lee, M. C. Vuran, and S. Mohanty, "Next generation/dynamic spectrum access/cognitive radio wireless networks: A survey," *Computer Networks*, vol. 50, pp. 2127–2159, Sept. 2006.

[33] G. Cheng, W. Liu, Y. Li, and W. Cheng, "Spectrum aware on-demand routing in cognitive radio networks," in *Proc. IEEE Symp. New Frontiers Dynamic Spectrum Access Networks (DySPAN)*, Dublin, Ireland, 2007.

[34] O. B. Akan and I. F. Akyildiz, "ATL: An adaptive transport layer suite for next generation wireless Internet," *IEEE J. Sel. Areas Commun.*, vol. 22, pp. 802–817, Jun. 2004.

[35] R. Chen, J. M. Park, and J. H. Reed, "Defense against primary user emulation attacks in cognitive radio networks," *IEEE J. Sel. Areas Commun.*, vol. 26, pp. 25–37, Jan. 2008.

[36] P. Kaligineedi, M. Khabbazian, and V. K. Bharava, "Secure cooperative sensing techniques for cognitive radio systems," in *Proc. IEEE Int. Conf. Commun. (ICC)*, Beijing, China, 2008.

[37] ITU, "Definition of software defined radio (SDR) and cognitive radio system (CRS)," *ITU*, Geneva, Switzerland, ITU-R. SM.2152, Sep. 2009.

[38] C. Stevenson, G. Chouinard, Z. Lei, W. Hu, S. Shellhammer, and W. Caldwell, "IEEE 802.22: The first cognitive radio wireless regional area network standard," *IEEE Commun. Mag.*, vol. 47, pp. 130–138, Jan. 2009.

[39] R. Kennedy and P. Ecclesine. (2010, Jul.). IEEE 802.11af tutorial [Online]. Available: https://mentor.ieee.org/802.11/dcn/10/11-10-0742-00-0000-p802-11aftutorial. ppt

[40] J. Wang, M. S. Song, S. Santhiveeran, K. Lim, G. Ko, K. Kim, S. H. Hwang, M. Ghosh, V. Gaddam, and K. Challapali, "First cognitive radio networking standard for persoanl/portable devices in TV white spaces," in *Proc. IEEE Symp. New Frontiers Dynamic Spectrum Access Networks (DySPAN)*, Singapore, 2010.

[41] S. Deb, V. Srinivasan, and R. Maheshwari, "Dynamic spectrum access in DTV whitespaces: Design rules, architecture and algorithms," in *Proc. The 15th Annu. Int. Conf. Mobile Computing and Networking(MobiCom)*, Beijing, China, 2009.

[42] ECMA-392: MAC and PHY for operation in TV white space, ECMA, Dec. 2009.

[43] M. Mueck, A. Piipponen, K. Kalliojarvi, G. Dimitrakopoulos, K. Tsagkaris, P. Demestichas, F. Casadevall, J. Perez-Romero, O. Sallent, G. Baldini, S. Filin, H. Harada, M. Debbah, T. Haustein, J. Gebert, B. Deschamps, P. Bender, M. Street, S. Kandeepan, J. Lota, and A. Hayar, "ETSI reconfigurable radio systems: status and future directions on software defined radio and cognitive radio standars," *IEEE Commun. Mag.* , vol. 48, pp. 78–86, Sept. 2010.

[44] F. F. Digham, M. S. Alouini, and M. K. Simon, "On the energy detection of unknown signals over fading channels," *IEEE Trans. Commun.*, vol. 55, pp. 21–24, Jan. 2007.

[45] R. Fantacci and A. Tani, "Performance evaluation of a spectrum-sensing techniques for cognitive radio applications in B-VHF communication systems," *IEEE Trans. Veh. Technol.*, vol. 58, pp. 1722–1730, May. 2009.

[46] A. T. Walden, D. B. Percival, and E. J. McCoy, "Spectrum estimation by wavelet thresholding of multitaper estimators," *IEEE Trans. Signal Process.*, vol. 46, pp. 3153–3165, Dec. 1998.

[47] J. K. Tugnait, "Wavelet-thresholded multitaper spectrum sensing for cognitive radios in unknown noise," in *Proc. IEEE Int. Conf. Commun. (ICC)*, Cape Town, South Africa, 2010.

[48] C. Cordeiro, M. Ghosh, D. Cavalcanti, and K. Challapali, "Spectrum sensing for dynamic spectrum access of TV bands," in *Proc. IEEE 2nd Int. Conf. Cognitive Radio Oriented Wireless Networks and Commun. (CROWNCOM)*, Orlando, FL, 2007.

[49] W. A. Gardner, "Exploitation of spectral redundancy in cyclostationary signals," *IEEE Signal Process. Mag.*, vol. 8, pp. 14–36, Apr. 1991.

[50] Y. Zeng, C. L. Koh, and Y. C. Liang, "Maximum eigenvalue detection: Theory and application," in *Proc. IEEE Int. Conf. Commun. (ICC)*, Beijing, China, 2008.

[51] Z. Tian and G. B. Giannakis, "A wavelet approach to wideband spectrum sensing for cognitive radios," in *Proc. IEEE 1st Int. Conf. Cognitive Radio Oriented Wireless Networks and Commun. (CROWNCOM)*, Mykonos Island, Greece, 2006.

142

[52] A. Wiesler, R. Machauer, and F. Jondral, "Comparison of GMSK and linear approximated GMSK for use in software radio," in *Proc. IEEE 5th Int. Symp. Spread Spectrum Tech. and Applicat.*, Sun City, South Africa, 1998.

[53] P. Jung, "Laurent's representation of binary digital continuous phase modulated signals with modulation index 1/2 revisited," *IEEE Trans. Commun.*, vol. 42, pp. 221–224, Feb. 1994.

[54] S. M. Kay, *Fundamentals of Statistical Signal Processing Volume II: Detection Theory.* Upper Saddle River, NJ: Prentice Hall, 1998.

[55] T.W. Anderson, *An Introduction to Multivariate Statistical Analysis*, 2nd Ed. New York, NY: NY John Wiley, 1984.

[56] D. Cabric, S. Mishra, and R.W. Broderson, "Implementation issues in spectrum sensing for cognitive radios," in *Proc. IEEE 38th Asilomar Conf. Signals, Systems, Computers*, Pacific Grove, CA, 2004.

[57] D. Cabric, A. Tkachenko, and R.W. Broderson, "Experimental study of spectrum sensing based on energy detection and network cooperation," in *Proc. ACM 1st Int. Workshop Tech. and Policy Accessing Spectrum (TAPAS)*, Boston, MA, 2006.

[58] S. Chaudhari, V. Koivunen and H.V. Poor, "Autocorrelation-based decentralized sequential detection of OFDM signals in cognitive radios," *IEEE Trans. Signal Proc.*, vol. 57, no. 7, pp. 2690–2700, Jul. 2009.

[59] A.V. Dandawate and G.B. Giannakis, "Statistical tests for presence of cyclostationarity," *IEEE Trans. Signal Process.* vol. 42, pp. 2255-2369, Sep. 1994.

[60] S. Haykin, D.J. Thomson and J.H. Reed, "Spectrum sensing for cognitive radio," *Proc. IEEE*, vol. 97, pp. 849-877, May. 2009.

[61] C.W. Helstrom, *Elements of Signal Detection and Estimation.* Englewood Cliffs, NJ: Prentice Hall, 1995.

[62] P. Jallon, "A spread signals detection algorithm based on the second order statistics in semi-blind contexts" in *Proc. IEEE 3rd Int. Conf. Cognitive Radio Oriented Wireless Networks and Commun. (CROWNCOM)*, Singapore, 2008.

[63] P. Jallon, "An algorithm for detection of DVB-T signals based on their second-order statistics" *EURASIP J. Wireless Commun. Networking*, vol. 2008, pp. 1-9 Jan. 2008.

[64] J. Lunden, V. Koivunen, A. Huttunen and H.V. Poor, "Collaborative cyclostationary spectrum sensing for cognitive radio systems," *IEEE Trans. Signal Process.*, vol. 57, pp. 4182-4195, Nov. 2009.

[65] J. Ma, G.Y. Li and B.H. Juang, "Signal processing in cognitive radio," *Proc. IEEE*, vol. 97, pp. 805-823, May. 2009.

[66] K. Muraoka, M. Ariyoshi and T. Fujii, "A novel spectrum-sensing method based on maximum cyclic autocorrelation selection for cognitive radio system," in *Proc. IEEE Symp. New Frontiers Dynamics Spectrum Access Networks(DySPAN)*, Chicago, IL, 2008.

[67] M. Oner and F. Jondral, "Cyclostationarity based air interface recognition for software radio systems," in *Proc. IEEE Radio Wireless Conf.*, Atlanta, GA, 2004.

[68] M. Oner and F. Jondral, "On the extraction of the channel allocation information in spectrum pooling systems," *J. Sel. Areas Commun.*, vol. 25, pp. 558-565, Apr. 2007.

[69] V. Osa, C. Herranz, J.F. Monserrat and X. Gelabert, "Implementing opportunistic spectrum access in LTE-advanced," *EURASIP J. Wireless Commun. Networking*, 2012, 2012:99

[70] T. Söderström, P. Stoica, *System Identification*. New York, NY: Prentice Hall, 1989.

[71] A. Tani and R. Fantacci, "Low-complexity cyclostationary-based spectrum sensing for UWB and WiMAX coexistence with noise uncertainty," *IEEE Trans. Veh. Technol.*, vol. 59, pp. 2940-2950, Jul. 2010.

[72] J.K. Tugnait and G. Huang, "Cyclic autocorrelation based spectrum sensing in colored Gaussian noise," in *Proc. 2012 IEEE Wireless Commun. Networking Conf. (WCNC 2012)*, Paris, France, Apr. 2012.

[73] G. Zhong, J. Guo, Z. Zhao and D. Qu, "Cyclostationarity based multi-antenna spectrum sensing in cognitive radio networks," in *Proc. IEEE Veh. Tech. Conf. (VTC Spring)*, Taipei, 2010.

[74] G. Huang and J. K. Tugnait, "On cyclic autocorrelation-based spectrum sensing for cognitive radio systems in Gaussian noise," in *Proc. 49th Annual Allerton Conf. Commun., Control, Computing,*, Urbana-Champaign, IL, 2011.

[75] E. Axell and E. G. Larsson, "Optimal and suboptimal spectrum sensing of OFDM signals in known and unknown noise variance," *IEEE J. Sel. Areas Commun.*, vol. 29, pp. 290–304, Feb. 2011.

[76] E. Axell and E.G. Larsson, "Multiantenna spectrum sensing of a second-order cyclostationary signal," in *Proc. 2011 4th IEEE Intern. Workshop Computational Advances in Multi-Sensor Adaptive Processing (CAMSAP)*, San Juan, Puerto Rico, Dec. 2011.

[77] Z. Hasan, H. Boostanimehr, and V. K. Bhargava, "Green cellular networks: A survey, some research issues and challenges," *IEEE Commun. Surveys Tuts.*, vol. 13, pp. 524–540, Forth Quarter. 2011.

[78] H. Yu, W. Tang, and S. Li, "Joint sensing and power allocation in multiple-channel cognitive radio networks," *IEICE Trans. Commun.*, vol. E95-B, pp. 672–675, Feb. 2012.

[79] H. Mu and J. Tugnait, "Joint soft-decision cooperative spectrum sensing and power control in multiband cognitive networks," in *Proc. IEEE Intern. Conf. Commun (ICC)*, Ottawa, Canada, 2012.

[80] T. V. Nguyen, H. Shin, T. Q. S. Quek, and M. Z. Win, "Sensing and probing cardinalities for active cognitive radios," *IEEE Trans. Signal Process.*, vol. 60, pp. 1833–1848, Apr. 2012.

[81] Y. Pei, Y. C. Liang, K. C. Teh, and K. H. Li, "Energy-efficient design of sequential channel sensing in cognitive radio networks: optimal sensing strategy, power allocation ,and sensing order," *IEEE J. Sel. Areas Commun.*, vol. 29, pp. 1648–1659, Sep. 2011.

[82] L. Li, X. Zhou, H. Xu, G. Y. Li, D. Wang, and A. Soong, "Energy-efficient transmission in cognitive radio networks," in *Proc. 7th IEEE Consumer Commun. Networking Conf. (CCNC)*, Las Vegas, NV, 2010.

[83] Y. Chen, Q. Zhao, and A. Swami, "Distributed spectrum sensing and access in cognitive radio networks with energy constraint," *IEEE Trans. Signal Process.*, vol. 57, pp. 783–797, Feb. 2009.

[84] A. T. Hoang, Y. C. Liang, D. T. C. Wong, Y. Zeng, and R. Zhang, "Opportunistic spectrum access for energy-constrained cognitive radios," *IEEE Trans. Wireless Commun.*, vol. 8, pp. 1206–1211, March. 2009.

[85] X. Feng, X. Gan, and X. Wang, "Energy-constrained cooperative spectrum sensing in cognitive radio networks," in *Proc. IEEE Global Telecom. Conf. (GLOBECOM)*, Houston, TX, 2011.

[86] H. Su and X. Zhang, "Cross-layer based opportunistic MAC protocols for QoS provisionings over cognitive radio wireless networks," *IEEE J. Sel. Areas Commun.*, vol. 26, pp. 118–129, Jan. 2008.

[87] D. Hu and S. Mao, "Design and analysis of a sensing error-aware MAC protocol for cognitive radio networks," in *Proc. IEEE Global Telecom. Conf. (GLOBECOM)*, Honolulu, Hawaii, 2009.

[88] S. Boyd and L. Vandenberghe, *Convex Optimization.* Cambridge, UK: Cambridge Univ. Press, 2004.

[89] E.V. Belmega and S. Lasaulce, "Energy-efficient precoding for multi-antenna terminals," *IEEE Trans. Signal Process.*, vol. 59, pp. 329-340, Jan. 2011.

[90] L. Fu, Y. Zhang and J. Huang, "Energy efficient transmission in MIMO cognitive radio networks," in *Proc. 46th Annual Conf. Information Sciences & Systems*, Princeton, NJ, 2012.

[91] M. Grant and S. Boyd. (2011, Apr.). CVX: Matlab software for disciplined convex programming, version 1.21[Online]. Available: http://www.cvxr.com/cvx

[92] A. He et al, "Power consumption minimization for MIMO Systems - A cognitive radio approach," *IEEE J. Sel. Areas Commun.*, vol. 29, pp. 469-479, Feb. 2011.

[93] C. Jiang et al, "A survey of energy-efficient wireless communications," *IEEE Commun. Surveys Tuts.*, to appear (early access on IEEE Xplore).

[94] G.Y. Li et al, "Energy-efficient wireless communications: Tutorial, survey, and open issues," *IEEE Trans. Wireless Commun.*, vol. 18, pp. 28-35, Dec. 2011.

[95] F. Meriaus, Y. Hayel, S. Lasaulce and A. Garnaev, "Long-term Energy Constraints and Power Control in Cognitive Radio Networks,' in *Proc. 17th Int. Conf. Digital Signal Process.*, Corfu, Greece, 2011.

[96] D. Tse and P. Viswanathan, *Fundamentals of Wireless Communication.* Cambridge, UK: Cambridge Univ. Press, 2005.

[97] R. Zhang and Y. Liang, "Exploiting multi-antennas for opportunistic spectrum sharing in cognitive radio networks," *IEEE J. Sel. Topics Signal Process.*, vol. 2, pp. 88-102, Feb. 2008.

[98] Q. Zhao and B.M. Sadler, "A survey of dynamic spectrum access," *IEEE Signal Process. Mag.*, vol. 24, no. 3, pp. 79-89, May 2007.

[99] L. Zhang, Y. Xin, Y. C. Liang, and H. V. Poor, "Cognitive multiple access channels: Optimal power allocation for weighted sum rate maximization," *IEEE Trans. Commun.*, vol. 57, pp. 2754–2762, Sep. 2009.

[100] N. Jindal, W. Rhee, S. Vishwanath, S. A. Jafar, and A. Goldsmith, "Sum power iterative water-filling for multi-antenna Gaussian broadcast channels," *IEEE Trans. Inf. Theory*, vol. 51, pp. 1570–1580, Apr. 2005.

[101] M. Kobayashi and G. Caire, "An Iterative waterfilling for maximum weighted sum-rate of Gaussian MIMO-BC," in *IEEE J. Sel. Areas Commun.*, vol. 24, pp. 1640–1646, Aug. 2006.

[102] J. Chen and K. K. Wong, "Improving energy efficiency for multiuser MIMO systems with effective capacity constraints," in *Proc. IEEE Veh. Tech. Conf. (VTC Spring)*, Barcelona, Spain, 2009.

[103] E. Jorswieck, H. Boche, and S. Naid, "Energy-aware utility regions: Multiple access Pareto boundary," *IEEE Trans. Wirel. Commun.*, vol. 9, pp. 2216–2226, Jul. 2010.

[104] D. Tse and S. Hanly, "Multiaccess fading channels-part I: Polymatriod structure, optimal resource allocation and throughput capacities," *IEEE Trans. Inf. Theory*, vol. 44, pp. 2796–2815, Nov. 1998.

[105] *Handbook of Global Optimization*, Kluwer Academic Publishers, Dordrecht, Netherlands, pp. 405-602, 1995

[106] W. Yu, W. Rhee, S. Boyd, and J.M. Cioffi, "Iterative water-filling for gaussian vector multiple-access channels," *IEEE Trans. Inf. Theory*, vol. 50, no. 1, pp. 145–152, Jan. 2004.

146

[107] W. Yu, "Sum-capacity computation for the Gaussian vector broadcast channel via dual decomposition," *IEEE Trans. Info. Theory*, vol. 52, no. 2, pp. 754–759, Feb. 2006.

[108] J. Xu, L. Qiu and S.Q. Zhang, "Energy efficient iterative waterfilling for the MIMO broadcasting channels, " in *Proc. IEEE Wireless Commun. and Networking Conf.(WCNC)*, Paris, France, 2012.

[109] J. Xu, L. Qiu, "Energy efficiency optimization for MIMO broadcasting channels", `arXiv:1202.3510v2 [cs.IT]`, Jun. 2012.

[110] C. Isheden, Z. Chong, E. Jorswieck, and G. Fettweis, "Framework for link-level energy efficiency optimization with informed transmitter, " *IEEE Trans. Wireless Commun.*, vol. 11, no. 8, pp. 2946–2957, Aug. 2012.

[111] E.V. Belmega, S. Lasaulce, and M. Debbah, "A survey on energy-efficient communications, " in *Proc. IEEE Intl. Symp. Personal, Indoor and Mobile Radio Commun. (PIMRC)*, Istanbul, Turkey, Sep. 2010.

Appendices

Appendix A

Proof of Lemma 1 of Chapter 4

We have

$$E\{\hat{R}_{ik,x}(\alpha;\tau)\} = R_{ik,x}(\tau)[\frac{1}{M}\sum_{m=1}^{M}e^{-j2\pi\alpha m}] \tag{A.1}$$

and

$$E\{x_i(m_1)x_j^*(m_1+\tau_1)e^{-j2\pi\alpha m_1}x_k^*(m_2)x_l(m_2+\tau_2)e^{j2\pi\beta m_2}\}$$

$$= \text{cum}_4\left(x_i(m_1), x_j^*(m_1+\tau_1), x_k^*(m_2), x_l(m_2+\tau_2)\right)$$

$$\times e^{-j2\pi(\alpha m_1-\beta m_2)} + R_{ij,x}(\tau_1)R_{kl,x}^*(\tau_2)e^{-j2\pi(\alpha m_1-\beta m_2)}$$

$$+R_{ik,x}(m_2-m_1)R_{lj,x}(m_1-m_2-\tau_2+\tau_1)e^{-j2\pi(\alpha m_1-\beta m_2)}. \tag{A.2}$$

For Gaussian sequences, the 4th cumulants are identically zero. Hence,

$$\text{cov}(\hat{R}_{ij,x}(\alpha;\tau_1), \hat{R}_{kl,x}^*(\beta;\tau_2))$$

$$= E\{\hat{R}_{ij,x}(\alpha;\tau_1)\hat{R}_{kl,x}^*(\beta;\tau_2)\} - E\{\hat{R}_{ij,x}(\alpha;\tau_1)\}E\{\hat{R}_{kl,x}^*(\beta;\tau_2)\}$$

$$= \frac{1}{M^2}\sum_{m_1=1}^{M}\sum_{m_2=1}^{M}[R_{ik,x}(m_2-m_1)R_{lj,x}(m_1-m_2-\tau_2+\tau_1)$$

$$\times e^{-j2\pi(\alpha m_1-\beta m_2)}] =: A. \tag{A.3}$$

Setting $m_1 - m_2 = m$ in (A.3) and with $\mathbf{x}(k) = \mathbf{n}(k)$, we have

$$A = \frac{1}{M^2}\sum_{m=-(M-1)}^{M-1}e^{-j2\pi\beta m}R_{ik,n}(-m)R_{lj,n}(m+\tau_1-\tau_2) \times [\sum_{m_1=|m|+1}^{M}e^{-j2\pi(\alpha-\beta)m_1}]. \tag{A.4}$$

We have

$$\frac{1}{M}\sum_{k=1}^{M}e^{-j2\pi(\alpha-\beta)k} = \begin{cases} 1 \text{ for } \alpha = \beta \in \mathcal{A} \\ \frac{e^{-j\pi(\alpha-\beta)(M+1)}}{M}\frac{\sin(\pi(\alpha-\beta)M)}{\sin(\pi(\alpha-\beta))} \\ \text{ for } \alpha \neq \beta, \quad \alpha, \beta \in \mathcal{A}. \end{cases} \tag{A.5}$$

It then follows that for any fixed m,

$$\lim_{M\to\infty}\frac{1}{M}\sum_{k=|m|+1}^{M}e^{-j2\pi(\alpha-\beta)k} = \lim_{M\to\infty}\frac{1}{M}[\sum_{k=1}^{M}e^{-j2\pi(\alpha-\beta)k} - \sum_{k=1}^{|m|}e^{-j2\pi(\alpha-\beta)k}] = \delta_{\alpha,\beta}. \tag{A.6}$$

Using (A.3), (A.4), (A.6) and the fact that $\mathbf{n}(k)$ is spatially uncorrelated, we obtain (4.10). Using (4.9) it follows that

$$\hat{R}^*_{ik,x}(\alpha;\tau) = \hat{R}_{ki,x}(-\alpha;-\tau) = \hat{R}_{ki,x}(1-\alpha;-\tau). \tag{A.7}$$

Therefore, from (4.10) and (A.7), we obtain (4.11). $\square$

Appendix B

Proof of Lemma 2 of Chapter 4

When $\mathbf{n}(k)$ is WSS, circularly symmetric, complex-valued, zero-mean colored Gaussian and $\mathbf{x}(k) = \mathbf{n}(k)$, it follows easily that $E\{\hat{\mathbf{R}}_{nn(*)}(\alpha; \tau)\} = 0$ and

$$\mathrm{cov}(\hat{R}_{(*)ij,n}(\alpha; \tau_1), \hat{R}_{(*)kl,n}(\beta; \tau_2))$$

$$= E\{\hat{R}_{(*)ij,n}(\alpha; \tau_1)\hat{R}_{(*)kl,n}(\beta; \tau_2)\} = 0 \tag{B.1}$$

where $R_{(*)ik,x}(\tau) := E\{x_i(m)x_k(m + \tau)\}$. Mimicking Sec. 4.3.1 (and setting $m_2 - m_1 = m$), we have

$$\mathrm{cov}(\hat{R}_{(*)ij,n}(\alpha; \tau_1), \hat{R}_{(*)kl,n}^*(\beta; \tau_2))$$

$$= \frac{1}{M^2} \sum_{m_1=1}^{M} \sum_{m_2=1}^{M} [R_{ik,n}(m_2 - m_1)R_{jl,n}(m_2 - m_1 + \tau_2 - \tau_1)$$

$$+ R_{il,n}(m_2 - m_1 + \tau_2)R_{jk,n}(m_2 - m_1 - \tau_1)]e^{-j2\pi(\alpha m_1 - \beta m_2)}$$

$$= \frac{1}{M^2} \sum_{m=-(M-1)}^{M-1} e^{j2\pi\alpha m}[R_{ik,n}(m)R_{jl,n}(m + \tau_2 - \tau_1)$$

$$+ R_{il,n}(m + \tau_2)R_{jk,n}(m - \tau_1)] \times [\sum_{m_2=|m|+1}^{M} e^{-j2\pi(\alpha-\beta)m_2}]. \tag{B.2}$$

Eqn. (4.18) then follows. $\quad\square$

Appendix C

Fractional Programming

In [105], fractional programming is introduced. Consider the following fractional program

$$\mathbf{CF}_1: \quad \max_{\mathbf{x} \in \mathcal{C}_1} F_1(\mathbf{x}) \text{ where } F_1(\mathbf{x}) = \frac{f(\mathbf{x})}{g(\mathbf{x})}, \tag{C.1}$$

$\mathcal{C}_1 \subseteq \mathbb{R}^n$ is a compact convex set, $f(\mathbf{x})$ is nonnegative and concave on $\mathcal{C}_1$, and $g(\mathbf{x})$ is positive and convex on $\mathcal{C}_1$.

Problem $\mathbf{CF}_1$ is said to be a concave fractional program if the numerator $f(\mathbf{x})$ of $F_1(\mathbf{x})$ is concave on $\mathcal{C}_1$, and $g(\mathbf{x})$ and $\mathcal{C}_1$ are convex function and set, respectively. In addition it is assumed that $f(\mathbf{x})$ is nonnegative on $\mathcal{C}_1$ if $g(\mathbf{x})$ is not affine. $\quad \square$